CHEMICAL REVIEWS

Review

Electrochemical Monitoring of Single Cell Secretion: Vesicular Exocytosis and Oxidative Stress

Christian Amatore, Ste#phane Arbault, Manon Guille, and Fre#de#ric Lemai#tre

Chem. Rev., **2008**, 108 (7), 2585-2621 • DOI: 10.1021/cr068062g • Publication Date (Web): 11 July 2008

Electrochemical Monitoring of Single Cell Secretion: Vesicular Exocytosis and Oxidative Stress

Christian Amatore,* Stéphane Arbault, Manon Guille, and Frédéric Lemaître

Département de Chimie, Ecole Normale Supérieure, 75005 Paris, France

Received September 10, 2007

Contents

* To whom correspondence should be addressed. Tel: 33-1-4432-3388. Fax: 33-1-4432-3863. E-mail: Christian.Amatore@ens.fr.

1. Introduction

Communication between cellular organisms occurs, among other mechanisms, through the release of specific biochemical or chemical messengers by an emitting cell, generally coupled to a specific detection of these messengers by a receiving cell. According to the target or the scope of the information exchanged, these messengers are released into biological fluids (for instance, into the blood flow), a restricted volume (i.e., a

10.1021/cr068062g CCC: $71.00
Published on Web 07/11/2008

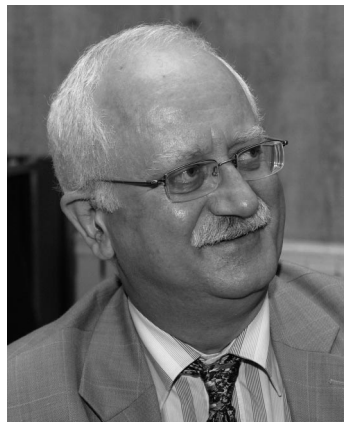

Christian Amatore, 56, is a Full Member of the French Académie Des Sciences and of the High Council of Science and Technology, advising the French President on scientific matters. His ultramicroelectrodes have allowed electrochemical investigations of organic, inorganic, and organometallic chemistries or living cells. These works correspond to over 330 publications with over 10800 citations (H = 55). He has received many renowned international prizes and distinctions and is Doctor Honoris Causa of many universities in Europe and Asia.

Stéphane Arbault, 39, was born in Reims, Champagne, France. After studying Photography and History of Arts, he chose to study Biology and Physical Chemistry. Then, during his Ph.D. in the laboratory of Dr. C. Amatore, he developed an electrochemical method to study oxidative stress on single human cells and defended his thesis in 1996. His interest in the biology and chemistry of carcinogenesis lead him to be involved in a European project based on a network of labs from Belgum, Spain, and France. In 1998, he was appointed by CNRS to a permanent position of Researcher in Dr. Amatore's group at ENS-Paris. His current research interests range from the detection and characterization of biological mechanisms involving nitric oxide and its derivatives, as well as studies of cell secretion of neuromediators via the exocytosis process or the development of novel methodologies, combining several technical approaches (electrochemistry, fluorescence microscopy, electrophysiology, and microfluidics), for fundamental studies or industrial research and development. Stéphane received several French and international young investigator prizes from the Societies of Electrochemistry or Nitric Oxide.

Manon Guille was born in 1979 in Les Lilas, France. She achieved her Ph.D. in 2005 in the Bioelectrochemistry field (physicochemistry of exocytosis, nitric oxide effects on neurovascular coupling in rat brain slices) from Université Pierre & Marie Curie, Paris 6, France. During her postdoctoral research at the University of Warwick, Coventry, United Kingdom (Marie-Curie IntraEuropean Fellowship; direction of Dr. J. V. Macpherson and Prof. P. R. Unwin), she worked on the electrochemical properties of single wall carbon nanotubes. She obtained an Assistant Professor position (Maître de Conférences) in September 2006 at the Université Pierre & Marie Curie, in the laboratory of Dr. Christian Amatore. Manon's research interests focus on SECM on living cells and brain tissues as well as on microfluidics applied to the study of biological phenomena.

Frédéric Lemaître, 30, was born in Saint-Rémy, Burgundy, France. He did a joint thesis between the Université de Bourgogne (France) and the Université de Sherbrooke (Canada) and received a double Ph.D. degree in 2003. His thesis works dealt with electrochemistry of palladium clusters. After doing postdoctoral research in Dr. Amatore's group at the Ecole Normale Supérieure de Paris (palladium catalysis), Frédéric obtained an Assistant Professor position (Maître de Conférences at the Université Pierre et Marie Curie) in September 2004. His research works are still performed in Dr. Amatore's group at ENS and concern the detection of secretion processes at the single cell level.

synapse), or the extra-body environment (as for pheromones). Whatever the communication procedures are, an infinitely minute number of molecules are released during a brief fraction of time (i.e., milliseconds to seconds) by a living cell outside its cytoplasm, that is, in the extracellular medium. Such infinitely small quantities thus represent a challenge as compared with the actual analytical standards. Moreover, the completion of the whole secretion event within a very short time, as well as the fact that the moment of release is "decided" by the cell itself, obviously increase the difficulties of such an analytical detection.

The huge difficulty of the analytical detection of these events can be transposed in terms of the signal-to-noise ratio, that is, the main requirement for the quality of the biological information. Taking for granted that the receptor of the material released has been selected to be thermodynamically and kinetically adequate, a good signal-to-noise ratio requires only a sufficient concentration (and not a sufficient amount since only chemical recognition rates matter) of the chemical or biochemical messengers near the receptor. As a consequence, the signal-to-noise constraint can be overcome by constraining the release of a small number of molecules to the local area of the receptor to give a large concentration only in the close vicinity of the receptor. This is easily done by restricting the volume in which the messengers are released. It must be emphasized that this is the solution retained by Nature in its biological synapses, so as to detect kinetically with a high signal-to-noise ratio the release of

zepto- to attomoles of chemical messengers released during a millisecond time scale.

As we will present in this review, this solution is readily adaptable to electroanalytical purposes. Indeed, whether the molecules released are electroactive and identifiable electrochemically, positioning an electrode at micrometric or submicrometric distances from a living cell allows restriction of the extracellular volume in which the molecules produced by the cell are released. It then ensures an adequate signal-to-noise ratio and a complete collection of fluxes of chemical messengers emitted by the cell under the electrode surface. For instance, one femtomole delivered in a volume of a thousand cubic micrometers creates a millimolar concentration rise, that is, a concentration variation that can be monitored kinetically via electrochemical techniques with an excellent signal-to-noise ratio, provided that the electrode does not pick up too much noise through its surface.

Ultimately, electrodes pick up electrical noise through their capacitance (through their overall conducting surface area), while the analytical information (the faradaic current) arises only from the surface area exposed to the cell release. Thus, using an electrode with an active surface matching that of the examined cell decreases the noise, while it does not affect at all the collection and provides the required quality and intensity to the analytical information. This maximizes the signal-to-noise ratio and simultaneously ensures a quantitative collection efficiency from different release points since this artificial synaptic cleft covers the whole cell-emitting surface. Indeed, because cell dimensions are in the micrometer range, using microelectrodes therefore allows one to perform measurements at the single cell or few cells level. Furthermore, positioning a microelectrode at micrometric distances from an isolated living cell ensures the most adequate signal-to-noise ratio and guarantees that the collection of electroactive chemicals released at the surface of a single living cell is quantitative. In other words, the microelectrode/living cell assembly (Figure 1) constitutes a semi-artificial synapse with all of the advantages of those built by Nature.

This solution has been mostly used purposely or intuitively for the investigation of biochemical material release and has allowed several important biological mechanisms to be clarified. In this review, we wish to report several important contributions of electroanalytical techniques over the past 20 years for investigating three major biological processes at the single cell level (or at least a few cells population): vesicular exocytosis, oxidative stress, and nitric oxide metabolism in brain.

2. Monitoring the Exocytosis at Single Living Cells

2.1. Introduction

2.1.1. Principles of Vesicular Exocytosis

As already mentioned in the Introduction, intercellular communication occurs through the release of chemical (or biochemical) messengers from an emitting cell to a target cell. This transmission is mostly achieved by vesicular exocytosis, such as in neurons, neuroendocrine cells, or for the control of hormonal fluxes in blood.[1] The expulsion of the messengers from the emitting cell and their further diffusion toward the neighboring cells can be briefly described as follows. First of all, secretory vesicles located in the emitting cell cytoplasm are initially filled with the

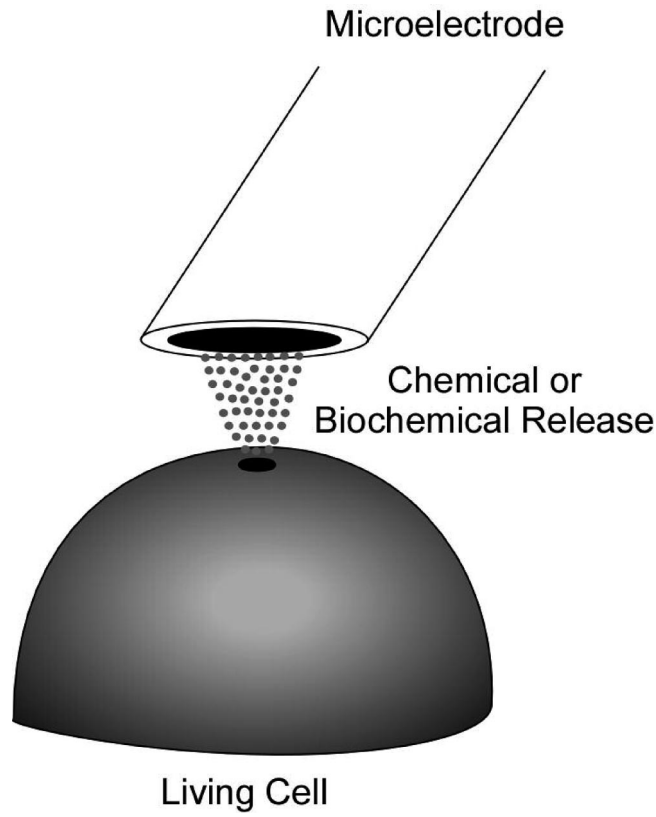

Figure 1. Principle of the semi-artificial synapse configuration, in which a microelectrode is positioned at the top of a living cell that releases electroactive species.

biochemical messengers (neurotransmitters, hormones, and peptides).[2] Second, following an appropriate cell stimulation (which provokes a Ca^{2+} entry or increase), the available vesicles dock to the cell membrane through a step requiring multiple protein−protein interactions, that is, the formation of SNAREs (soluble *N*-ethylmaleimide sensitive fusion protein attachment receptors) complexes (Figure 2, step a).[3] By overcoming the natural electrostatic repulsions between the cell and vesicular membranes, SNAREs allow membranes to interact at molecular distances so that the electrical field carried by each electroporates them. By local reorganization of phospholipidic bilayers, the formation of a fusion pore ensues through which the release of the vesicular content toward the extracellular medium onsets (Figure 2, step b). In most cell models investigated experimentally, exocytosis implies "dense-core" vesicles, whose intrinsic properties make them a better analytical target (see section 2.1.3 for details). Thus, the cationic messengers are compacted into a matrix behaving like a polyelectrolytic gel and constituted of polyanionic proteins such as chromogranins, which fill the vesicle core.[4] Because of the formation of the fusion pore, the first ionic exchanges between this matrix and the extracellular medium occur spontaneously by allowing partition of the cations. This provokes a local exchange with the cations of the external medium and thus a destructuration of the gel due to the different molecular and supramolecular interactions. In a natural environment, each messenger cation is exchanged by a fully hydrated small cation (Na^+, H_3O^+), and a local matrix swelling is induced. This increases the Laplace tension over the membranes junction area, which may ultimately counterbalance the pore edge energy. The expansion of the pore then takes place, leading to the release of a larger flux of the chemical messengers into the

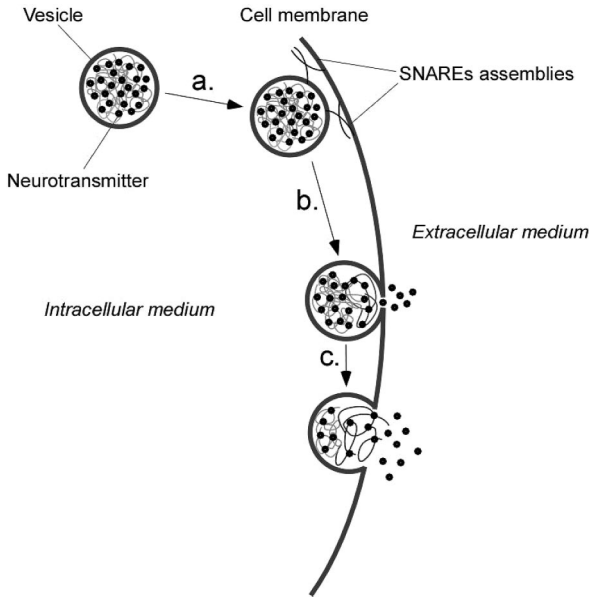

Figure 2. Schematic representation of the main phases of dense-core vesicles exocytosis. After appropriate stimulation, vesicles that are primed to undergo exocytosis dock to the cell membrane by the mean of SNAREs complexes (step a). The cell and vesicular membranes mix and evolve to the formation of a fusion pore, through which neurotransmitters begin to diffuse out the vesicular matrix (step b). Resulting from the ionic exchanges (catecholamines cations vs Na^+ or H_3O^+) and water entry between the intravesicular and the extracellular media, the vesicular matrix swells and provokes the fusion pore expansion (step c).

extracellular medium (Figure 2, step c), so that an autoaccelerating release takes place, leading eventually to the full fusion of the vesicle with the cell membrane. It must be added that the increase of the cytosolic Ca^{2+} concentration has been evidenced to play concomitantly an important role during almost all steps of the whole exocytotic process (for instance, as the disassembly of the actin cytoskeleton).[1]

2.1.2. Fast Scan Cyclic Voltammetry and Amperometry: Respective Advantages

Aerobic living cells require oxygen-containing solutions to perform as close as possible to physiological conditions. Because O_2 is in high or comparable concentrations (0.23 mM) vs the released species flowing into the semiartificial synapse, reductive detection is generally prohibited. Electrochemical measurements of a cell secretion then generally rely on the oxidation of the molecules released at the electrode surface located close to the cell membrane. The recorded currents thus evidence the nature of the molecules released and their quantities as well as the dynamics of the release itself. Two main electrochemical techniques have been used, amperometry and cyclic voltammetry. In amperometry, the working electrode is held at a constant potential at which the molecules under investigation are oxidizable. It ensues a continuous recording of the oxidation current as a function of the time without severe contamination by capacitive current. However, the "potential information" is lost. In cyclic voltammetry, the current is recorded as a function of the potential applied at the electrode (triangular voltage ramps), so discontinuous monitoring ensues, and capacitive currents may impede measurements, whenever they are not stable enough to be subtracted. In the absence of a semi-artificial synapse configuration, electrochemistry is coupled to another analytical technique (liquid chromatography or capillary electrophoresis). Unfortunately, although such measurements may be achieved at the single cell level, they merely report confirmations once the whole exocytotic process has ended.[5] For instance, the catecholamines content of a single bovine chromaffin cell can be determined by analyzing the extracellular solution (resulting from the cell lysis or after exocytosis has occurred) through microcolumn liquid chromatography coupled with amperometry at a carbon fiber electrode (that is directly inserted into the end of the capillary column).[6] This type of study has allowed the quantification of the amount of catecholamines per cell, and it has further evidenced that chromaffin cells are classified in either a single type of catecholamines secreted (75% of cells, only adrenaline release or nor-adrenaline) or a mixture of species (25%, adrenaline/nor-adrenaline) released. Additionally, the individual cells have been shown to deliver catecholamines in the same proportions in which they store catecholamines.[7,8] Similar studies (in which the coupled electrochemical technique is voltammetry) were also performed on individual neurons.[9,10]

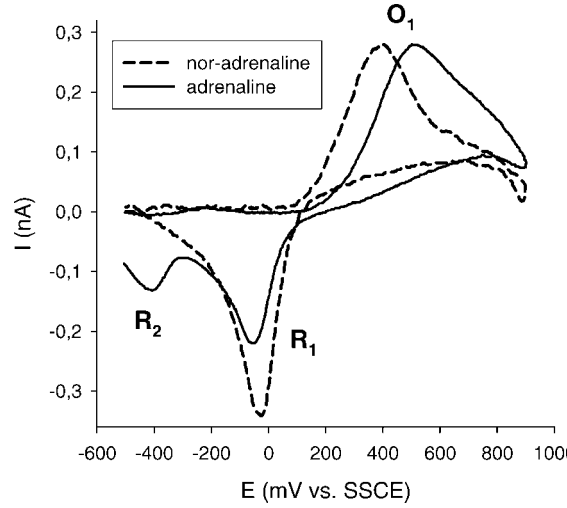

Figure 3. Background-substracted cyclic voltammograms at 10 V s^{-1} of nor-adrenaline (dashed plots) and adrenaline (thin plots) (20 μM) at a Nafion-coated carbon fiber electrode in pH 7.4-buffered physiological solution (adapted from ref 7).

Although these postanalytical methods can provide essential data concerning the vesicular content, no temporal and spatial information could be obtained during the very exocytotic release act. In the "semi-artificial synapse" mode, amperometry or voltammetry can be achieved along the occurrence of effective exocytotic events. Indeed, the whole release of neurotransmitters by a single cell is the summation of a series of spatially and temporally independent exocytotic events.

For example, successive cyclic voltammograms performed on chromaffin cells at relatively low scan rates (10 V s^{-1}; Figure 3) during exocytosis afforded a clear discrimination between adrenaline and nor-adrenaline releases. Indeed, for a given voltammogram of catecholamines under physiologically compatible conditions, a first oxidation/reduction (O_1/R_1) system can be observed (oxidation of the catechol framework into *o*-quinone during the anodic scan and subsequent reduction of the latter during the reverse cathodic scan) (Scheme 1). An additional peak (R_2) is detected on the reverse reduction scan for adrenaline, due to a fast intracyclization reaction that eventually leads to the formation of a reducible adrenochrome, which is reduced at R_2 (Figure 3). The cyclization is impossible during the voltammetric

Scheme 1

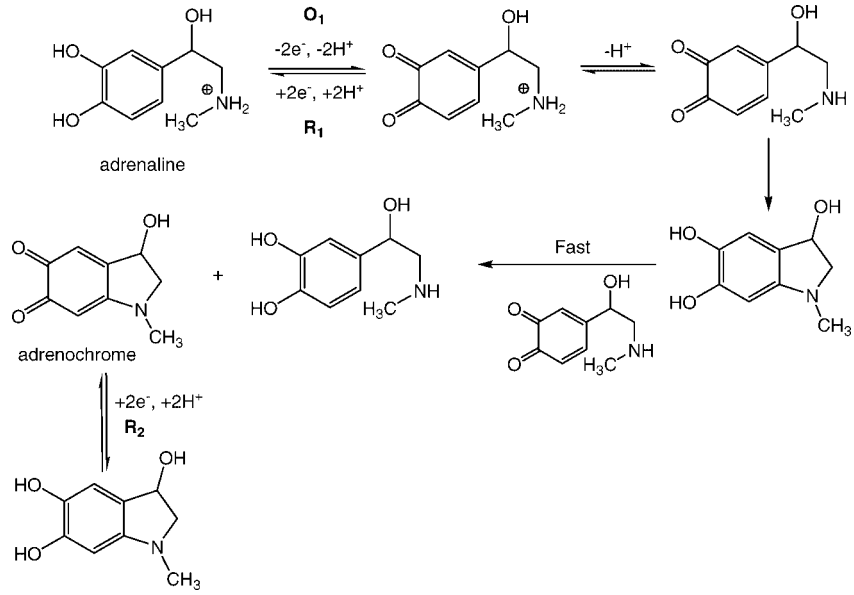

scan for nor-adrenaline, so that both molecules may be discriminated through analysis of the R_1 and R_2 peak currents.[11]

Voltammetric studies performed during the exocytotic release by a single living cell could thus confirm the results obtained with chromatography, that is, at least three classes of chromaffin cells (one that only releases adrenaline, a second one that only releases nor-adrenaline, and a last one that releases a mixture of adrenaline and nor-adrenaline) may be implied during catecholamines secretion in adrenal glands.[7] To improve the collection rate of the cyclic voltammograms during a single cell measurement, a real-time analysis by fast scan cyclic voltammetry has been developed. For instance, the temporal resolution falls in the millisecond range for scan rates of 200−300 V s^{-1}.[12−14] Thus, fast scan voltammetry (usually $\upsilon = 800$ V s^{-1}) also allows the continuous differentiation of adrenaline and nor-adrenaline. Indeed, in that case, a second oxidation wave is only observed for adrenaline at very positive potentials, being presumably due to the adsorption of the *o*-quinone form onto the electrode surface and the subsequent irreversible oxidation of the amine to imine.[15]

As already mentioned above, electrochemical measurements only require that the vesicular content released may be oxidized at the surface electrode. Such experiments were thus also designed to monitor the secretion of peptide hormone from single melanocytes of the intermediate lobe of the rat pituitary (oxidation of tryptophan and tyrosine residues of small proopiocortin-derived peptides secreted from the cells).[16,17]

Yet, because of the discontinuous monitoring and possible corruption by capacitive currents, cyclic voltammetry mainly allows the chemical identification of the secreted molecules. Conversely, amperometry provides much more precise kinetic information on the exocytotic process itself. Actually, amperometric analysis of the secretion of neurotransmitters by a single living cell allows evaluation in real-time of the whole efficiency of the exocytotic process with a very high precision from analytical (zeptomoles), temporal (millisecond), and spatial (electrode diameter, ~7 μm) points of view.[18−20] Practically, a glass micropipette can be positioned near the cell investigated in the semiartificial synapse configuration and is used to administer secretagogues, that is, stimulating agents that trigger exocytosis (for instance, nicotine, a K^+/Ca^{2+}, or digitonine/Ca^{2+} mixture, Ba^{2+}, etc.[14,21,22]) via pressure ejection.[18] Stimulation can also be performed with action potentials in the presence of Ca^{2+} or by flash photolysis of caged coumpounds.[23−26] Whatever the stimulation is, exocytosis is amperometrically depicted as a series of current spikes that correspond to the detection of successive exocytotic events, each spike corresponding to one exocytotic event.[14] As compared to cyclic voltammetry measurements, complex features of the dynamics of the exocytotic events can be amperometrically obtained. Globally, four main parameters of the amperometric trace have been evidenced to reveal the features of secretion events at a single cell. The first one deals with the number of events detected per cell (frequency of release), and the others concern the characteristics of the individual amperometric spikes and provide individual and statistical data about the progress of the event itself. The mean frequency of the events (evaluated experimentally upon counting the number of events occurring within a selected duration of the secretion process; see a representative amperometric trace in Figure 4A) testifies to the number of exocytotic events that occur when the cell is stimulated.

Several mean kinetic parameters can be deduced by examination of each individual event, that is, of each amperometric spike (Figure 4B). For instance, the maximum oxidation current I_{max} (pA) directly gives the maximum flux of neurotransmitters released during an event. Additionally, time parameters such as the half-width $t_{1/2}$ (ms; evaluated at 50% of I_{max}), a rise-time (between the beginning and the maximum of the spike), or a spike falling-time (delay between the maximum and the end of the peak or a time constant resulting from exponentional fits) are readily determined with a submillisecond precision.[27] Because of the high signal/noise ratio (rms noise between 0.2 and 1 pA), the messenger fluxes can be amperometrically measured with a precision in the range of 1000 molecules per ms.[20] Besides these quantitative data, the morphology of a spike is directly linked to the steps of the exocytotic event. Thus, once the formation of the fusion pore occurs (see section 2.2.1.), neurotransmitters begin to diffuse out of the fused vesicle,

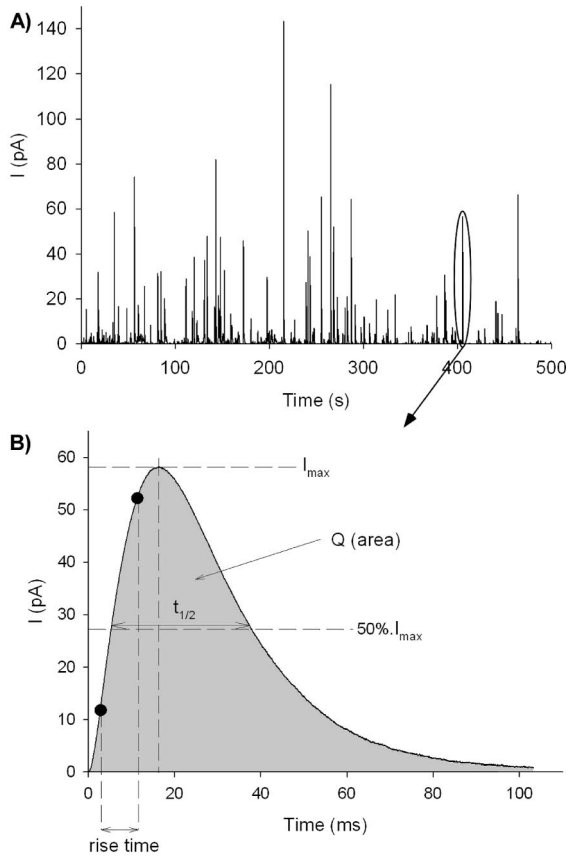

Figure 4. (A) Representative amperometric trace obtained during exocytosis of a single chromaffin cell (the potential of the carbon fiber microelectrode is held at 650 mV vs Ag/AgCl; at this value, all of the catecholamines released during an exocytotic event are oxidized). (B) Usual amperometric analysis of an exocytotic event: major relevant quantitative and kinetic parameters extracted from an amperometric spike.

sometimes leading to different pre-spike features (PSFs) termed generally as a "foot". The expansion of the pore is then detected as a sudden drastic current increase, while the following current decreases, featuring the end of the event and then the diffusion of the last neurotransmitters released.[28]

Finally, the area of a current spike corresponds to an electrical charge Q (fC or pC) that directly reflects (by the mean of the Faraday's law) the amount of molecules collected during one individual event. Because collection is quantitative when the electrode is in the close vicinity of the cell, this represents the effective quantity released.[29] It must be emphasized that the detection threshold ranges between 1000 and 10000 molecules for an individual event, depending on the experimental conditions. Finally, the high number of data collected (between 50 and 200 nonoverlapping spikes per amperogram are generally analyzed) allows a statistical and comprehensive analysis of the phenomenon.

Exocytosis of neurotransmitters that can not be easily oxidized (glutamate, acetylcholine, etc.) is obviously not amenable to direct amperometry,[5] although indirect detection may be applied as for many bioelectrochemical sensors. This is however at the expenses of collection efficiency and time resolution. Nevertheless, amperometric measurements allow precise kinetic quantification of many messengers of importance in natural exocytotic events and are henceforth considered as a usual and powerful analytical tool with large scope. It is worth mentionning that some cells that release nonelectroactive molecules, such as dog pancreatic duct epithelial cells, may be incubated with dopamine (that is oxidable electrochemically) to amperometrically monitor their exocytosis subsequently to other analytical techniques.[30–32]

2.1.3. Cell Models Typically Investigated

Generally, exocytosis is investigated on nonsynaptic cell models that possess comparatively large-sized vesicles (0.25−1 μm diameter) vs synaptic vesicles (~20−50 nm diameter) and high neurotransmitter concentrations, which allow a remarkable detection sensitivity.[33] Hence, this avoids the usual difficulties in studies of real synapses among which are the difficulty of neurons culture, the low size of synaptic vesicles, the weak amount of neurotransmitters released, and the impossibility of inserting the electrochemical probe into a synapse without inducing its destructuration.[33] Although they are amperometrically limited by the requirement of an electroactive substance released during the exocytotic process, numerous cell types are available as model systems. This mainly includes adrenal (bovine, calf, rat, or even human) chromaffin cells (that release a mixture of catecholamines: adrenaline, nor-adrenaline, and dopamine),[13,14,21,25,34–36] rat pheochromocytoma (PC12) cells (that release dopamine after incubation and are derived from cancerous rat adrenal gland),[37–39] mast cells from normal or beige mice [corelease that of 5-hydroxytryptamine (serotonin) and histamine but involve giant vesicles][40–42] or RBL-2H3 mucosal mast cells (serotonin-loaded),[43,44] human or mouse pancreatic β-cells (insulin release, preloading procedures also allow serotonin release),[45–47] dog pancreatic duct epithelial cells (dopamine-loaded),[32] trans-differentiated bovine chromaffin cells thus acquiring a neuronal phenotype,[48] enterochromaffin cells of the guinea pig ileum (serotonin),[49,50] and single melanotrophs of the intermediate lobe of the rat pituitary (melanocytes secreting hormones and related peptides).[16,17]

Although not involving real synapses (i.e., no intrusion of the electrochemical probe into the synaptic cleft), works dealing with neuronal systems have been reported on invertebrate systems, such as the leech *Hirudo medicinalis* (serotonin),[51–53] the pond snails *Planorbis corneus* (dopamine)[54–58] and *Lymnaea stagnalis* (serotonin and catecholamines),[59] and the sea hare *Aplysia californica* (serotonin),[60] or on mammalian neuronal systems, such as superior cervical ganglion neurons from neonatal rats (catecholamines mixture),[61] cultured ventral midbrain neurons of rat (dopamine loaded),[62] or dissociated neurons of the sea pansy *Renilla koellikeri* (in this case, after cell-loading procedures with dopamine and nor-adrealine).[63] Eventually, amperometric measurements have also been achieved on somata of Substantia Nigra neurons in rat midbrain slices,[64] axonal varicosities of rat midbrain dopaminergic neurons,[65] or individual dopaminergic neurons isolated from the mouse retina.[66]

2.1.4. Typical Microelectrodes

Generally, electrochemical measurements aimed to investigate exocytosis are achieved with carbon fiber microelectrodes (usually from 1 to 10 μm diameter). The carbon fiber can be sealed and encased into a glass capillary.[13,67] Optimized procedures involve a polymer insulation of protruding carbon fibers [for instance, polyethylene,[68] polypropylene,[69] or poly(oxyphenylene)[70]] before or after glass sealing. Furthermore, coating of the carbon fiber with a thin film of the perfluorinated cation-exchange material Nafion

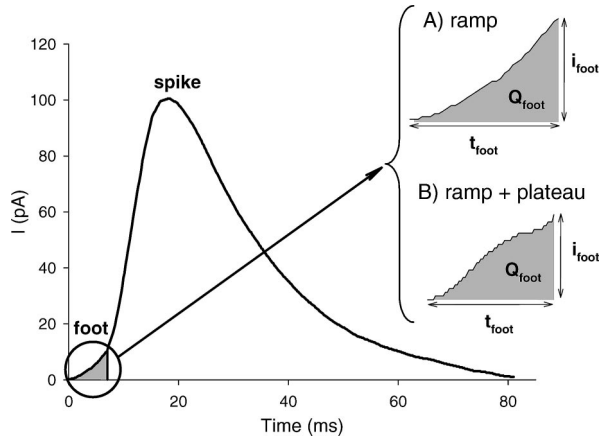

Figure 5. Schematic representation of two main amperometric spikes with a pre-spike feature of foot (PSF). (A) With a "ramp"-shaped foot. (B) With a "ramp + plateau"-shaped foot. Quantitative foot parameters I_{foot}, t_{foot}, and Q_{foot} calculated before the rising phase of the spike are given for both PSFs.

has been shown to enhance the selectivity (only the cations, such as the protonated catecholamines at chromaffin cells, may then easily permeate the film), although this decreases the temporal resolution due to the time necessary for secreted substances to diffuse slowly through the polymer film.[13] Coated carbon fiber ultramicrodisk electrodes (CUMDEs) can also be prepared by means of cathodic electrophoresis paint to electrically and chemically insulate the carbon fiber protruding from a pulled glass capillary.[71] Moreover, amperometric measurements at pancreatic β-cells (insulin release) have required the use of carbon fiber microelectrodes modified with a polynuclear ruthenium oxide/cyanoruthenate film. Such a chemical modification induces a fast catalysis of insulin oxidation, thus allowing its anodic detection in physiological buffers.[45,72]

Recently, "diamond" microelectrodes have been used to record serotonin release from enterochromaffin cells of the intenstinal mucosal layer.[49,50] The diamond microelectrode was formed by overcoating a sharpened 76 μm diameter Pt wire with a thin layer of conducting diamond. Subsequent insulation with polypropylene allows a conically shaped microelectrode with a diameter of about 10 μm at the tip.

2.2. Insights Directly Provided by Amperometry

2.2.1. Detection of the Fusion Pore

The fusion pore phase can be detected amperometrically, although its structure (proteic or lipidic) cannot be solved by this analytical technique.[73] The detection of an amperometric foot related to the pre-release through the fusion pore was first reported by R. H. Chow et al.,[68] followed a few months later by the group of G. A. de Toledo.[74] Both have shown that a significant proportion (for instance, about 30% in chromaffin cells, depending on the experimental conditions and the analysis; see below) of the amperometric exocytotic events display a foot (commonly named the prespike feature or PSF). This reflects the onset of the catecholamine release through the transient fusion pore.[75] Consequently, the amperometric foot (whose shape generally resembles a ramp or a ramp followed by a plateau of current) directly informs on the existence of the fusion pore (Figure 5).[76] Four PSF parameters are commonly analyzed: its duration (t_{foot}, which is ascribed to the lifetime of the pore), the charge (Q_{foot}, which is linked to the number of molecules released through the pore), the maximum current (I_{foot}, which is correlated to the flux of neurotransmitters released), and the percentage of spikes with a foot (or PSF frequency) by comparison with the whole set of spikes analyzed. It must be nevertheless emphasized that the studies in which these four parameters are analyzed together are rather scarce because of the intrinsic difficulty of these measurements (low foot current) by comparison with those dealing with entire spikes.

The works dealing with the detection of an amperometric foot are miscellaneous. For instance, several data have raised the question whether the amperometric foot is linked to the predissociation of the vesicular matrix.[75,77,78] Furthermore, recent studies on chromaffin and PC12 cells suggested that the presence of an amperometric foot is correlated to the vesicular content and size and possibly to the presence of a liquid film (named a halo) containing few dissolved neurotransmitters molecules when the matrix core is not adherent to the vesicle membrane.[76,79] Indeed, in some vesicles, the vesicular membrane may not fit tightly around the dense core, leaving in electron microscopy an electron-lucent halo separating the dense core from the vesicular membrane.[80] This halo is thus associated with the existence of a liquid film into some vesicles or at least of a medium in which the diffusion coefficient of catecholamines is larger than in the dense matrix.

Hence, at chromaffin and PC12 cells, although a PSF detected during an exocytotic event reveals that a flux of catecholamines occurs during the phase of the initial fusion pore opening, experimental observations based on modifications of the vesicular content (by L-DOPA or reserpine treatment) or of the mechanical cell membrane properties suggest that an amperometric foot does not only correspond to a prerelease of catecholamines from the vesicular matrix but also of catecholamines contained in a halo present in a fraction of vesicles.[79,81,82] Thus, only these halo-equipped vesicles would give rise to an amperometric PSF. This brings up in particular the notion that the PSF frequency would not be linked to the dynamics of the fusion pore, which is an intrinsic property of the fusing vesicles. The percentage of spikes with a foot and the stability of the fusion pore may then be two independent phenomena that are not necessarily correlated. A PSF would thus only reflect the presence of a sufficiently sized halo.[81] Interestingly, amperometric studies of exocytosis at rat pancreatic β-cells coreleasing GABA, ATP, and serotonin have evidenced that PSFs are less frequently observed when ATP is released than for serotonin or GABA, but also that the relative amplitude of PSF (amplitude of foot as compared to those of the whole spike) also depends on the substance released. The PSF events thus exhibit fusion pore selectivity and compounds may be differentially released depending on their chemical properties.[83] For a lipidic pore, this seems difficult to rationalize unless the selectivity is linked to the halo composition, so that such experiments add to the present view rather than to the predissociation mechanism.

Additionally, the percentage of spikes with foot has been evidenced to depend sometimes on the secretagogue, in agreement with the recognized dependence of vesicular fusing populations on the stimulus of exocytosis.[84] For instance, the PSF frequency for chromaffin cells varies when comparing digitonin/Ca^{2+} with nicotine,[85] whereas the absence of dependence is observed when comparing Ba^{2+} and K^+/Ca^{2+} stimulations.[86]

In two works reported, a proportion of foot signals did exhibit rapid fluctuations, and this was interpreted as evidence of the flickering of the fusion pore, the number and frequency of the foot flickering being modified by intracellular Ca^{2+} concentration.[87,88] However, this appears as a scarce experimental observation. Furthermore, some effects of SNAREs assemblies on the stability of the fusion pore have also been deduced from the analysis of the amperometric foot.[89–95]

Actually, the scarceness of studies in which all of the foot parameters are analyzed together as well as the method of detection of an amperometric foot (which often depends on the group) have promoted different interpretations of what a PSF exactly represents. For instance, a PSF could sometimes be confused with the superimposition of two independent spikes temporally close together. Hence, the relative lack of precision required for amperometry in this case implies that the amperometric detection of the fusion pore is henceforth associated to capacitance and conductance measurements (see section 2.4.).[96–98]

2.2.2. Mapping the Cell Surface

Usually, the diameter of the carbon fiber microelectrode is approximately 7−10 μm, that is, equivalent to the size of a single cell, for the reasons of information collection that we have described above. Decreasing the electrode size to a lower scale (~1 μm) can be achieved through the fabrication of etched electrodes (mostly carbon fiber electrodes).[70] In that case, exocytosis can also be monitored without any clear modification of the spikes parameters (as compared to those monitored at the 10 μm fiber electrode),[77] except for a reduced spike frequency (in agreement with the reduced collection due to a lower electroactive surface relative to the emission surface area of the cell). This basic property has been used to map the chromaffin cell surface during the secretion.[99,100] Also, the simultaneous recordings of cell secretion with two etched electrodes has been shown to reveal that different release sites are present on endocrine cells. Notably, the correlation between the active zones and a high local intracellular calcium concentration ("hotspots") has been clearly evidenced, suggesting that calcium pumps are spatially close from fusing points equipped with SNAREs machineries.[100]

Etched electrodes have also been used to map neurite-emitting chromaffin cells.[101] Indeed, after 3−4 days of plating, there is a large proportion of chromaffin cells that become non-spherical. Mapping the release of such bipolar or tripolar cells has revealed that, contrary to ovoid cells, the release distribution is not randomly located. It must be added that the mapping of the cell surface by the means of etched electrodes has also been successfully achieved on pancreatic β-cells.[102,103]

Additionally, studies dealing with the amperometric detection of exocytosis at PC12 cells with nanoelectrodes (ca. 100 nm) have been reported.[104] In that case, the nanoelectrode size corresponded to the vesicle diameter range, and exocytosis was rarely detected when the nanoelectrode was randomly positioned at the top of the cell. Indeed, there was no detection during ca. 70% of the recordings, and only one to a few spikes per cell (5 min of recording) were observed when exocytosis occurred beneath the nanoelectrode. Therefore, these results support what was already described above, that is, the existence as well as the distribution of active and inactive release zones of cell membrane.[104]

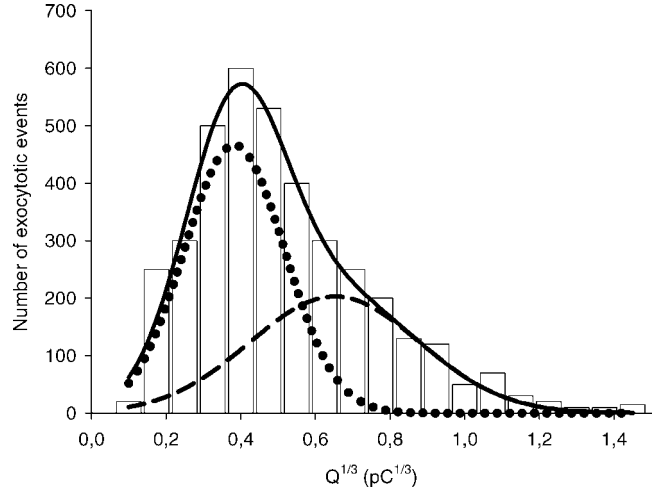

Figure 6. Example of quantitative analysis of dense-core vesicle size provided by amperometric measurements (the vesicle diameter is assumed to be proportional to the cube root of the amperometric spike charge). Two vesicular populations can be fitted with the sum of two Gaussian distributions. Direct analysis of dense-core vesicle diameter obtained by electron microscopic measurements gives the same statistical distributions (adapted from ref 21).

Recently, the fabrication and characterization of carbon microelectrode arrays (MEAs) have been reported. The carbon MEAs are composed of few (two, three, or seven) individually 5 μm diameter carbon microdisks embedded in glass, leading to a 20−40 μm diameter array.[105] Amperometric measurements with MEAs have been achieved on PC12 cells and thus allow one to obtain information about the spatial heterogeneity of the exocytotic events with a convenient experimental device.

2.2.3. Evidences of Multiple Vesicular Populations

The modulatory role by intracellular vesicles in the chemical transmission appears to be related to a distribution of sizes.[38] This leads somehow to question if different types of vesicular populations are implied during exocytosis. Amperometric data may easily be used to examine this question. Indeed, the released charge (Q) per amperometric spike, which represents the number of molecules released per exocytotic event (also improperly thought as the quantal size[106]) is related to the vesicular radius by combining the Faraday's law and the formula of the spherical volume:[14]

$$r = \left(\frac{3Q}{8\pi F C_{ves}}\right)^{\frac{1}{3}} \quad (1)$$

Assuming that the intravesicular concentration C_{ves} is a constant value, as imposed by the very supramolecular binding of neurotransmitters inside the matrix, one obtains

$$r \alpha Q^{1/3} \quad (2)$$

Whenever this basic equation holds, it shows that analysis of the amperometric charge (more particularly its cube root) is tantamount of the vesicular size. Although chromaffin cells are usually thought to have a single population of secretory vesicles, Grabner et al. showed by both electron microscopy and amperometric analyses that exocytosis at chromaffin cells involves a dual size-differentiated population of vesicles (see an example in Figure 6). Indeed, the size distribution (estimated by optical microscopy or by the mean of $Q^{1/3}$) was well-described as the sum of two Gaussians, suggesting

that secretory vesicles are bimodally distributed with both large and small events. The very similar distributions obtained by microscopy (vesicular radius) and amperometry ($Q^{1/3}$) were shown to be consistent, further adding to the view that chromaffin cells possess at least two populations of dense-core vesicles with specific secretory properties.[21] Furthermore, a hypotonic extracellular environment increases the ratio between large- and small-sized vesicles. Indeed, under hypotonic conditions, the population of smaller vesicular contents, and therefore of smaller sizes, results in depressed by comparison with isotonic conditions.[107]

The notion that at least two vesicular populations participate concurrently in exocytosis appears to be extendable to other cell types. For instance, similar amperometric results were recorded on the cell body of the dopamine-containing neuron of *Planorbis corneus*.[108] As above, the statistical distribution of $Q^{1/3}$ values evidenced a release of dopamine from two classes of vesicles.[54,55,57,58] Additionally, amperometric measurements performed from undifferentiated rat PC12 cells[109] or Retzius cells of the leech (*Hirudo medicinalis*) led to similar results.[51–53]

Actually, a more accurate analysis of the charge from amperometric data showed that in chromaffin cells, the $Q^{1/3}$ distribution is more reasonably described by the presence of at least three Gaussian individual populations.[34] Moreover, the mean charge, as well as the relative proportion of each vesicular population, are clearly affected by the duration of the cell culture before experiments.[34]

2.2.4. Mathematical Models Applied to Amperometric Spikes

As explained above, the extraction of spikes parameters is expected to offer a better understanding of the exocytotic process. To go further, some works have reported on mathematical models that could provide additional information. For instance, A. G. Ewing and colleagues reported on the amperometric study of exocytosis by PC12 cells or *Planorbis corneus* neurons.[38,58] In such works, it was assumed that the shape of the decreasing phase of an amperometric spike follows a Cottrell-like behavior. Combination with Faraday's law affords one to correlate the vesicular radius with the charge released without assuming a priori a constant intravesicular concentration:

$$r_{\mathrm{ves}} = \frac{D^{1/2}}{t^{1/2}\pi^{1/2}} \cdot \frac{3Q}{i(t)} \tag{3}$$

On the basis of the same hypotheses, a second model connected the vesicular and electrode radii and the charge released:

$$r' = \frac{(r_{\mathrm{ves}})^3}{(r_e)^2} = \frac{D^{1/2}}{i(t)\cdot t^{1/2}} \cdot \frac{3Q}{4\pi^{1/2}} \tag{4}$$

As a result, vesicular size distributions were extracted from a combination of the electrochemical current and charge. The comparison with literature data (provided by electron microscopy analysis) showed that the model behaves very satisfactorily, although it provides only relative distributions. Indeed, the value of the diffusion coefficient cannot be measured with accuracy within this framework.

A full theorical and mathematical model was provided by C. Amatore and colleagues to describe the shape of an individual amperometric spike.[28,29,35,78,110,111] The diffusion coefficient of the neurotransmitter inside the swollen parts of the vesicle matrix could then be determined for each event. This, as for the Ewing simplified model, allowed through comparison to the charge Q, an accurate determination of the intravesicular concentration, showing that it is reasonably constant, although with a distribution-like behavior.[38,110]

Thus, a full mathematical way analysis could be developed upon considering that an amperometric spike results from the convolution of an opening sigmoid type function with a purely diffusional function. In a first approach, this convolution was approximated by the integral of the product of an exponential decaying branch (diffusion from the spherical matrix) by a Gaussian (derivative of the sigmoid like opening function) curve.[28] Satisfactory results were thus obtained while fitting an amperometric spike with the ensuing exponentially modified Gaussian curves. The Gaussian portion has been evidenced to reflect a rate-limiting opening of the pore, whereas the final exponential part is consistent with the diffusional control of the release, that is, the dissociation of vesicular matrix. This model, prone to be more realistic and precise than the one described above, showed clearly that physical chemistry plays a significant role during exocytotic events and that the diffusion of the vesicular content is not rate limiting during the first stages of the process. Physically, the raising part of the spikes is mostly determined by the fusion itself, while the descending branch mainly illustrates the rate of diffusional release from the swollen exposed matrix (Figure 7A).

Several other models have been proposed, in particular by Y. A. Chizmadzhev et al., to rationalize exocytosis by taking into account the effect of membrane mechanics and particularly the effects of surface tensions on the stability of the initial fusion pore.[112,113] Yet, in these models, the reasons for changes of membrane surface tensions were not explained, and furthermore, the membrane dynamics were not related to amperometric measurements. Besides, three other models have been developed to face amperometric measurements with the physicochemical characteristics of exocytotic events. The origin of the driving force of exocytosis was noteworthily emphasized, from where it ensues that the main effect is due to changes of Laplace surface tension of membranes provoked by the swelling of the vesicle matrix during exocytosis.[78,110,111,114,115] Moreover, these three models tempted to couple the membrane dynamics to the flux of neurotransmitters, measured electrochemically, as based on two main rate-determining phenomena: (i) the surface tension-induced rate of the pore opening (i.e., the rate at which the vesicle membrane is incorporated into the cell membrane) and (ii) the increasing diffusion rate of neurotransmitters out of the swollen matrix through its increasing exposed area.

These three models rely on the same conceptual framework in which each individual amperometric spike $i(\tau)$ was assumed to result from the convolution of an opening function $S(\tau)$ and a diffusion one $\Psi(\tau)$ (Figure 7B, τ being an adimensional time).[78,110,111]

$$i(\tau) = 2F \cdot \int_0^{\tau} \Psi(\tau - u) \cdot \frac{\mathrm{d}S(\tau)}{\mathrm{d}\tau} \cdot \mathrm{d}u \tag{5}$$

The diffusion function was independently obtained by the mean of Brownian fits of the descending branch, while the opening function was linked to the variation of the

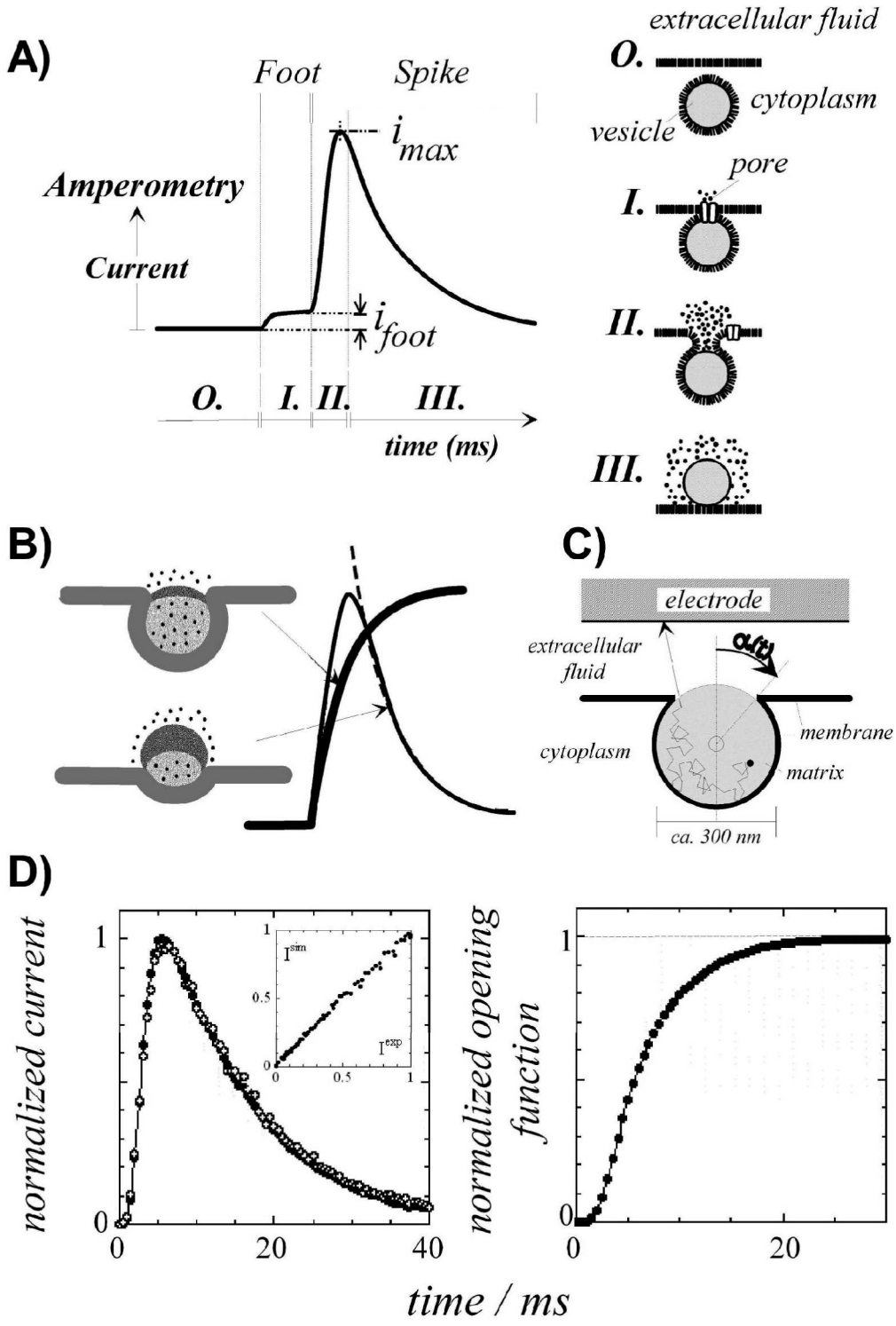

Figure 7. (A) Schematic representations of the different phases of vesicular exocytosis as observed by amperometry. (B) Rationalization of an amperometric spike (thin solid curve) by the time convolution between membrane fusion (thick solid curve and top left cartoon) and free spherical diffusion (dashed curve and bottom left cartoon). (C) Schematic representation of a 2D cross-section of the physicochemical model used to describe the convolution sketched in part B. (D) Left: modeling (symbols) of a typical spike (solid curve) by random walk simulations as sketched in part C. The inset evidences the perfect agreement between the experimental spike and its physico-chemical model. Right: opening function extracted after deconvolution of the spike shown on the left. Data from references 78, 110, 111.

vesicular uncovered surface as a function of time (Figure 7C):

$$S(t) = \frac{1 - \cos \alpha(t)}{2} \tag{6}$$

By means of geometrical restriction to diffusion due to the time-dependent circular section of the fusion junction zone, this allowed a full Brownian motion fitting of each spike so that $S(\tau)$ could be determined for each event without requiring any a priori assumption except for that of correctness of the formulation in eq 5.

This deconvolution procedure that removes the diffusion function could be computerized so as to allow the almost in-time analysis of thousands of experimental spikes, by the

use of a homemade software to extract each individual opening function with an extremely high precision through subsequent iterative procedures (Figure 7D). The excellent fits that were obtained are consistent with the key role played by the matrix swelling in producing the driving energy, the rate of release of which is finely tuned by membrane dynamics. Furthermore, this model permitted elucidation of the whole process from an energetic point of view. Indeed, the refrained swelling of vesicular matrix induces a pressure onto the vesicle/cell membrane assembly after the initial fusion pore, which is converted into an increasing virtual surface tension of the membrane through Laplace's law.[78,110,111] Ultimately, this dominates the edge energy of the initial fusion pore and provokes its rupture and its further enlargement. During this phase, the corresponding released energy is assumed to be converted into heat dissipation due to the membrane leaflets slipping against each other and against the intra- and extracellular solutions. As a consequence, the evolution of the radius R of the rim connecting the cell and vesicle membranes can be described following eq 7 (where η is the viscosity of the cell membrane, and σ is the equivalent surface tension maintained by the continuous swelling):[78,110,111]

$$W_{\text{released}}(\alpha < \pi/2) = \pi\sigma R^2 = W_{\text{viscous}} = 4\pi\eta R\frac{dR}{dt} \quad (7)$$

This equation has been shown to be experimentally valid during the first full-fusion phase ($\alpha < 90°$). However, when the forces exerted by matrix swelling do not apply anymore onto the membranes (i.e., after the matrix has been exposed beyond its diametrical plane, $\alpha > 90°$), the smaller released energy can be treated as a pseudoedge energy,[78,110,111] so that the radius R of the rim connecting the cell and vesicle membranes now decreases and its rate of evolution can thus be written as follows (where ρ is the equivalent edge energy of the system):

$$W_{\text{released}}(\alpha > \pi/2) = -2\pi\rho R = W_{\text{viscous}} = 4\pi\eta R\frac{dR}{dt} \quad (8)$$

The resolution of the eqs 7 and 8 allows the prediction of the variation of R as a function of the time. Because the opening function (extracted from the experimental amperometric spikes) can be related to R (for instance, during the first full-fusion phase, $R(t) = R_0 \sin \alpha(t)$, where R_0 is the initial unswollen matrix radius), the comparison between predicted and experimentally deduced temporal evolutions of R showed that the model predicts very satisfactorily the dynamics of fusion and release. This emphasizes the importance of physicochemical parameters during the exocytotic process for which the energy released by the vesicular matrix swelling through the membranes is dissipated viscously by membrane slipping during the pore enlargement. Finally, it has to be emphasized that the role played by the cell membrane viscosity as well as the mechanical membrane tension has been experimentally confirmed by the mean of modifications on the extracellular osmolarity or environment.[35] These purposely designed experiments thus confirmed the present view of dense-core vesicular release and offered a strong qualitative background to rationalize many reported observations.

The experimental testing of these three models required independent knowledge of several parameters (vesicle radius, transmitter diffusivity within the swollen matrix, surface tension and viscosity of membranes, etc.),[78,110,111,114,115] so that the analytical treatment of current variations observed could be used to describe the effective membrane dynamics. In the first model,[78,110,111] these crucial data were extracted from each single event observed upon using different fractions of the current−time spike. Treatment of several hundreds of spikes from the same cells or a series of cells evidenced that—as could be guessed because of cellular variability—these parameters experienced relatively large variabilities and thus contributed in part to the particular shape of each spike. In the two other models,[114,115] the authors treated only a few spikes and decided to rely on average data for these crucial parameters. In our opinion, beyond the great qualities of each methodology, this potentially introduced a severe bias in the overall treatment. Indeed, any neglected variations of the key parameters vs their assumed average values may have been likely compensated by an appropriate bias into the extracted membrane mechanics.

2.3. Using Amperometry as a Routine Technique

As described above, investigations of the exocytotic process are essentially performed on cell models in which vesicles are dense-core granules. Neurotransmitters are stored into a vesicular matrix whose role is not only devoted to the neurotransmitters storage, although this is a most efficient way for forming nanopackets. For instance, vesicles in adrenal chromaffin cells store catecholamines (adrenaline, nor-adrenaline) at high concentrations (~0.5 M) and at low pH (~5.5) with other soluble components (ATP, Ca^{2+}, ascorbic acid, etc.) and mainly chromogranins, which allow the matrix to behave statically (storage) and dynamically (swelling driving force) as a polyelectrolytic gel. The cohesion of this complex assembly is notably maintained by interactions (mainly electrostatic forces and hydrogen bonds) between the deprotonated carboxylic functions of chromogranins, the positively charged catecholamines, and the Ca^{2+} ions. Once the fusion pore formation onsets, ionic exchanges with the extracellular medium induce a destructuration of the matrix by modifying the local packing forces and hence its further swelling. As a consequence, it is expected that the composition of the external environment (pH, nature and concentration of ions, etc.) have to play a role on the exocytotic process. More generally, physical and chemical properties of the systems have been evidenced to play an important role during the exocytotic mechanism in addition to biological controlling factors.[116] Yet, the ensuing energy is dissipated viscously by the membranes. Thus, on a physicochemical point of view, the exocytotic efficiency and dynamics are finely regulated by the membrane properties (resulting from the phospholipidic composition, the mechanical tension, or the cell membrane viscosity) concomitantly to the vesicular matrix role. The situation is akin to a powerful steam engine (here, the matrix) regulated by a Watt's pendulum (here, the membrane) although the operating energy of the latter is much weaker. Moreover, the biological parameters, such as the enzymatic systems, proteins, intracellular calcium concentration, actin cytoskeleton, the nature of the secretagogues classically used, and the cellular machinery that they implied or the biosynthesis of the secretory vesicles, have been evidenced to have a

crucial influence, for example, for the docking stage, but certainly also because they overall tune the membrane viscosities.

In that way, because of the excellent temporal resolution as well as the comprehensive dynamic data provided by amperometry, electrochemical studies have permitted to obtain some important results that were hidden to other techniques (for instance, such as patch-clamp; see section 2.4.) or too much corrupted by noise (local optical probes) to allow a fine understanding at a quantitative level. It must be specified that the works and results dealing with the influence of pure biological parameters on exocytosis rarely involve lone amperometric measurements but use them in addition to other complementary analytical techniques that provide important other information. Yet, because of the scope of this review and the ubiquity of amperometric investigations,[2,19,117] the following sections will be mostly devoted to the reports in which amperometry is the main analytical tool.

2.3.1. pH Dependence of the Exocytotic Release

Because the catecholamines are positively charged due to their nitrogen protonation, the rate of dissociation of the matrix (initially at pH ~5.5 before the ionic exchanges with the extracellular medium) is predicted to increase by imposing higher external pH, that is, by creating a higher pH gradient. Moreover, because the chromogranin A structure is pH-dependent, the external pH is also expected to affect the destructuration of the vesicular matrix. R. M. Wightman et al. showed that this is the case at adrenal chromaffin cells by performing amperometric studies at different extracellular pH values (5.5, 7.4, and 8.2). Although results depend on the secretagogue used to elicit exocytosis, the changes observed in spike size and shape are qualitatively consistent with the interactions between catecholamines and other intravesicular components.[22,77] For instance, because chromogranin A is a dimer or tetramer species at pH 7.5 and 5.5, respectively, exocytosis at acidic pH is clearly slower than at physiological pH, in agreement with the stronger chromogranin aggregation and thus a better binding capacity with the catecholamines and other cations present inside the matrix. Furthermore, frequency of the exocytotic events has been evidenced to decrease at pH 5.5, in line with the annihilation of the pH gradient.

Unfortunately, the results obtained at chromaffin cells are difficult to extend to other cell types, due to differences of compound storage and nature. Thus, amperometric measurements at pancreatic β-cells (release of insulin and 5-HT) evidence that acidic pH as compared to physiological pH (7.4) only affects the insulin release, which thus does not occur at pH 6.4.[118] Indeed, contrary to 5-HT (that is presumably stored in liquid-containing vesicles), vesicular insulin is enclosed as a hexamer unit associated with two Zn^{2+} ions. Therefore, the release of insulin requires the dissolution of the granule, that is, the dissociation of this Zn−insulin complex. The insolubility of the Zn−insulin assembly for pH < 7 totally prevents the exocytotic release of insulin at pH 6.4. In the same way, increasing the extracellular pH from 6.9 to 7.9 (6.9, 7.05, 7.4, and 7.9) induces faster insulin release (narrower insulin spikes) without affecting the amount of insulin released, whereas the same treatments had no effect on 5-HT secretion.[47]

Finally, the external pH dependence of the exocytotic release without any secretagogue has been amperometrically studied at PC12 cells.[119] Thus, decreasing the external pH from 7.4 to 6.8 has been shown to elicit the exocytotic process. It is suggested that extracellular acidosis causes secretion by intracellular acidification.

Internal vesicular pH obviously affects the efficiency of the release by exocytosis as well. For instance, E. N. Pothos et al. evidenced amperometrically at chromaffin cells and enteric neurons that the decrease of the intravesicular pH enhances the uptake of the secretory vesicles.[80] Conversely, using several drugs that block the vesicle proton pumps and thus induce a rise of the intravesicular pH causes a deceleration in the kinetics of exocytosis and a reduction in the catecholamine released content.[120] Indeed, all of the experimental conditions that disrupt the pH gradient limit the exocytotic release. The effects of the disruption depend obviously on the drugs used and the amount of catecholamines released that can be modified while kinetics remain unaffected.[121] As already explained above, the "dense-core" vesicular structure maintains the pH gradient between extra- and intravesicular media. Thus, at pancreatic β-cells that release both 5-HT (the 5-HT secretory vesicles have no dense-core) and insulin (via dense-core vesicles), amperometric measurements showed that only the exocytosis of insulin is significantly affected by the intravesicular pH increase.[47]

2.3.2. Effects of the SNAREs Complexes

The first step of a fusion event between the cell and the vesicular membrane requires an assistance provided by SNAREs (soluble NSF attachment protein receptor) complexes. Their physicochemical role is to counteract electrostatic repulsions between phospholipid head groups when the two membranes approach beyond the distance required for complete double layer screening, viz., enough to molecularly interact. Briefly, vesicle membrane proteins (VAMP/synaptobrevin, named v-SNAREs) link to those of the target cell membrane (SNAP-25 and syntaxin, named t-SNAREs).[3] The progressive tightening of the resulting complex then pulls the two membranes to within angstromic distances of each other,[122,123] so that the electrical field induced locally may raise enough to electroporate both membranes. After fusion, v-SNAREs and t-SNAREs evolve into the fused membrane by forming another extremely stable complex that will be subsequently disassembled to be reused. Although such complexes are not supposed anymore to play any energetic game, they may still play a kinetic role by imposing the local membrane viscosity and curvature and therefore in tuning the rate of full fusion (see eq 7).

The essential role of the SNAREs complexes during the tethering and priming of the vesicles with the cell membrane has been amperometrically confirmed. For instance, fusion is inhibited when SNAREs are cleaved by neurotoxins[124–127] or after modifications on the amino acid sequence of one specific SNARE,[128] both leading to a drastic decrease of the frequency of exocytotic events. Except for viscosity effects, SNAREs assemblies are not expected to intrinsically alter the dynamics of individual fusion events after the initial pore has been formed. Nevertheless, the formation of the SNAREs assemblies involves other regulatory-specific proteins that can significantly affect the bilayer mixing rate and thus the regulatory kinetics of the exocytotic events itself through changes in energy dissipation ability. Such an effect has been shown to depend on the step in which the protein operates,

as for instance, α-SNAP, Csp,[129] munc 18,[92,94,130,131] protein kinase C,[126] or complexin.[132]

2.3.3. Role of the Cell Membrane Physicochemical Properties

The high temporal and spatial resolution of amperometric measurements allowed testing the effects due to insertion of exogenous lipids compounds on the exocytotic events kinetics. For instance, short incubation times with dilute solutions of lyso-phosphatidylcholine (LPC) or arachidonic acid (AA) have been shown to affect the whole exocytotic process at chromaffin cells by supposedly altering slightly the composition of the cell membrane outer leaflet. Indeed, LPC favors the catecholamine release (rate, events frequency, and charge released), while AA disfavors the exocytotic process. The observed kinetic features are consistent with a lipidic fusion pore formation and the physical topological constraints applied to the cell membrane by the presence of LPC and AA diluted in the external leaflet (alterations of the membrane curvature through changes of lipid cone angle).[133] Additionally, similar works at PC12 cells were performed with other phospholipids such as phosphatidylcholine (PC), phosphatidylethanolamine (PE), sphingomyelin (SM), and phosphatidylserine (PS), although at higher incubating doses and exposures.[134] These studies evidenced again that the differences in membrane composition, that is, the localization of the exogenous lipid into the cell membrane (inner or outer cell membrane leaflet) as well as the phospholipids electrical charge, directly affect exocytosis.[134]

2.3.4. Role of the Extracellular Osmolarity

The role of the extracellular osmolarity (315 mOsm under isotonic conditions) on the exocytotic phenomenon has been studied amperometrically at chromaffin cells. Indeed, once its external osmolarity is perturbed, a chromaffin cell will lose (hypertonic extracellular medium) or gain water (hypotonic extracellular medium) to restore a new osmotic equilibrium between its extra- and intracellular medium. Yet, during short times, the cell cannot change its surface membrane area. As a consequence, from a physicochemical point of view, this provokes an alteration of the cell membrane properties (viscosity and mechanical tension), which indirectly results from the cell swelling or shrinking. Amperometric measurements evidenced that exocytosis is drastically favored (frequency, kinetics, and charge released) under hypotonic conditions (200 mOsm),[28,107,135] while hypertonic conditions (630−970 mOsm) tend to inhibit the exocytotic events.[35,135,136] Interestingly, under drastic hypertonic conditions (more than 1000 mOsm), only a few spikes of low amperometric magnitude remain by comparison with isotonic conditions, being suggested to feature the intermediate exocytotic state called "kiss-and-hold" since full fusion is kinetically hampered.[136] All of these results are in agreement with the above model predictions, that is, the cell membrane tension increase (respectively decrease) and its viscosity decrease (respectively increase) when the cell is bathed in a hypotonic (respectively hypertonic) medium, thus modifying the σ/η ratio in eq 7. Concomitantly, modifying the external osmolarity necessarily affects the matrix swelling energy and kinetics. Thus, the experimental results also support the importance of the ionic exchanges between the matrix and the extracellular medium. Indeed, once the matrix surface is in contact with the extracellular medium, catecholamine cations start leaving the matrix, due to the high concentration gradient created. Because of electroneutrality, this flow of cations must be compensated by cation exchanges (H_3O^+, Na^+ vs catecholamines) and water entry from the extracellular medium. For instance, under hypertonic conditions, the higher external ionic strength minimizes electrostatic repulsions. Therefore, this may reduce the ease of fracturation of the compacted matrix, inducing a decrease of the number of exocytotic events and hence disfavoring the release of catecholamines. Both predictions have been observed experimentally.[35,107,135,136]

2.3.5. Effects of the Ionic Extracellular Composition

The works evaluating the effects of the presence of different cations in the extracellular medium toward the exocytotic release are numerous. For instance, increasing the extracellular Zn^{2+} concentration during the secretion of pancreatic β-cells increases the kinetics and decreases the amount of insulin released without affecting serotonin secretion.[47] As already described above, such results are consistent with the internal structure of the secretory vesicles since vesicular insulin is stored as a Zn complex. As a consequence, a Zn^{2+} excess is expected to inhibit the assembly dissociation.[47]

The effects of the presence of some cations as Zn^{2+} or Cs^+ were amperometrically investigated at chromaffin cells and beige mouse mast cells (that store histamine and serotonin in a similar manner than chromaffin cells, that is, by the mean of a protein intragranular complex). The exocytotic process from both types of cells was altered in the same way. For instance, the amount of secretion decreased with the divalent cation zinc but increased with the monovalent cation cesium. Additionally, the maximum current of the amperometric spikes recorded in the presence of Zn^{2+} cations was smaller than those observed with Cs^+ or controls.[40] Those results are consistent with the expected compaction of the vesicular matrix by divalent cations, which thus cross-link negative charges. Conversely, monovalent cations as Cs^+ can not perform such a cross-linking but rather help the vesicular matrix to swell by dislodging the endogenous cations.

The presence of extracellular La^{3+} cations during exocytosis at chromaffin cells induces a striking decrease in the exocytotic events frequency as well as an increase of the kinetics of release of the remaining ones. This is consistent with percolation of trivalent cations into the matrix (strong interactions with the matrix anionic sites), thus causing the decrease of its swelling and its further efficiency.[35] It must be added that similar ionic effects than those reported above were also amperometrically observed on isolated granules of beige mouse mast cells, thus bringing direct support to the above rationalizations.[137]

Yet, the situation is not as simple. For instance, amperometric measurements at PC12 cells evidenced in a particular case (exocytosis evoked by muscarine) that high (1 mM) external La^{3+} or Zn^{2+} concentration blocked the extracellular Ca^{2+} entry, which is essential in triggering the exocytotic mechanisms.[138] More precisely, exocytosis elicited by muscarine triggers the muscarinic receptor activation, the latter stimulating Ca^{2+} release from intracellular stores. Such a release provokes an extracellular Ca^{2+} entry that could be blocked by La^{3+} and Zn^{2+}, thus inhibiting the exocytotic process.

Alterations of the exocytotic release at chromaffin cells by extracellular Na^+ concentration were also reported.[139] The absence of extracellular Na^+ ions increases the amount of catecholamines released as well as fastening the kinetics of the whole process. Additional cytosolic calcium measurements showed that Na^+ cations also contribute to a Na−Ca exchange, the latter influencing the local cytosolic Ca^{2+} signal responsible for the catecholamines release.

Influence of lanthanide trivalent cations (La^{3+}, Ce^{3+}, and Pr^{3+}) on Ca^{2+} channels during catecholamine secretion in PC12 and chromaffin cells was also reported.[140] Amperometric measurements then evidenced that replacing Ca^{2+} with La^{3+} or other lanthanide ions supported exocytosis in divalent ion-free solution. Moreover, La^{3+} cations have been evidenced not to entry into the cytoplasm, while the lanthanide efficacy seems to depend on ionic radius ($La^{3+} > Ce^{3+} > Pr^{3+}$). Globally, those results are consistent with a size-selective binding interface of trivalent cations at the L type voltage-gated Ca^{2+} channel (VGCC) pore. As a consequence, occupancy of the channel pore by an impermeable cation would lead to a conformational change that is transmitted to the exocytotic machinery upstream of intracellular cation build-up (intracellular Ca^{2+} concentration).

2.3.6. Effects of the External Temperature

For experimental convenience, the majority of amperometric studies on exocytotic processes are performed at room temperature (22−25 °C) and thus not under physiological conditions (37 °C). Nevertheless, several works were designed to evaluate amperometrically how the external temperature affects the efficiency of the whole process. Then, increasing the external temperature from 21 to 37 °C has been shown to significantly affect the exocytosis of mast and chromaffin cells.[40]

More particularly, kinetics have been evidenced to be faster, the amount of catecholamines released increasing at higher temperature.[40,141] The frequency of the events also increases when the temperature is raised from 22 to 37 °C. The effects are reversible; the basic cell functions observed at room temperature are not altered afterwhile. This suggests that the temperature dependence of the biosynthesis of catecholamines does not prevail in this case. Actually, the temperature seems to essentially affect the dissociation rate of the vesicular content, that is, the swelling of the matrix.[40,141,142] From a thermodynamical point of view, the intravesicular polymer matrix storing the catecholamines content in chromaffin cells should be more disordered as temperature increases, due to magnification of entropic contributions. This is expected to enhance the exocytotic release efficiency by allowing an easier swelling.

Furthermore, the external temperature can play significantly on the physical properties of the cell membrane as well as the phospholipid molecules forming the fusion pore.[81] From this point of view, a higher temperature is expected to decrease the membrane viscosity, therefore contributing to a higher efficiency of the exocytotic events.

2.3.7. Other Modifications of the Extracellular Environment

Alterations of exocytosis by weak bases were performed at chromaffin cells. For instance, methylamine, amphetamine, or tyramine have been evidenced to induce exocytotic release by allowing the vesicles to trigger their own exocytosis (by disrupting some granules after the amine entry into the cytoplasm, therefore increasing the intracellular Ca^{2+} concentration).[143] Conversely, hydrazaline (a weak base that is an antihypersensitive agent) does not seem to evoke exocytosis but rather slows down the rate of catecholamine exocytosis by reducing the amount of catecholamines released. This weak base seems to accumulate within secretory vesicles and to interfere with the storage of catecholamines.[144]

The effects of hypoxia on exocytosis were also investigated. Thus, amperometric studies on PC12 cells showed that hypoxic conditions (PO_2 = 11 mmHg) can elicit the catecholamines release without using any subsequent secretagogue. This result is consistent with an increased activity of voltage-gated Ca^{2+} channels, leading to an increased Ca^{2+} influx.[119,145]How hypoxia affects the exocytotic process has also been studied at intact neuroepithelial body cells (release of serotonin) in rabbit lung slices.[146] Similar conclusions were then obtained, that is, exocytosis evoked by hypoxia implies specific Ca^{2+} channels.

The effects of nitric oxide ($NO^{\bullet}$) on the late phase of exocytosis have been amperometrically studied on chromaffin cells.[147] Acute incubation of the cells with $NO^{\bullet}$ or $NO^{\bullet}$ donors has been evidenced to exacerbate the exocytotic release, whereas the converse result is obtained after a treatment with $NO^{\bullet}$ scavengers or NO synthase inhibitors. No clear explanation exists up to date. It is suggested that $NO^{\bullet}$ does not interfere with fusion pores but modifies the affinity of catecholamines toward the intravesicular matrix, although the mechanism is unclear.[147]

Finally, acute effects of toluene on vesicular catecholamine release from PC12 cells have been amperometrically investigated in toxicological studies. As compared to a K^+ depolarization-evoked secretion, toluene causes an increase in release frequency, although the kinetics and amount of dopamine released are unchanged. However, these effects are difficult to rationalize since the toluene-induced exocytosis mechanism is likely to be nonspecific.[148] Nevertheless, exocytosis evoked by toluene may depend on the influx of Ca^{2+} through voltage-activated Ca^{2+} channels, so the effect would be linked to an indirect increase in intracellular Ca^{2+} concentration.

2.4. Coupling between Amperometry and Other Analytical Techniques

2.4.1. Other Techniques that Afford Detection with Real-Time Resolution

Real-time information about the exocytotic phenomenon can be obtained by two other important analytical techniques. These measurements (based on fluorescence or capacitance variations) obviously give access to complementary data by comparison with those provided by amperometry.[73,117,149,150]

Patch-clamp measurements allow the recording of the cell membrane surface variation since, upon assuming invariant composition of the resulting double layer, the cell membrane capacitance is directly proportional to its own surface. As a consequence, because each vesicle fusion increases the cell membrane surface, each exocytotic event is depicted as a capacitance step during the time course of the exocytotic release. Practically, a patch of cell membrane is sealed ohmically at the tip of a micropipette ("cell-attached" mode; see Figure 8A). For instance, two different configurations can then be used. The patch can be isolated from the cell

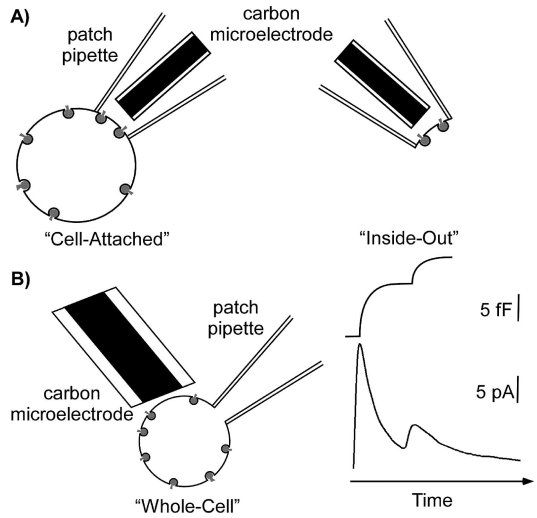

Figure 8. Schematic representation of the three main patch-clamp/amperometry combinations. (A) Left, picture of the cell-attached configuration/amperometry device; right, picture of the inside-out configuration/amperometry device. In both cases, the carbon fiber microelectrode that allows the amperometric detection is located inside the patch pipet. (B) Left, picture of the whole-cell configuration/amperometry device; right, schematic example of temporal correlation between capacitance and amperometric recordings.

("inside-out" configuration in which the extracellular side of the patched cell membrane faces the internal medium of the pipet; see Figure 8A). Alternatively, the patch can be broken, thus creating a hole in the plasma membrane and allowing contact between the pipet solution and the intracellular medium ("whole-cell" configuration in which the whole cell membrane is immobilized at the tip of the pipet; see Figure 8B). By comparison with the amperometric monitoring, the capacitance measurements afford detection of both exocytotic (fusion between vesicle and cell membranes) and endocytotic (cell membrane retrieval that counteracts the cell membrane increase by exocytosis) events. Additionally, exocytotic events implying empty vesicles (obviously amperometrically silent) can be detected. Conversely, no data dealing with the vesicular content may be provided, and as the amperometric detection, investigation of the dynamics of the exocytotic process from individual vesicles is achieved once the fusion event onsets. Furthemore, the exocytotic events can not be localized at the cell membrane surface.

Fluorescence techniques allow visualizing or recording intracellular changes. For example, the fluorescence imaging or monitoring of Ca^{2+} intracellular concentration involves a probe (Indo-1, Fura-2, Fluo-3...) whose fluorescent properties depends on its binding with the free Ca^{2+} cations, so changes in fluorescence activity ensues from calcium release. More particularly, optical techniques based on fluorescence microscopy allow visualizing the different stages (displacement, docking and fusion) of vesicles during the exocytotic process. Owing to the fluorescent probe supramolecular binding properties, specific probes may be targeted to selected bodies of a cell. For instance, FM 1−43 is a fluorescent dye whose fluorescence is high when bound to membranes and low in aqueous medium; green fluorescent proteins (GFP) are localized into the granule matrix, *etc*. Furthermore, evanescent wave fluorescence microscopy allows the detection in the vicinity of the cell membrane ($\sim$ 100 nm). As a consequence, the traffic of secretory vesicles that eventually undergo fusion may be performed in real-time. Nevertheless, this technique is generally used for interrogating the status of the vesicles before and during fusion and not on the exocytotic event itself. All these methods rely on a specific decrease of the light noise so that the signal-to-noise ratio increases, though the signals remain too weak to allow precise kinetic investigations.

2.4.2. Coupling between Amperometry and Capacitance Measurements

The first combination between capacitance measurements and amperometry at carbon fiber microelectrodes was introduced 15 years ago for investigating exocytosis at chromaffin and beige mouse mast cells.[68,74] In these studies, the patch-clamp measurements were performed in the whole-cell configuration (Figure 8B), and a microelectrode was present outside the micropipette. Correlation between the amperometric spikes and changes in the cell membrane capacitance thus allows one to obtain comprehensive information (frequency, kinetics, and cell membrane variation) on the release process. Although several problems are intrinsic such as a possible delay between the amperometric and the capacitance recordings,[26,41,151] this experimental combination is henceforth very popular.[87,152–155] Simultaneous amperometric and patch-clamp recordings allowed significative improvements on experimental monitoring of the fusion pore formation and its evolution.[73] Other contributions of interest are miscellaneous. For instance, the coupling between both techniques has been evidenced to accurately estimate the endocytosis/exocytosis ratio (Successive exocytotic events induce an increase of the cell membrane surface area as well as its composition modification. To keep globally constant the cell membrane surface area, endocytotic processes concomitantly occur. Endocytosis deals with the formation of empty vesicles from the cell membrane).[156,157] In mouse pancreatic β-cells, capacitance measurements evidenced two major exocytotic modes, in which the slowest one only was accompanied by amperometric events. Amperometric spikes could then be kinetically classified in two groups, leading to the conclusion that several exocytotic pathways with divergent fusion kinetics occur in β-cells.[158] Furthermore, a detailed comparison of capacitance and amperometric measurements in bovine chromaffin cells was attempted by comparing the experimental amperometric signals with generated amperometric spikes from a given measured capacitance increase through Monte Carlo simulations.[23]

Whole-cell capacitance measurements reflect the surface changes due to exocytosis on the total cell membrane, while amperometric detection is spatially limited to an electrode surface that only covers a portion of the cell surface. This problem can be prevented by achieving such measurements with the "inside-out" or "cell-attached" modes, upon which the carbon fiber microelectrode is inserted into the patch pipet (Figure 8A).[96,97,159] By comparison with the "whole-cell" experiments, both configurations enhance the capacitance measurements resolution, thus allowing studies of "kiss-and-run" events (i.e., those in which secretory vesicles fuse transiently with the plasma membrane before they are internalized and before the full-fusion step may occur),[160] the refinement of the fusion pore analysis,[98] or investigations on the process by which vesicles adapt their membrane area as a function of the alteration of their catecholamines content.[161] Nevertheless, a distortion of the amperometric spikes shape can not always be avoided, since the control

of the distance between the electrode and the patched cell membrane remains difficult. Indeed, the relatively large distance of the carbon electrode from the patch can provoke a diffusion broadening of the spikes morphology.[96,97,159]

2.4.3. Combination of Fluorescence Microscopy and Amperometry

Direct combination of the amperometric recordings with intracellular Ca^{2+} concentration measurements by fluorimetry is now common and has unambiguously established the correlation between the exocytotic phenomenon and the increase of the Ca^{2+} intracellular concentration.[22,43,121,162–164] Moreover, fluorescence imaging of Ca^{2+} intracellular concentration may also be coupled with amperometry. Notably, at chromaffin cells, using etched electrodes proved that the fluorescent Ca^{2+}-"hotspots" (or partial rings found immediately beneath the plasma membrane) are colocalized with the zones where the catecholamines are released.[100] Similarly, association of amperometry and confocal microscopy with Zinquin (a fluorogenic Zn^{2+}-specific indicator) was used for spatially and temporally coupled measurements of Zn^{2+} efflux and insulin release from single pancreatic β-cells. Once again, using etched electrodes provides the correlation between the insulin release and the Zn^{2+} flux sites.[103] Additional attempts were performed to improve the convenience of the combination, that is, by achieving amperometric and fluorescence measurements using the same sensor. To do so, fabrication of a dual microsensor was achieved to simultaneously detect Ca^{2+} and catecholamines from individual chromaffin cells. In that case, calcium green-1 dextran was used as the fluorescent dye being linked to the tip of a carbon fiber electrode by cross-linking with 5% glutaraldehyde.[165]

In all of the above combinations, the fluorescence measurements dealt with the detection of divalent cations (Ca^{2+}, Zn^{2+}) through specific molecular probes. To correlate the fusion zones and the subsequent release of vesicles, amperometric and FM1-43 fluorescence measurements were performed at pancreatic β-cells. In the presence of FM1-43, once the cell undergoes exocytosis, the increase in membrane area induces uneven fluorescence increases around the surface of the cell. By means of etched electrodes, amperometric spikes could then be recorded only at strong fluorescent zones whereas cell regions that gave small increases in membrane fluorescence led to no amperometric detection.[102]

Works that couple a fluorescence imaging of the fusing vesicles with a good amperometric resolution have still not been reported. Currently, two methodologies seem to pave the way for such a combination. First of all, M. Lindau and colleagues reported the microfabrication of electrochemical detector arrays that consist of four platinum microelectrodes on a glass coverslip (Figure 9A).[166] As a consequence, four cell membrane exocytotic zones can be simultaneously recorded amperometrically. Furthermore, concomitant fluorescence imaging of release of acridine orange (a dye that accumulates in acidic compartments at high concentrations) from individual vesicles confirmed the electrochemical position assignments. Indeed, fluorescence flashes could be spatially correlated with the position of individual release events (determined after random walk simulations from the fraction of catecholamines recorded by the individual electrodes).[166] A different strategy involves the simultaneous observation of fluorescence and amperometric measurements of exocytosis by single adrenal chromaffin cells on transparent ITO (indium tin oxide) microelectrodes (Figure 9B).[167] Thus, glass slides were coated with a film of ITO (500 nm thickness). Micrometric disk surfaces of ITO were delimited by photolithography, affording transparent surfaces of 40−100 μm diameter. On such micrometric surfaces of ITO, the amperometric detection of the exocytosis at single chromaffin cells could be achieved with a high signal/noise ratio, while fluorescence observation (where acridine orange is the fluorescent probe) of exocytotic release was simultaneously performed on the same support.

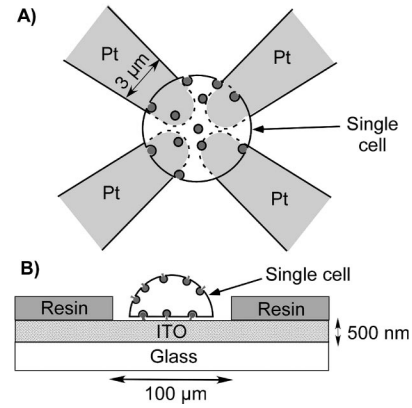

Figure 9. (A) Scheme of a cell releasing neurotransmitters and locating on electrochemical detector arrays (adapted from ref 166) consisting of four platinum microelectrodes on a glass coverslip. The present scheme depicts the cell upper view. Note that the exocytotic events drawn in the scheme (black circles) occur under the bottom of the cell. (B) Representation of a secreting cell (exocytotic events are depicted as black circles) that is adhered onto a transparent ITO microelectrode device (adapted from ref 167).

2.5. Conclusions and Perspectives

Nowadays, methods of microelectrodes fabrication have extensively been improved.[53,71,168,169] Nevertheless, although amperometry at carbon fiber microelectrodes remains a very powerful tool, further improvements are currently required to go further along the detection and analysis of biological phenomena as exocytosis. In that sense, many works deal with modifications of the nature as well as the localization of the electrochemical sensor. For instance, K. D. Gillis et al. have reported the amperometric detection of the release of catecholamines by chromaffin cells on electrochemical detectors (Au-SiO_2) in picoliter-sized wells.[170] It must be emphasized that each well-electrode conforms to the shape of the cell to capture a large fraction of released catecholamine (Figure 10A). Subsequently, combination of amperometric recording on the chip with patch-clamp recordings of membrane capacitance (whole-cell configuration) can be performed.

Moreover, a microchip device that uses transparent ITO electrodes in microfluidic channels has been developed to measure exocytosis from chromaffin cells (Figure 10B).[171] Unfortunately, only amperometric measurements relative to a cell population could be achieved. Nevertheless, this configuration has been extended to the development of transparent microchip devices that enable photorelease of caged Ca^{2+}, together with electrochemical detection of catecholamines secretion from cell arrays or individual cells and concomitant fluorescent measurements of intracellular Ca^{2+}.[172]

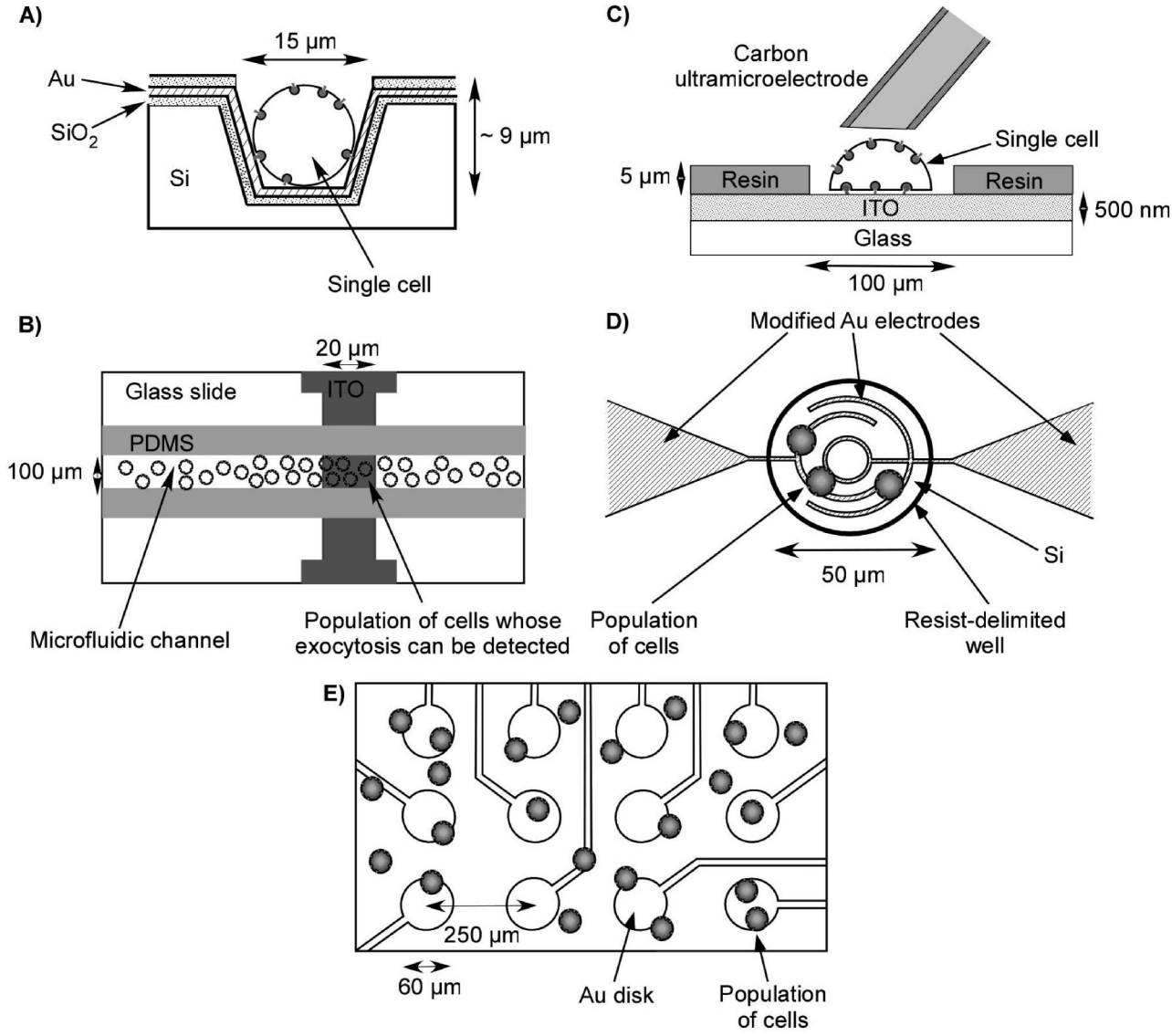

Figure 10. Schematic representations (dimensions are not to scale for more clarity) of micrometric devices used for amperometric measurements of exocytosis. (A) Detection of neurotransmitter release of a single cell on Au-SiO_2 electrodes in picoliter-sized wells.[170] (B) Detection of neurotransmitter release by a cell population on an ITO electrode-incorporated microchip device.[171] (C) Detection of neurotransmitter exocytosis of a single cell located into a well on the transparent ITO microelectrode.[167] Basal exocytotic events are detected at the ITO electrode, while apical events can be monitored by positioning a carbon fiber microlectrode at the apex of the cell.[173] (D) Detection of exocytosis of one or a few cells on a circular interdigitated structure of mercaptopropionic acid-modified gold electrodes.[174] (E) Detection of exocytosis of a cell population on a MEA-integrated biochip.[176]

As already described above, simultaneous amperometric detection and visualization of the exocytosis at a single chromaffin cell positioned in a well on transparent ITO microelectrode have been reported (Figure 9B).[167] Contrary to the usual studies performed with a carbon fiber microlectrode, exocytotic events are thus detected at the basal pole of a single cell. Thus, beyond the potential coupling with fluorescence techniques, this configuration allows the comparison of two active zones (apical and basal with both a carbon fiber and a ITO electrodes, respectively; see Figure 10C) with the same technique, indicating that the efficiency of the whole process strongly depends on the particular pole of secretion.[173]

Furthermore, C. Spégel et al. achieved the determination of dopamine exocytosis at PC12 cells by using mercaptopropionic acid-modified gold electrodes (MPA prevents the dopamine polymerization resulting from the electrochemical detection).[174,175] In this work, a microchip has been developed for monitoring the release of dopamine by one or a few cells (Figure 10D). Once again, analysis of exocytotic events is performed at the basal pole of the cell.

As already mentioned above, the detection of exocytosis at the single cell level by means of a four platinum microelectrodes detector was reported by M. Lindau and coworkers (Figure 9A). Basal exocytosis from a single chromaffin cell positioned on top of the array was detected by the four individual electrodes with a low noise. As a consequence, the localization of individual release events is determined from the fraction of catecholamines recorded by the individual electrodes. Additionally, the electrochemical position assignments were confirmed by concomitant fluorescence imaging of release from secretory vesicles.[166]

Eventually, a biochip integrating a MEA was elaborated by H. F. Cui et al. to detect exocytosis from dopaminergic cells, as MN9D cells (Figure 10E).[176] This biochip involved a silicon-based 5×5 array of Au disk microelectrodes (from 10 to 90 μm diameter). This device does not currently allow a detection at the single cell level, the amperometric signals

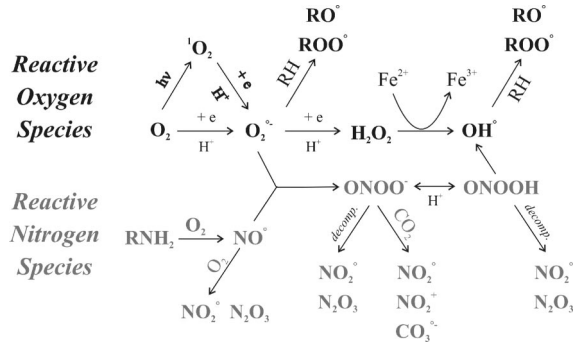

Figure 11. Main reactive oxygen species (ROS) and reactive nitrogen species (RNS) derived from the biological conversion of oxygen into superoxide ion ($O_2^{\bullet -}$) and nitric oxide ($NO^{\bullet}$).

arising from a cell population that adheres randomly to each Au pad. However, it must be added that in this work, the cell line could be grown on the surface of the biochip chamber, showing the biocompatibility of the device.

Additionally, some works report on the implementation of carbon-fiber microelectrodes in a scanning electrochemical microscope to combine topographical and electrochemical studies on the release processes by cellular organisms, particularly exocytosis at chromaffin or PC12 cells. This should allow examination of topographical data about the regions of interest on the cell membrane that are further spatially addressed with the microelectrode.[177–180]

3. Monitoring Oxidative Stress at Single Living Cells

3.1. Introduction

3.1.1. Oxidative Stress Processes

Oxidative stress is a hazardous metabolic situation encountered or controlled by aerobic organisms during their whole life. Aerobic organisms derive ultimately most of their energy from the controlled oxidation of fat and sugars via oxygen-atom transfer catalyzed by metalloenzymes. Also, these metalloenzymes are central actors of the respiratory chain in mitochondria. However, the same enzymes are generally good reducing agents, prone to open a side route in activating dioxygen (the yield may range from a fraction of a percent to a few percent) leading to oxygen reduction into superoxide ion ($O_2^{\bullet -}$). Superoxide is the precursor of a whole series of hazardous species for living systems, coined the "reactive oxygen species" (ROS; see Figure 11).[181–184]

At physiological pH, superoxide ion is readily scavenged through its second-order disproportionation ($k = 2 \times 10^5$ M^{-1} s^{-1}, $T = 25$ °C, pH 7.4) into hydrogen peroxide and oxygen. This may be even more rapid in living cells when catalyzed ($k = 2 \times 10^9$ M^{-1} s^{-1}, $T = 25$ °C, pH 7.4) by superoxide dismutases (SOD) (eq 9):

$$2O_2^{\bullet -}(+ 2H^+) \rightarrow H_2O_2 + O_2 \qquad (9)$$

Two main types of SOD are present in mammalian aerobic cells: a Mn-based enzymatic center form (Mn SOD) located in mitochondria and a Cu/Zn-based form (Cu/Zn SOD) located in cytoplasm, in specific granules and possibly in membranes.[185–191] These enzymes are prone to protect cells from superoxide oxidation of R−H bonds, although this reaction is generally slow, and also from the reaction of superoxide with other radicals such as nitric oxide that may generate more hazardous compounds (Figure 11 and explanations below).

H_2O_2 formed by $O_2^{\bullet -}$ disproportionation is an even more potent cytotoxic chemical than superoxide since its lifetime is sufficient to allow its diffusion to almost any cellular compartment, where it may act as a potential source of hydroxyl radicals $OH^{\bullet}$ (Figure 11) through the Fenton reaction. Yet, this requires the presence of iron(II) free ions or metalloenzymes.[182,183] Hydroxyl radicals being among the best hydrogen atom acceptors, they are prone to induce a large variety of biological modifications among which the peroxidation of cell membrane bilipids through the Haber−Weiss reaction of proteins, DNA bases, and backbone oxidation or hydroxylation.[182,183,192]

In living cells, H_2O_2 is scavenged primarily by catalase and second by peroxidases (glutathione peroxidase), which catalyze, respectively, its fast disproportionation into oxygen and water or into oxidized organic substrates and water, so that its concentration is usually maintained at nanomolar steady-state levels, preventing from the lethal routes mentioned above.[181,193–196] However, catalase and peroxidases are inhibited by their substrate, viz. at high concentrations of hydrogen peroxide (typically a few tens to a few hundred millimolars).[197,198] Thus, aerobic cells might remain unprotected against H_2O_2 and other ensuing ROS whenever their concentrations rise rapidly at levels significantly beyond normal physiological ones.

Besides, the production of superoxide and others ROS may not only result from side routes of the normal oxidative or energetic metabolism of cells. Specific processes are used on purpose by many cell types for communication, for the control of redox-sensitive mechanisms (gene expression) leading eventually to the controlled cell death by apoptosis or for defense against xenobiotics (bacteria, virus, etc.), for example, as in the case of phagocytes (macrophages and neutrophils). Several aerobic cells may change their normal oxygen metabolism so as to produce deliberately important quantities of superoxide and ROS through the involvement of specific enzymes such as NADPH oxidases, which catalyze the following reaction (eq 10):[199–203]

$$2O_2 + NADPH \rightarrow 2O_2^{\bullet -} + NADP^+ + H^+ \qquad (10)$$

NADPH oxidase (from the NOX family) activity is of particular importance in the phagocytosis of bacteria and viruses by macrophages or neutrophils, the bactericidal activity being provided essentially by the ROS (and RNS, see below).

However, uncontrolled excess of ROS production by active or passive mechanisms amplifies cell damages over long periods of time. These damages might be prevented by enzymes (SOD, catalase, and peroxidases mentioned above), which are aimed to wipe out the ROS excess, and soluble antioxidant molecules (vitamins, glutathione, and uric acid, etc.) or repaired by specific enzymes (DNA repair systems, lysosomes fusion for membrane repair, etc.). Nevertheless, this may be out of control leading to a critical situation termed "oxidative stress". This basically describes an acute or chronic imbalance between the production of ROS and the antioxidant and repairing capacities of living cells and organisms. Oxidative stress processes are suspected to be involved directly or indirectly (apoptosis) in many human pathologies (aging, cancers, Parkinson and Alzheimer diseases, autoimmune pathologies, arthritis, etc.). Over the last three decades, this has prompted a very large number of

research groups from several disciplines of biology and medicine to investigate the different stages of oxidative stress.

Current research in this domain has established that the imbrication of ROS metabolism with that of nitric oxide ($NO^{\bullet}$) in oxidative stress is general and appears ubiquitous in many physiological or pathological situations. Nitric oxide (more properly nitrogen monoxide) displays very different effects (positive or negative) in organisms as a function of its concentration and of the local conditions prevailing in vivo. $NO^{\bullet}$ mostly originates from the activation of a class of enzymes, the NO synthases (three different mammalian types, plus a supposed mitochondrial form), which catalyze its formation along two steps (eqs 11 and 12):[204–207]

$$\text{L-arginine} + 1\text{NADPH} + O_2 \rightarrow \text{N}^{\omega}\text{-hydroxy-L-arginine} + 1\text{NADP}^+ + H_2O \quad (11)$$

$$\text{N}^{\omega}\text{-hydroxy-L-arginine} + 0.5\text{NADPH} + O_2 \rightarrow NO^{\bullet} + \text{L-citrulline} + 1.5\text{NADP}^+ + H_2O \quad (12)$$

Nitric oxide is a weak oxidant by itself and alone does not cause oxidative stress. In fact, it is at most a weak reductant associated with the strong oxidizing species NO^+.[208] Nevertheless, it reacts extremely fast with paramagnetic species, so whenever $O_2^{\bullet -}$ and $NO^{\bullet}$ are produced in the same cell environment or in closely related ones, they may couple at a rate close to the diffusion limit ($\sim 3-19 \times 10^9$ M^{-1} s^{-1}, eq 13)[208–210] to form the potent peroxynitrite anion:

$$O_2^{\bullet -} + NO^{\bullet} \rightarrow ONOO^- \quad (13)$$

Peroxynitrite is reported to be the source of many oxidative, nitrating, or nitrosating processes involving several cell components and has therefore been the focus of broad research over the past decade. At physiological pH, peroxynitrite may decompose through the intermediate formation of its conjugated acid ONOOH ($pK_a \approx 6.8$),[211–215] which undergoes two facile decomposition routes. One goes through the formation of the very reactive radicals $NO_2^{\bullet}$ and $OH^{\bullet}$ and is considered as biologically feasible, especially in nonpolar environments (e.g., membranes) where the lipophilic ONOOH species may accumulate spontaneously. Besides, peroxynitrite anion $ONOO^-$ may react in biological conditions with carbon dioxide (overall constant $k = 3-6 \times 10^4$ M^{-1} s^{-1}).[214,216–218] This mechanism competes with the direct decomposition of $ONOO^-$ since CO_2 concentration in vivo is quite high (12−30 mM in blood). It appears that a significant fraction of the short time living species $ONOOCO_2^-$, forming along this process, ends up into the potent nitrating and caboxylating radicals $NO_2^{\bullet}$ and $CO_3^{\bullet -}$.

Similarly, when diffusing over significant distances from its source, $NO^{\bullet}$ is expected to react significantly ($k = 2 \times 10^6$ M^{-1} s^{-1})[219,220] with oxygen (eq 14) although more slowly than with superoxide. Yet, this species is present at rather important concentrations (ca. 0.23 mM in air saturated physiological solutions) in extracellular fluid or in blood:

$$4NO^{\bullet} + O_2 + 2H_2O \rightarrow 4NO_2^- + 4H^+ \quad (14)$$

The side reactions of nitric oxide oxidation may form species such as $NO_2^{\bullet}$ and N_2O_3, which are also very efficient nitrating and nitrosating compounds. Finally, although the in vitro decomposition of nitric oxide and peroxynitrite leads ultimately to a combination of the very stable nitrite and nitrate ions. Depending on nitric oxide concentration in vivo, these ions may accumulate in cells and their environment. Such processes may then generate very reactive intermediates such as $NO_2^{\bullet}$, N_2O_3, or NO^+, suspected to be at the origin of nitrated, nitrosated derivatives of amino acids, thiols, and other important biological components.

The existence of such a series of complex and intricately interconnected pathways, which necessarily follow any simultaneous production of superoxide and nitrogen monoxide by living cells, explains why determining the very nature of the ROS and/or RNS compounds and quantifying them has not yet been fully characterized in the majority of oxidative stress processes. The origin and mechanism of these processes have been mostly hypothesized based upon the observation of cell metabolites (requiring hours to years to appear) or biological cascades triggered by specific effects on cellular activation mechanisms such as gene expression (hours or days). Despite the apparent ubiquity and importance in aerobic cells of the ROS and RNS, few analytical methods have been developed to monitor directly their production by living cells, that is, for investigating the processes at the very origin of oxidative stress and henceforth primarily responsible for its severe consequences. As for the investigations on the exocytotic release, electrochemistry on microelectrodes became a method of choice in this regard during the last 15 years because of the electroactivity of several important ROS and RNS, as discussed below. We wish to report in the following an overview of the studies that have demonstrated at the single cell level or in some cases on a small group of cells, the range of applications of electrochemical measurements of oxidative stress processes.

3.1.2. Electroactive Species Implicated in Oxidative Stress

The ability of the electrochemical methods to detect in biological conditions some of the ROS and RNS mentioned above (or presented in Figure 11) obviously depends on two main factors: the half-wave potential of the redox couple involving a given ROS or RNS and the time-life of this compound when produced by a living cell, since this latter commands its permanence and diffusion into cells or tissues and eventually toward the electrode surface. Moreover, the ultimate goal here being the analysis on single aerobic living cells, measurements must be conducted in aqueous medium (buffer) in the presence of oxygen (solutions in equilibrium with normal atmosphere). As already mentioned previously, this condition mostly precludes the use of the reduction domain for electrochemical analyses since the reduction of oxygen takes place at low reductive potentials on most electrode surfaces [e.g., −0.1 V vs SCE (saturated sodium calomel electrode) on platinum microelectrodes], while oxygen concentration in the close environment of the cell may vary during oxidative stress processes due to its consumption. Thus, a direct reductive analysis of any other electroactive species would be generally convoluted with oxygen detection although this has been neglected in many reports pretending to detect superoxide. The reductive detection may then only be used through indirect processes via the recycling of a mediator oxidized at the electrode surface at low potentials. Examples of such mediated detections of RNS are described in section 3.3 of the review.

Hydroxyl radical $OH^{\bullet}$ is among the most reactive radical found in biochemistry since it can abstract a hydrogen atom from any C−H bond. This species is thus definitively not able to diffuse anywhere from its generation point in the cell, and particularly toward an electrode surface without

reacting with other molecules, such as the cell membrane constituents. The eventuality of its detection would require positioning the electrode surface at a nanometric distance from its source, which is out of our present experimental limits in electrochemistry at living cells. In agreement, to our best knowledge, the direct electrochemical detection of hydroxyl radicals in vivo has not yet been reported.

The nitrogen dioxide $NO_2^{\bullet}$ time life is reported to be significantly longer under biological conditions than that of hydroxyl radical (microsecond domain vs nanosecond domain, respectively). This would be compatible with a direct electrochemical detection although it would represent an analytical challenge. Furthermore, the standard potential of the redox couple for the oxidation of $NO_2^{\bullet}$ into NO_2^{+} has been measured as $E^{\circ\prime}(NO_2^{+}/NO_2^{\bullet}) = +1.56$ V vs NHE,[208,209,221,222] which imposes high potentials close to the water oxidation wall. These conditions strongly limit the probability for a direct detection of $NO_2^{\bullet}$ through its oxidation, and to the best of our knowledge, such results have not been reported so far into biological conditions.

Conversely, the primary radical species that lead to the complex family of ROS and RNS, that is, superoxide and nitric oxide, are certainly more "easy" targets for their electrochemical detection by oxidation. Moreover, detecting the primary species of oxidative or nitrosative stress is of large interest for understanding the initiation steps of these processes. The thermodynamic data providing the following standard potential of the redox couple for the oxidation of $NO^{\bullet}$ [$E^{\circ\prime}(NO^{+}/NO^{\bullet}) = +1.21$ V vs NHE] and a standard potential of the redox couple for the oxidation of $O_2^{\bullet-}$ [$E^{\circ\prime}(O_2/O_2^{\bullet-}) = -0.33$ V vs NHE] do not preclude a priori their detection.[208,209,221] From a kinetic point of view, the life span of each of these primary species strongly depends on the local conditions in cells for their production. Nitric oxide at nano- to micromolar local concentrations may diffuse over micrometric distances, and its detection in the extracellular space is thus feasible. Moreover, the high lipophilic character of $NO^{\bullet}$ and the slight lipophilic character of $O_2^{\bullet-}$ allow their diffusion through cell membranes and henceforth their detection by a microelectrode placed outside the cell, provided that the diffusing fluxes are sufficient to be monitored with a sufficient signal/noise ratio. Besides, the possibility that these species can be produced by enzymatic systems located in cell membranes, such as the NADPH oxidases (NOX family) for superoxide and constitutive NO synthases for $NO^{\bullet}$, has to be considered. Under such conditions, the distance between the two sources should minimize direct reactions between $NO^{\bullet}$ or $O_2^{\bullet-}$, thus providing a better probability for their observation.

Several other neutral or anionic ROS and RNS are also good candidates for their detection and the characterization of oxidative or nitrosative stress at living cells. Concerning ROS, hydrogen peroxide is probably the most stable compound among this family of species albeit its reputation. Its lifetime in vivo depends essentially on its possible reaction with free metallic ions such as iron(II) or catalase present in the medium. The redox potential of its couple [$E^{\circ\prime}(H_2O_2/O_2) = -0.146$ V vs NHE] makes it a good candidate for direct detection on cells. Nitrite anion is also a very stable compound in vivo, and the redox potential of its couple [$E^{\circ\prime}(NO_2^{\bullet}/NO_2^{-}) = +0.99$ V vs NHE] is compatible with direct electrochemical oxidation. Nitrite anions are essentially the end products of nitric oxide metabolism and are classically used as an indirect marker of oxidative or nitrosative stress with the problem that its basal levels may be quite high. Nitrate anions are extremely difficult to oxidize [$E^{\circ\prime}(NO_3^{\bullet}/NO_3^{-}) = +2.50$ V vs NHE] in the absence of an enzymatic transducing system and are also stable end products of RNS.[208,209,221] Then, these two compounds did not stimulate much interest for their direct analysis on single cells. Conversely, the most intermediate and reactive species, peroxynitrite (both anionic and acidic form), is a proper target for electrochemical measurements. Other methods reported in the literature for peroxynitrite detection are rooted on fluorimetric and chemiluminescence analysis although they are indirect and not very selective.[223–226] Quantization and kinetic profiles of species release by single cells or a small population are also impossible by such methods. In contrast, electrochemistry at microelectrodes offers the considerable advantage of a direct and local detection of peroxynitrite at the single cell level. The basic form $ONOO^{-}$, the major one in aqueous media at physiological pH, is the best candidate for analysis since its formal redox potential is quite low [$E^{\circ\prime}(ONOO^{\bullet}/ONOO^{-}) = +0.20$ V vs NHE], making its direct oxidation possible. The acidic form ONOOH is a priori only reducible at potentials lower than -1 V.[227] Besides, the overall decomposition kinetic of peroxynitrite is in the subsecond range.[208,209,221,228] Consequently, considering an electrochemical sensor positioned close to the cell source of peroxynitrite, that is, under some conditions equivalent to the ones used for $NO^{\bullet}$ or $O_2^{\bullet-}$detection (actually the species that lead to $ONOO^{-}$ and ONOOH), it may be possible to detect and monitor peroxynitrite before it reacts with its biological targets or before its spontaneous decomposition.

3.1.3. Electrode Surface Modifications for the Selective Detection of Specific ROS and RNS

Among the different species mentioned above, several of them are oxidizable at bare surfaces of carbon (carbon fiber), platinum, or even gold, although in this latter case the usable range of potentials in oxidation is rather limited (typically below 0.4 V vs Ag/AgCl). First, the primary species of oxidative stress, $NO^{\bullet}$ or $O_2^{\bullet-}$, can be detected at the usual bare microelectrode surfaces, platinum and carbon. This property was used initially for in vitro purposes but also in the first attempts of detection at living cells, as shown in the different examples of application below. Apart from kinetic considerations that determine the lifetime of a species such as superoxide, as detailed above in section 3.1, $O_2^{\bullet-}$ is thermodynamically oxidizable at low potentials, typically +0.1 V vs Ag/AgCl at carbon fiber microelectrodes.[229,230] This feature is advantageous since it precludes easily from the simultaneous detection of oxidizable interferences that can be found in biological media (uric acid, ascorbic acid, etc.). Despite, many groups have developed more sophisticated sensors to obtain a high selectivity of detection for superoxide. This subject was recently reviewed by M. Yuasa and K. Oyaizu[231] who distinguished sensors modified with either a protein, cytochrome *c* (used apart for spectrophotometric measurements of superoxide), or SOD (the natural selective scavenger) or with synthetic materials, including polypyrole films containing metal particles or porphyrin complexes. Cell measurements of superoxide, as detailed below, have been, however, mostly based on the use of carbon surfaces or cytochrome *c*-modified gold electrodes.

Although nitric oxide is also oxidizable with a moderate overpotential at platinum or platinized surfaces and to a lesser extent at carbon surfaces, its detection potential that provides

a maximum sensitivity is about 0.7 V vs Ag/AgCl.[232–235] Many biological substances are oxidizable at this potential, and it is therefore necessary in many cases of analysis to increase the selectivity by a surface modification of the electrode. On that purpose, different types of films have been reported in the literature as tools to limit, by size exclusion (polymethylcellulose for instance) or charge exclusion (Nafion) processes, the diffusion of other undesired molecules toward the electrode surface. Several important results regarding biological mechanisms that involve nitric oxide (see sections 3.6 and 3.7) such as in the brain were obtained based on the use of millimetric or micrometric, platinum or carbon electrodes simply modified by one or two different layers of these polymers. In the mid-nineties, several groups reported a second generation of nitric oxide sensors based on carbon or platinum surfaces modified by redox polymers.[236–238] A first advantage was the ability to electrodeposit films of redox complexes such as porphyrins and thus to control the surface topology and eventually the electrode sensitivity. The sensitivity is increased due to the catalytic effect provided by a porphyrin (metal centers of Ni, Cu, Co, or Mn) enabling it to reach concentration levels of NO in the range of a few nanomolars.[239,240] Another advantage has been the better selectivity afforded by the porphyrin catalyst since the different ROS and RNS are not oxidized as easily as nitric oxide on that surface. Besides, microelectrodes modified by porphyrin complexes were developed in the last years for the detection of a major RNS, the peroxynitrite anion (see below). L. T. Jin and colleagues[241] and recently F. Bedioui and colleagues[242] reported the reduction of $ONOO^-$ at manganese tetraaminophthalocyanine-modified electrodes, although the exact mechanism of detection was not identified. The main advantage of these electrodes is the low potential (0 to −0.5 V vs Ag/AgCl) applied for peroxynitrite detection and consequently their almost immunity vs interfering oxidizable compounds.

3.2. Detection of Superoxide and Hydrogen Peroxide Released by Cells in Culture

3.2.1. Detection of Superoxide at Bare Carbon and Gold Microelectrodes on Phagocytes and Vascular Cells

Pioneering work in the field of detection of species related to oxidative stress was reported by the group of H. A. O. Hill in the mid-eighties. This group worked previously on SOD activity and investigated the possibility to detect superoxide anion release by human blood neutrophils.[229,230,243] Two main series of results were reported. In the first one, superoxide anion was detected directly by its oxidation wave at low potential (+50 mV vs Ag/AgCl) on the surface of a millimetric pyrolytic graphite electrode. The electrode was "opsonized", that is, its surface was modified by depositing an immunological factor, the immunoglobulin G (IgG). This was obtained by adsorbing the immunological factor through simple dipping of the electrode into a solution of IgG. Measurements were made into a buffer solution containing neutrophils previously purified and used in suspension. The neutrophils that met the electrode surface were activated by the deposit of IgG and rapidly initiated a respiratory burst response. Such a typical response of neutrophils and macrophages during immunological processes is indeed known for decades to be a key factor of phagocytosis. The increase of oxygen consumption (the respiratory burst) by activated phagocytes correlated with the activation of their NADPH oxidases that catalyze the formation of superoxide and hydrogen peroxide. Furthermore, $O_2^{\bullet -}$ released by neutrophils in their environment has been shown to be detected on the graphite electrode surface. The selectivity for $O_2^{\bullet -}$ of such an analysis was supported by the observation of a strong decrease of response when SOD or when *N*-ethyl-maleimide (NEM, a strong but nonselective inhibitor of NADPH oxidases) was injected into the medium.

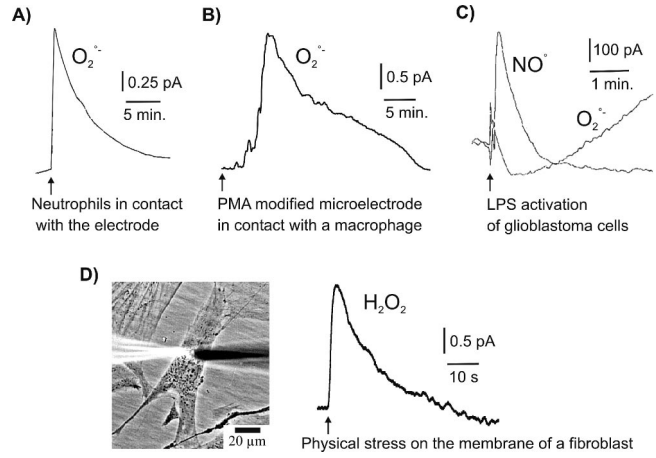

Figure 12. (A) Detection on an opsonized (IgG modified) gold microelectrode of superoxide release by a single neutrophil. At time *t* (indicated by an arrow), neutrophils were added to the buffer solution where the microelectrode is placed and one of them is supposed to encounter the microelectrode surface and be activated (adapted from ref 230). (B) Detection on a PMA-modified carbon fiber microelectrode of superoxide release by a single phagocyte (HL-60 cell line). The microelectrode surface was positioned in contact with one isolated cell at $t = 0$ min (adapted from ref 244). (C) Detection of $O_2^{\bullet -}$ on a ferricytochrome c-modified gold electrode and detection of $NO^{\bullet}$ on a commercial selective electrode at a submillimetric distance from a layer of 10^6 glioblastoma cells (A172 line). The LPS stimulation was applied to cells preactivated by IFN-γ for 24 h (adapted from ref 253). (D) Detection on a platinized carbon fiber microelectrode (10−15 μm diameter) of hydrogen peroxide release by a single human fibroblast in culture. Left, view under the microscope of the experimental setup; right, typical response detected on a single fibroblast after its membrane depolarization by a microcapillary.

In a second series of experiments, a gold microelectrode of 10 μm diameter was used instead of the classical pyrolytic graphite millimetric electrode.[230] The microelectrode surface was again opsonized by IgG and placed into a suspension of fresh neutrophils, as described before. The contact between cells and the microelectrode surface induced very low variations of current, in the range of 1−1.5 pA, with a spike-shaped kinetic profile (see Figure 12A). Control experiments in the presence of SOD or NEM (see above) showed that superoxide was responsible for this oxidation current or at least was primarily related to the oxidized species. Measurements of the oxygen consumption rate by the neutrophils and its ensuing evaluation for a single cell led the authors to conclude that the oxidative bursts detected on their opsonized microelectrode originated in most of cases from the activation of a single neutrophil being in contact with the electrode surface. These seminal results seem to be the first demonstration of the perfect suitability of electrochemical methods for the detection of ROS species implicated in oxidative stress at the level of one living cell.

In 1996, K. Tanaka et al. reported studies[244,245] that confirmed and refined the work of H. A. O. Hill et al. Superoxide production by phagocytes in culture (HL-60 cell line) was detected on a 10 μm diameter carbon fiber

microelectrode. The microelectrode surface was also opsonized by dipping it into a solution of human IgG, a procedure akin to that of Hill's group, or modified by adsorption of an activator, the phorbol ester PMA (4-phorbol-12-β-myristate-13-acetate). Cells were immobilized on coverslips and, consequently, easy to localize for analysis without relying on a hypothetical interaction between the cells in suspension and the electrode surface. When the microelectrode surface was set in contact with the surface of a phagocyte, the cell shape changed, and a phagocytosis process initiated. As reported in Figure 12B, amperometric currents detected at +0.1 V vs Ag/AgCl, a potential sufficient to oxidize superoxide into oxygen on the carbon surface, provided slow developing signals in both condition of cell activation. Their maximum amplitude was in the range of a few picoampers. The authors assumed that the collection efficiency of superoxide secretion from the cell attached to the electrode surface was total, so that they could estimate the maximum rate and total amount of release: 1.2 fmol min^{-1} and 15 fmol total for IgG activation and 0.4 fmol min^{-1} and 30 fmol total for PMA activation. The very low noise level of the background current (about 0.1 pA) led these authors to draw the conclusion that the oscillations on the cell signal analyzed for 1−3 h originated from variations of the cofactor NADPH. Indeed, this may be used by cells to modulate their NADPH oxidase activity or other enzymes activity also dependent on NADPH metabolism.

On the basis of the work of K. Tanaka et al., several groups have used carbon fiber microelectrodes to monitor superoxide release by living cells into biological situations different as the one exposed above.[246–249] In particular, C. Privat et al. have reported measurements of $O_2^{\bullet-}$ produced by vascular cells (endothelial and smooth muscle cells).[250] Indeed, oxidative stress following overproduction of superoxide (and possibly nitric oxide) at the vascular level may lead to local dysfunctions. This has been recognized as a key factor in atherosclerosis, ischemia/reperfusion injury, etc. The electrode surfaces were electrochemically pretreated, and measurements were conducted by differential pulse amperometry between 0 and +0.1 V vs SCE. The authors also carefully calibrated their carbon fiber microelectrodes (7 μm diameter) against superoxide solutions prepared from dissolved KO_2 over a wide range of pH values (7.4−14). This procedure offered an excellent sensitivity for $O_2^{\bullet-}$ (0.8 nM/pA), while the low potential applied provided selectivity. In these experiments, the sensing property of the electrodes was separated from the cell stimulating step, that is, did not involve adsorption of chemical or immunological agents on the electrode surface. Vascular cells in culture were stimulated independently by cytokine IL-1β, after positioning via a micromanipulator the microelectrode surface at close distance from cells, that is, supposedly a few tens of micrometers. The configuration ensured an efficient collection of superoxide release, without a priori any significant loss of response due to reaction with $NO^{\bullet}$, which was not supposed to be produced in these conditions. These hypotheses were supported by the low local concentrations of superoxide detected, being in the range of tens of nanomolar. However, because the superoxide disproportionation involves a second order dependence on its concentration (eq 9), such a low level may result either from the fact that effectively such low level production occurred (i.e., $O_2^{\bullet-}$ could diffuse unaltered to the electrode surface) or from the fact that a larger level production was almost entirely scavenged by the disproportionation before its detection could occur. This is a general caveat in the detection of superoxide flows out a cell and applies as well to Hill's or Tanaka's reports. Therefore, one may be extremely careful when deriving interpretations based on the low levels of superoxide (nM) in cellular bursts. Note that this applies as well to the cases described hereafter since the problem is independent of the nature of the detection step but depends only on the distance traveled by the superoxide ion from its source to the electrode surface.

3.2.2. Detection of Superoxide by Cytochrome c-Modified Gold Electrodes on Neuronal Cells

Let us present a seminal study from the group of C. J. McNeil. Starting in 1989, these authors have proposed a new concept for electrodes preparation to improve their selectivity toward superoxide.[251] These studies were based on millimetric electrodes and did not apply initially to single cell but to confluent cell layers. We believe nevertheless that the present principle of electrode modification may be used for the preparation of microelectrodes and that single cell analysis would be possible with such sensors. Hence, the authors have developed millimetric gold electrodes modified by a deposit of ferricytochrome c,[252–255] a protein classically used for indirect spectrophotometric measurements of superoxide produced by living cells in culture since the reaction between the two compounds is very fast ($k = 2 \times 10^6$ M^{-1} s^{-1}, eq 15):[256]

$$\text{ferricytochrome c } (Fe^{3+}) + O_2^{\bullet-} \rightarrow \text{ferrocytochrome c } (Fe^{2+}) + O_2 \quad (15)$$

Ferricytochrome c was covalently immobilized by a thiol derivative (DTSSP) linker interacting with the protein and the gold surface (SAM formation through Au−S bonds). This was decided for providing a better selectivity for $O_2^{\bullet-}$, particularly against $NO^{\bullet}$, than that offered by neat carbon or gold electrodes. A complete study in vitro with solutions of superoxide generated enzymatically by a system xanthine/xanthine oxidase established the interest of the concept based on the electro-oxidation of the reduced cytochrome *c*, thus providing a catalytic effect on the response. Consequently, these modified microelectrodes offered a high sensitivity for $O_2^{\bullet-}$, for example, 2 pM/pA.[253,254]

Each electrode was used in conjunction with a second electrode, a commercial $NO^{\bullet}$ sensor, for simultaneous measurements of $O_2^{\bullet-}$ and $NO^{\bullet}$ produced by neuronal cells in culture (different cell lines were analyzed). The data presented in Figure 12C were obtained from simultaneous measurements with the two types of sensor over a layer of adherent glioblastoma cells (A172 cell line).[253] Their oxidative stress response was stimulated by the addition of PMA (a phorbol ester activating NADPH oxidases as explained before) or LPS (lipopolysaccharide-α, an endotoxin originating from fragments of bacteria walls, known to activate NO synthases) to the buffer solution. On the basis of the in vitro tests, the authors assumed no possible interference between the two sensors, that is, that superoxide was not detected by the $NO^{\bullet}$ sensor and the $O_2^{\bullet-}$ sensor was insensitive to $NO^{\bullet}$. Simultaneous measurements gave them the ability to observe the cross-reaction between $O_2^{\bullet-}$ and $NO^{\bullet}$ under their experimental conditions. Following addition of the stimulus (LPS in Figure 12C), a rapid increase of $NO^{\bullet}$ was detected and even possibly amplified under conditions

of NO synthases preactivation (inducible NOS induction by the cytokine interferon-γ), while superoxide was not detected. When the production of $NO^{\bullet}$ decreased, superoxide began to be observed showing that in the initial phase of the cell response, $O_2^{\bullet-}$ was certainly titrated by the excess of $NO^{\bullet}$ to form $ONOO^-$. To the best of our knowledge, these studies reported one of the first examples of direct and selective simultaneous measurement of different primary species of oxidative stress at living cells and the observation of reaction between these species to form RNS.

The present experimental protocol and modified electrodes were used for different biological applications by several groups including the one of C. J. McNeil. Particularly, it was used to investigate the relations between oxidative stress and the growth of different neuron types in culture including motor neurons, as models of pathological processes occurring in the central nervous system.[257,258] However, the applicability of their analytical method to quantitative biological studies may have been limited by the low efficiency of superoxide collection for the submillimetric distances separating the electrode surface and the layer of cells. The spontaneous formation (viz., without catalase involvement) of H_2O_2 in these conditions is certainly not negligible (see above), although it was not evaluated. Similarly, peroxynitrite formed by coupling between $NO^{\bullet}$ and $O_2^{\bullet-}$ could not be measured directly. Yet, $ONOO^-$ may reoxidize ferricytochrome c and interfere with measurements over long times since the reaction is quite slow.[259] Nevertheless, these studies on cell colonies established that the detection of side products of superoxide and nitric oxide was feasible so that their extension would be of great importance for characterizing quantitatively and in real-time the very nature and origin of oxidative stress processes occurring in aerobic cells.

3.2.3. Detection of Hydrogen Peroxide by Platinized Carbon Fiber Microelectrodes on Skin Fibroblasts

Among the different ROS, hydrogen peroxide is the most stable one and is consequently an essential marker of oxidative stress. Our group decided to focus initially on its detection in the mid-nineties through the development of microelectrodes allowing its monitoring on single cells.[260] It was previously established that H_2O_2 oxidation was difficult on any type of carbon surfaces, while its oxidation on bare polished platinum surfaces induced the formation of platinum oxide and peroxide and, consequently, led to unstable electrochemical responses. Meanwhile, several groups working in the development of glucose sensors have shown that hydrogen peroxide produced by glucose oxidase could be easily and quantitatively detected by oxidation on black platinum or platinized electrode surfaces.[261,262] Black platinum was thus electrodeposited from a Pt(IV) solution following a $4e^-$ reduction into Pt(0) on a microelectrode surface (eq 16)

$$PtCl_6^{2-} + 4e^- \rightarrow Pt^0 + 6Cl^- \quad (16)$$

A stable irreversible voltammetric wave ($2e^-$ oxidation process, $E_{1/2} = +0.25$ V vs SSCE) for H_2O_2 could be observed on platinized carbon fiber microelectrodes (1−30 μm diameter). Moreover, the platinized surface being a rough deposit, such microelectrodes possess a huge active area, which ensures a high sensitivity for H_2O_2 detection. The limit of sensitivity determined by amperometry at +0.55 V vs SSCE was a few nanomolars, the selectivity being provided by the electrode potential, and was attested by control experiments in the presence of added catalase or *o*-dianisidine.

Because of their excellent analytical properties, these modified microelectrodes were applicable for monitoring oxidative stress responses on single human skin fibroblasts. These cells are the main constituents of skin dermis and as a consequence are the site of some of the oxidative damages induced by UV-A and -B from sunlight or other chemicals in contact with the skin. Under oxidative stress conditions, DNA alterations of fibroblasts might be amplified and lead the cell to shift toward a cancerous state.[183,263,264] S. Arbault et al. have shown that fibroblasts were able to produce oxidative bursts under depolarization of the cell membrane induced by a mechanical stress.[260,265] This was obtained by puncturing the membrane with the tip of a microcapillary without inducing cell disruption and death (the cells recovered all their functions after a few hours in culture medium). The shaft of microelectrodes was insulated to detect electroactive species only at their very tip surface. Because of their small size (10−15 μm tip diameter), they could be positioned via a micromanipulator at a few tens of micrometers above the cell surface, that is, in experimental conditions for which any loss of H_2O_2 through its reaction with other compounds should not occur. The variation of amperometric current detected immediately after the microcapillary puncture on the cell membrane (see Figure 12D) corresponded to an active response of the cell and not to the passive release of electroactive species diffusing from the cytosol or from storage vesicles. Experiments in the presence of scavengers (catalase or *o*-dianisidine, a substrate for peroxidases) showed that hydrogen peroxide was the major detected component of the cell response. In later studies, inhibitors of NADPH oxidases confirmed that H_2O_2 detected by the microelectrodes had an enzymatic origin[265] and that the kinetic profile of the oxidative bursts measured on fibroblasts (Figure 12D) or lymphocytes was dependent on metabolic factors governing NADPH oxidases activity.[265–267]

Nevertheless, several results led C. Amatore et al. to consider that oxidative bursts detected on different cell types were not exclusively related to hydrogen peroxide production. For instance, they reported that a residual signal was always observed in experiments with catalase but also that the amplitude of bursts was increasing at amperometric potentials higher than the one of H_2O_2 plateau potential. The hypothesis of a simultaneous production of $O_2^{\bullet-}/H_2O_2$ and $NO^{\bullet}$ has been further examined, as is detailed below.

3.3. Detection of Nitric Oxide and Peroxynitrite Releases by Single Cells in Culture

3.3.1. Detection of Nitric Oxide by Porphyrin Modified Microelectrodes at Single Cells from a Cardiac Endothelium

The group of T. Malinski was one of the first to describe an electrochemical $NO^{\bullet}$ sensor and its application to cell measurements of nitric oxide release. They reported in 1992 the development of a carbon fiber microelectrode whose surface was modified by the electrodeposit of a film of nickel porphyrin.[238] They have further used and adapted such sensors for numerous biomedical studies. Particulary, T. Malinski et al. have modified their electrodes to match the specific conditions of a single cell analysis on cells in culture or located on the surface of the endocardium (rabbit heart).[268] The active tip of the electrochemical sensor was reduced in

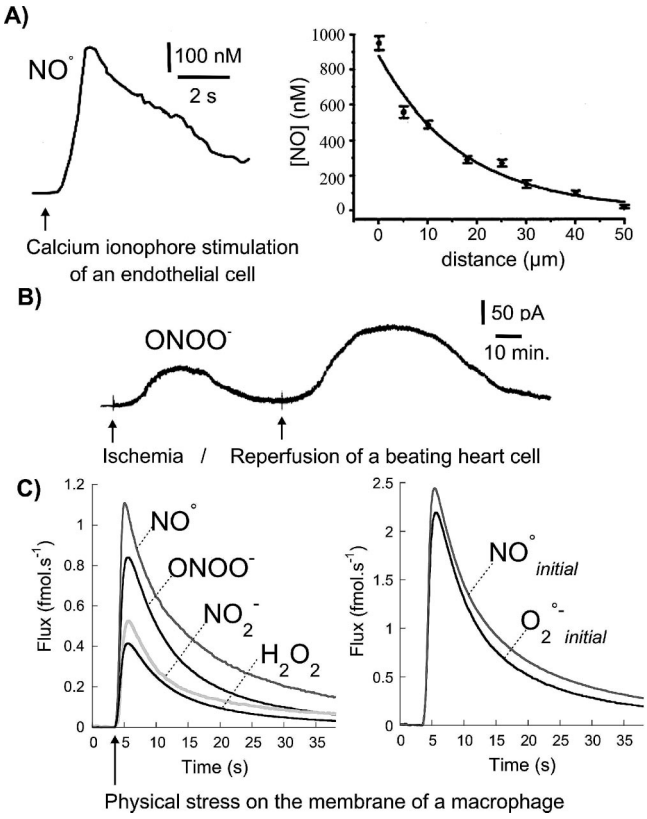

Figure 13. (A) Left, release of nitric oxide detected by a porphyrin-modified microelectrode placed 10 μm from the surface of an isolated endothelial cell (endocardium of rabbit) stimulated by a calcium ionophore (A23187) at $t = 0$ s; right, exponential decay of the signal amplitude with the distance between the sensor tip and the cell surface. (B) Time course of peroxynitrite detected by a Mn(TAPc)/PVP-modified microelectrode inside a single beating heart cell in culture after its ischemia/reperfusion. (C) Determination by platinized carbon fiber microelectrodes of the species (H_2O_2, $ONOO^-$, NO_2^-, and $NO^\bullet$) released by single murine macrophages during oxidative burst responses. Evaluation of the flux of the primary species ($O_2^{\bullet-}$ and $NO^\bullet$) produced by a macrophage.

diameter to reach a value of 2−5 μm instead of the initial value of 50−60 μm.[235,269,270] Second, the electrode was inserted into a catheter, so that the tip of the sensor was recessed (5−6 μm) within the catheter tip and was thus protected in the case of experiments performed directly in the tissue. Each electrode was tested and calibrated with pure $NO^\bullet$ solutions of concentration ranging from 5×10^{-9} to 3×10^{-6} mol L^{-1}.

Experiments were performed on cells mechanically removed from the surface of left heart ventricle of an anesthetized rabbit. Cells were subsequently plated on usual coverslips and maintained in life in an appropriate buffer. The tip of the porphyrinic microelectrode was then positioned via a micromanipulator over the surface of a single endothelial cell, considering that the zero distance was obtained when touching the cell membrane, which was evidenced by a signal artifact. Then, the electrode tip was retracted to a 10 μm height. The cell was subsequently stimulated following the injection into its environment of a calcium ionophore solution (compound A23187 that induces transient opening of calcium channels, 8 μM final concentration) leading to the activation of NO synthases (constitutive enzymes of endothelial type). The release of $NO^\bullet$ detected by amperometry started less than a second after the cell stimulation (see Figure 13A). The signal reached its maximum in about 1 s and returned to baseline after about 10 s. Its amplitude (in concentration of $NO^\bullet$) was highly dependent on the distance between the sensor tip and the cell surface. Logically, the maximum value, close to 1 μM, was obtained when placing the sensor nearest to the membrane surface (see Figure 13A). This observation is consistent with the principles described in the introduction of the chapter. The quantification of release from a single living cell is highly dependent on the collection efficiency of the electrode surface and of the volume of dilution defined by the distance between that sensor surface and the cell source of active species. Consequently, even for stable species released, minimizing this distance ensures better conditions for analysis of the true nature of the biological information, although this may lead to an indirect blasting of the cell surface by the products resulting from the electrochemical detection.

This first series of studies of $NO^\bullet$ detection on single cells allowed comparison of the response of endothelial cells obtained from the surface of endocardium of normal or hypertensive rats. Nitric oxide release was lower in hypertensive rats ($NO^\bullet$ is the major vaso-relaxing compound) in agreement with former studies reporting a weaker relaxation of smooth muscle cells from these animals as compared to the wild-type ones. However, the authors showed that the lower $NO^\bullet$ responses were very sensitive to SOD indicating that a large part of $NO^\bullet$ produced by cells was not detected by the electrode. It may be suggested that it was consumed through its reaction with $O_2^{\bullet-}$ before diffusing to smooth muscle cells and inducing their relaxation. Consequently, these studies hypothesized that the formation of RNS occurred preferentially in the hypertensive rats, this event leading potentially to the pathophysiological consequences observed in this animal model but also in humans.

3.3.2. Detection of Peroxynitrite by Modified Microelectrodes during Ischemia of Endothelial Cells from Heart

The direct electrochemical detection on living cells of peroxynitrite anion release was simultaneously reported by two groups in 2000, each one using a different type of electrode and focusing on a different biological application. We will emphasize first on studies reported by the group of L. T. Jin, who had previously reported the development of microelectrodes modified by metallophtalocyanines or Schiff bases as sensors for nitric oxide and superoxide.[249,271−273] In the studies that we wish to detail here, the authors have prepared cylindrical carbon fibers or platinum microelectrodes, whose surfaces were modified by the deposit of tetraaminophtalocyanine manganese(III) [Mn(TAPc)] as a catalyst for peroxynitrite reduction and subsequently modified by a membrane of the catanionic polymer polyvynilpyridine (PVP). Briefly, cylindrical carbon fiber microelectrodes (7 μm diameter) were chemically etched to provide electrodes of 1 μm diameter at the tip and tens of micrometers long. Then, their surfaces were electrochemically cleaned into H_2SO_4, dried, and modified by the electrodeposition of poly-Mn(TAPc) through voltammetric scanning of the potential between +0.5 and +1.0 V vs Ag/AgCl. Prior to in vitro tests or cell experiments, the electrodes were modified by a layer of PVP to perform as a cation repulsive barrier and also as a diffusional barrier for large biological molecules. These two characteristics are prone to significantly improve the selectivity of these microelectrodes for $ONOO^-$, although they may decrease the electrode response time. PVP was

simply deposited from a solution allowed to dry onto the electrode surface.

In vitro tests with pure peroxynitrite solutions established that this species was detectable by its reduction into nitrite and nitrogen dioxide electrocatalyzed by Mn(TAPc) at low potential (+0 V vs Ag/AgCl). This potential value in conjunction with PVP layer properties afforded a large immunity to many interferents including several ROS ($O_2^{\bullet -}$, H_2O_2), RNS ($NO^{\bullet}$, NO_2^-), dioxygen, or other molecules that may be present in cell cytosol (L-arginine, NADPH, ascorbic acid, etc.). These modified microelectrodes displayed a limit of sensitivity of 18 nM for $ONOO^-$ when used in conjunction with differential pulse amperometry (DPA). The useful analytical range was comprised between this lower limit up to a few hundreds of micromolars.

These electrodes were then used for intracellular measurements of $ONOO^-$ produced into myocardial cells isolated from the heart ventricle of neonatal rats. Peroxynitrite is suspected to be a major component of cardiac injury in the situation of heart ischemia, followed by reperfusion, although this hypothesis was previously inferred only on the basis of indirect markers of a nitrosative stress (staining of nitrotyrosine residues). The micrometric size tip of their microelectrodes was inserted into the beating heart cell. Despite the stress that it may induce in the cell (see below), they did not observe any significant change of baseline level of peroxynitrite concentration. After continuous ischemia of the cell, the signal ascribed to peroxynitrite progressively increased to reach a plateau after 15 min and stayed at the same level of concentration (70 nM) for about 15 other minutes (see Figure 13B). Then, the signal decreased until reperfusion of the cell that induced an increase of peroxynitrite concentration higher than the initial ischemic step. Control experiments involving an inhibitor of NO synthase or SOD or melatonin, a potent pharmaceutical inhibitor of $ONOO^-$, fully supported the conclusion that the variations of signal detected intracellularly by the modified microelectrodes reflected peroxynitrite concentration changes. These results provided a direct evidence that peroxynitrite was a major mediator of cardiac injuries occurring during ischemia/reperfusion process.

This hypothesis is further supported by results reported recently by the group of T. Malinski.[274] These authors have coupled three types of modified carbon microelectrodes (3−4 μm diameter, named nanosensors), poised at different potentials to detect simultaneously $O_2^{\bullet -}$, $NO^{\bullet}$, and $ONOO^-$ over the same layer of endothelial cells. Despite the fact that the authors did not discuss the occurrence of a possible simultaneous detection within a micrometric environment of the three different species, they reported the detection of peroxynitrite in the presence of its two mother species. Bursts of $O_2^{\bullet -}$, $NO^{\bullet}$, and $ONOO^-$ were simultaneously detected after a single endothelial cell stimulation by a calcium ionophore. These results were used to evaluate the ratio between nitric oxide and peroxynitrite concentrations detected in different conditions. Such a ratio clearly decreased in cells from hypertensive animals and following reperfusion of a vessel. These results recently reported by the group of Malinski demonstrated at most that electrochemical analysis at micro- or nanoelectrodes was a very powerful technique for studying local dysfunction of an endothelium in the in vivo condition.

3.3.3. Detection of Peroxynitrite by Platinized Microelectrodes on Single Skin Fibroblasts or Single Macrophages

Starting from the results described above in section 3.2.3, our group demonstrated in 2000 through the development of an original experimental protocol that oxidative bursts detected on single cells could be decomposed and quantified into their content in ROS and RNS.[228,275–277] In this series of studies, the distance between the microelectrode tip and the cell surface where the activation is applied was minimized to ensure the detection of species with short time lives, such as peroxynitrite, that would not be able to diffuse to the electrode surface before decomposing with the former arrangement.[260] The collection efficiency of the cell response increased and was maximal (>90%) when the distance was lower than 5 μm, indicating that species released by the cell in its environment were quantitatively detected, although the electrode−cell distance was large enough to avoid blasting the cell by the oxidation products of its released species.[276]

Then, numerous experiments conducted at different amperometric oxidative potentials on a large number of cells (about 1000 fibroblasts from the same wild type control strain) have shown that the cell oxidative response increased in amplitude with the potential and, consequently, that this response included the measurement of several electroactive species. These data enabled to construct an equivalent steady-state voltammogram of the average cell oxidative burst content by measuring the current vs the potential (over the potential range between +150 to +900 mV vs SSCE). The voltammogram depicted three different plateaus corresponding at least to three oxidation waves. Comparison of these waves to the oxidative responses obtained in vitro with the same electrodes for stable solutions of several ROS and RNS, potentially derived from superoxide and nitric oxide, led to the conclusion that the two higher potential waves featured (in terms of their potential position and transfer kinetic) the detection of $NO^{\bullet}$ and NO_2^-.[228,275,276] Conversely, the wave detected at low potentials did not correspond to the detection of a single species among all ROS and RNS, which could be tested. An exhaustive study of peroxynitrite anion electrochemistry, as well as that of H_2O_2, on platinum and platinized surface of electrodes established that this oxidation wave corresponded to a mixing of H_2O_2 and $ONOO^-$ oxidation waves, both being located within a near range of potentials.[228] Finally, the arithmetic addition of the voltammetric response of four different species (H_2O_2, $ONOO^-$, $NO^{\bullet}$, and NO_2^-) adjusted in concentration was in perfect agreement with the voltammogram determined from the cell oxidative response.[276,277] This analysis demonstrated that the evoked oxidative bursts of fibroblasts corresponded to the emission of a complex cocktail involving several ROS and RNS. Each species, including the very reactive peroxynitrite, could be characterized and selectively quantified by amperometric measurements at several potentials. Note that NO_3^- anions could not be detected due to their electroinactivity in our experimental conditions.

Further studies on cells (fibroblasts or macrophages) treated with different pharmacological agents, such as enzymatic inhibitors, established that this complexity reflected the simultaneous activation of two enzymatic systems of NADPH oxidase and NO synthase types following the cell stimulation. These were responsible for the separate production of the two primary species, $O_2^{\bullet -}$ and $NO^{\bullet}$ (Figure 11),[275,277] which could combine afterwhile. The determina-

tion of the individual fluxes of the different species released by the cells (Figure 13C, left) allowed us to reconstruct the fluxes of production of the primary species giving rise to these ROS and RNS (Figure 13C, right). Indeed, because all species originate from $O_2^{\bullet -}$ and $NO^{\bullet}$ (Figure 11), their primary fluxes could be evaluated based on matter conservation and Faraday's law:

$$(\Phi_{O_2^{\bullet -}})^{prod} = 2(\Phi_{H_2O_2})^{mes} + (\Phi_{ONOO^-})^{mes} + (\Phi_{NO_2^-})^{mes} \quad (17)$$

$$(\Phi_{NO^{\bullet}})^{prod} = (\Phi_{NO^{\bullet}})^{mes} + (\Phi_{ONO_2^-})^{mes} + (\Phi_{NO_2^-})^{mes} \quad (18)$$

Each curve was subsequently integrated and provided a measurement of the total amount of each compound produced during the oxidative burst. For both primary species, the quantities were found to lie in the range of tens of femtomoles and spectacularly consistent (Figure 13C, right). Although such magnitude may be considered as infinitely small from a macroscopic point of view as well as from the actual analytical standards, when considering the "living space" of a single cell (i.e., a few times its own dimensions), these amounts are not negligible in terms of local concentrations (viz., of the kinetic effects) that they produce. They indeed correspond to very high and therefore efficient concentrations of messenger, activator, or toxic molecules near the stimulated cell. The results presented here have led ultimately to several applications for biomedical purposes, such as studies of oxidative stress implication in HIV infection of blood lymphocytes[267,278] or oxidative stress implication in the carcinogenesis of skin fibroblasts.[265,266]

3.4. Future Analytical Challenges: The Development of Integrated Microsystems and Scanning Electrochemical Microscopy (SECM)

Current and future analytical challenges of oxidative stress studies at living cells concern the improvement of spatial and kinetic resolutions, as well as the achievement of statistically significant multiple parallel analyses to provide acute, efficient, and rapid systems for large-scale pharmacological and medical tests. Such improvement of spatial resolution for cell measurements is under process based on recent developments of SECM and nanoelectrodes. Several groups have shown recently that SECM (named BIO-SECM by some authors) was efficient to scan the surface of a single cell and thus to probe its membrane sites of secretion.[179,180,279–282] Particularly, the group of W. Schuhmann has reported the detection of $NO^{\bullet}$ released by single endothelial cells while precisely controlling the distance between the microelectrode's tip and the cell surface.[279] The best reported resolution of SECM on cells is about 1 μm,[279,281] that is, lower than the one provided by AFM techniques.[283] In the close future, the development of nanoelectrodes should efficiently lower this resolution and should provide the opportunity to distinguish different sites of release on a cell membrane. The decrease of sensor size will also logically favor an improvement of the kinetic resolution. Approaching closer to the source of electroactive species (without interfering with the cell activity) would diminish the response time (diffusion time) of the setup and may improve the detection of short time living species, such as peroxynitrite. One may further imagine the possibility to insert a nanometric tip size electrode into a cell without significantly disrupting its membrane or provoking intracellular damages (lethal damages) to measure intracellular oxidative events.[284]

In addition, the single cell experiments described in this chapter are highly time-consuming and involve high personnal expertises. Single cell studies, although important for resolution, are not statistically significant because of the rather large variation in cell metabolic activities. Hence, any significant information generally requires an average of 20−50 individual cell response measurements, which adds even more to the time consumption of experiments. Consequently, efforts are currently conducted in many groups to provide microsystems that may yield automatized analyses of single cells at a large scale. Recent reports by several groups established that microsystems integrating at least a set of three electrodes for measurements, a microfluidic chamber and channels for incubation and cell stimulation as well as a local pathway to other detection methods, is entirely feasible.[285–293] Different strategies have been explored, involving sensing microelectrodes that are microfabricated as pillar cones,[294] bands,[285] or as circle surfaces[287] located directly inside the chamber where the cells are cultured or separated from the chamber by a membrane through which molecules such as nitric oxide may diffuse easily.[289,292,295] As mentioned previously in the case of exocytosis studies (see section 2.5), a few microsystems aimed to single cell detection have already been reported, but this is a domain that is presently under constant and rapid evolution.

3.5. In Vivo Electrochemical Detection of Oxidative Stress: Particularities of Brain Studies

3.5.1. Analytical Properties of the Sensors Used in the Brain

This section is devoted to enlighten the electrochemical measurements of ROS or RNS, which had been performed in brain environment, including brain slices or the whole organ in living animals. Thus, we wish to focus on the amperometric detection of nitric oxide in brain tissues but also to report several rare studies on the direct electrochemical measurements in the brain of other direct oxidative stress markers such as superoxide anion. Moreover, we have limited this part of this review to the field of single cell measurements in brain tissues, at the most to several cells monitored by micrometric size electrodes. The reader of this *Chemical Reviews* issue is encouraged to consult the paper by R. M. Wightman et al., which deals more widely with the monitoring of neurotransmitters in the living brain.

Seminal studies on the $NO^{\bullet}$ electrochemical detection have been reported since the early nineties, simultaneously with the emergence of microelectrodes. The brain is a complex environment to screen analytically with chemical sensors because: (i) the analytes to be detected are frequently present in very low concentrations like micro- or nanomolar ranges, and generally, they are very unstable with short lifetimes, like for nitric oxide; (ii) they need to be detected in the presence of numerous other interferents, which often have high electrochemical activities toward common sensors; (iii) the biological, biochemical, and physiological processes that are investigated in these tissues have to be disturbed as little as possible by the invasion of the probe and without disturbing or destroying these delicate samples; (iv) a lot of surface sensor pollution, like protein fouling or adsorption, occurs while the measurements are performed and can affect

greatly the microelectrode response. All of these constraints make such detections arduous and challenging. Consequently, to perform significant surveys, the ideal analytical sensor must be highly sensitive and selective, must be calibrated before and after the measurements, must have a very fast response time, and must possess a micrometric size, and the general properties of the medium to be scrutinized must be perfectly understood. Obviously, a good analytical sensor for brain studies is a compromise between these different properties.[236,296–298]

In that way, measuring nitric oxide in the brain is complicated by the presence of numerous other endogenous electroactive species like dopamine metabolites such as 3,4-dihydroxyphenylacetic and homovanillic acids, the antioxidant ascorbic acid, or neurotransmitters (adrenaline, noradrenaline, dopamine, and serotonin).[298–300]

3.5.2. Advantages of Amperometry for Nitric Oxide Detection in the Brain

As already mentioned previously, amperometry is the simplest electrochemical experiment: In this method, the potential of the electrode is fixed so that the concentration of the detected analyte is maintained at zero at the microelectrode surface during the whole electrochemical measurement. Thus, the monitored current is only limited by the mass transport rate of the analyte toward the electrode surface. The current is then directly proportional to the average concentration of the analyte within the diffusion layer of the electrode at all times and is measured continuously at the microelectrode and generally implies long monitoring durations, so that its digital storage is generally required. This technique thus offers the best temporal resolution as compared to other electrochemical techniques. Indeed, it allows to follow the fast changes of chemical concentration that happen while neurochemical brain processes occur. However, amperometry has poor electrochemical selectivity; therefore, numerous surface modifications have been performed for nitric oxide detection in the brain such as those cited above (see section 3.1.3): incorporation of enzymes, ion-exchange membranes (like Nafion or other membranes in Clark type probes or commercial WPI probes), use of porphyrin, or deposit of black platinum. Enzymes produce enhancement of current via their substrates, but selectivity is not necessarily a guarantee of this surface modification since the enzyme or the membrane may be not selective under their conditions of use. The calibration for such modified sensors is then difficult in complex environments like the brain. Ion-exchange membranes are selective, like Nafion, which prevents access onto the microelectrode surface of anionic metabolites, such as nitrites, but they have the drawback of decreasing the temporal response of the sensor. Finally, the response time is also mainly fixed by the chosen digital sampling rate, the signal-to-noise ratio, and the filter of the used potentiostat. Among the other electrochemical approaches, chronoamperometry has less selectivity than voltammetry or differential pulse voltammetry since the potential information is lost but has a lower time resolution than fast scan cyclic voltammetry. Therefore, none of these various electrochemical techniques offers real universal advantages for brain measurements, but each of them has specific advantages for a particular problem. All in all, amperometry appears to be the most convenient method for in vivo detection of nitric oxide in the living brain, as we will discover below.

3.6. Detection of Oxidative Stress in the Central Nervous System

3.6.1. Electrochemical Detection of Nitric Oxide in Brain Slices

The first study using an electrochemical microprobe for detecting nitric oxide release in brain tissue was led by K. Shibuki.[232,301] The design of his $NO^{\bullet}$ probes was similar to that of miniature oxygen electrodes.[302] A glass micropipette was broken unevenly to form an oblique opening with a diameter between 150 and 250 μm and was filled with 30 mM NaCl and 0.3 mM HCl (pH 3.5). The tip was then sealed with a thin membrane of chloroprene rubber with a thickness less than 1 μm. As a cathode, a piece of platinum wire was inserted into the pipet, and as an anode, a piece of silver wire was inserted in it. The output current of the probe correlated linearly with the $NO^{\bullet}$ concentration at the tip, and the sensitivity of the probe was found to be between 3.5 and 106 pA per 1 μM change in $NO^{\bullet}$ concentration at the cathodic voltage of +0.8 V. This probe showed no sensitivity to oxygen or to oxidized derivatives of $NO^{\bullet}$. The $NO^{\bullet}$ release from sodium nitroprusside, a classical nitrovasodilator,[303] was successfully detected by the probe. The $NO^{\bullet}$ probe inserted into the molecular layer of a rat cerebellar slice detected a response corresponding to 8−58 nM of $NO^{\bullet}$ concentration following electrical stimulation of the white matter. This response was blocked reversibly by a toxin (tetrodotoxin, 1 μM) and was attenuated by hemoglobin (1 or 10 μM) present in the medium (Figure 14A). This seminal study demonstrated that an electrochemical $NO^{\bullet}$ probe was suited to the detection of endogenous $NO^{\bullet}$ release in a brain tissue. It had a sufficiently fast response time (1 s); however, its tip size was too big to achieve the monitoring of a single cell secretion, and one main inconvenience was the variability between different probes. Thus, the detection mostly concerned the emission of a group of neurons in the cerebellar slice with a specifically calibrated electrode for each measurement.

Nicotine-evoked nitric oxide release in a rat hippocampal slice was then performed in 1998 by a carbon fiber microelectrode covered with Nafion and *o*-phenylenediamine.[304] This study investigated the possible regulation of $NO^{\bullet}$ by cholinergic agonists in rat hippocampus. The electrochemical $NO^{\bullet}$ probe was a single (30 μm outer diameter) carbon fiber type modified with Nafion and *o*-phenylenediamine.[305] Acetylcholine or nicotine was delivered by injection from pipettes placed within 300 μm from the $NO^{\bullet}$ sensor (Figure 14B). Both induced $NO^{\bullet}$ signals rising up to a micromolar range concentration in the rat hippocampus slice and lasting for few minutes. These data supported the hypothesis that nicotine is able to evoke long-lasting $NO^{\bullet}$ release in the hippocampus. Moreover, these electrodes offered a better spatial resolution in allowing detection of nitric oxide from a few cells thanks to the reduced size of the sensor (30 μm).

C. S. Leonard et al. used in 2001 a porphyrinic microprobe to monitor $NO^{\bullet}$ in brain slices of the mesopontine tegmentum.[306] The sensor was modified for enhanced $NO^{\bullet}$ selectivity based on the work of Mitchell and Michaelis.[240] This involved carbon fiber-based sensors modified chemically thanks to the use of membranes of polymers such as nickel porphyrin, Nafion, immobilized ascorbic acid oxidase, and either polypyridinium or polylysine. These modifications provided good selectivity for anodic detection of $NO^{\bullet}$. The

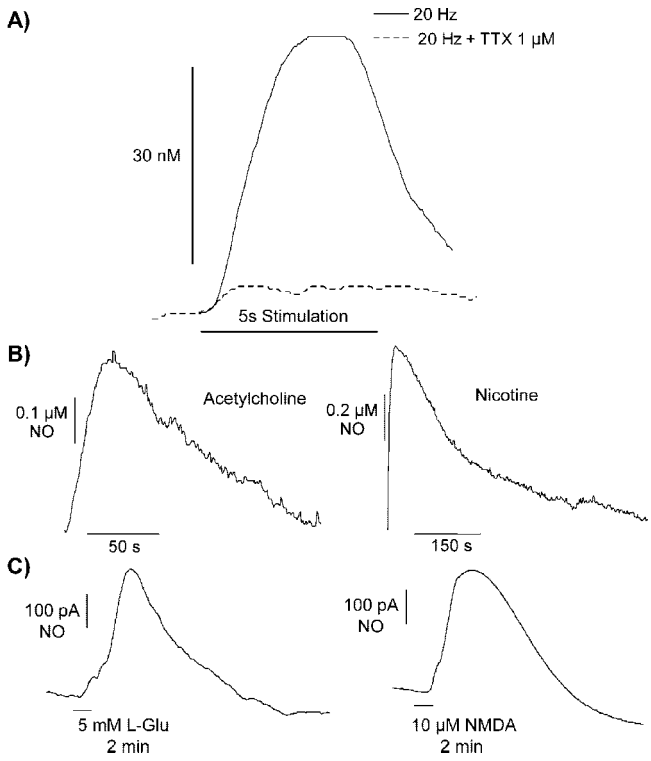

Figure 14. (A) Responses evoked by white matter stimulation and recorded through $NO^{\bullet}$ probes (similar to miniature oxygen electrodes) inserted into the molecular layer of cerebellar slices. The white matter was stimulated at 20 Hz for 5 s (horizontal bar), but for the dotted curve, there was an additional and simultaneous application of a toxin (1 μM tetrodotoxin). Adapted from ref 232. (B) Acetylcholine (left) and nicotine (right)-evoked overflow of $NO^{\bullet}$ in a rat hippocampal brain slice measured by a Nafion and *o*-phenylenediamine-treated carbon fiber microelectrode. Adapted from ref 304. (C) L-Glutamate-induced efflux (current/time profile) of $NO^{\bullet}$ recorded in the CA1 region of hippocampal slice following a 2 min perfusion of 5 mM L-glutamate (left) and 10 μM NMDA (right). Adapted from ref 307.

response time of these probes was found to be 500 ms, and the amperometric detection limit was 0.5 nM in $NO^{\bullet}$ concentration; L-arginine, L-NAME, and CO did not interfere since they were not detected by the probes. The efficiency of the sensors was tested ex vivo in brain slices and in the anesthetized brain where exogenous $NO^{\bullet}$ was injected, with detection limits of 8 and 173 nM $NO^{\bullet}$, respectively. Additionally, the cholinergic neurons of the mesopontine tegmentum were investigated since they appear to play a strategic role for generating arousal and rapid eye movement during sleep.[306] They express high levels of the enzymes NO synthases; therefore, the authors investigated whether or not their firing induced increases in local endogenous nitric oxide concentration levels. Such as in the work of D. A. Smith et al.,[304] $NO^{\bullet}$ measurements were made with a relatively small probe, allowing detection of the responses from a few neurons. Indeed, the microprobe measured 35 μm diameter and was inserted in brain slices. Local electrical stimulation at 10 or 100 Hz produced responses that were attributed to nitric oxide at a nanomolar range of concentration. A NO synthase inhibitor, N^{G}-nitro-L-arginine-methyl-ester at 1 mM, reduced the peak production by 92%, and the responses were shown to depend on extracellular Ca^{2+}, both controls validating the ascription of the signals to $NO^{\bullet}$. Collectively, all of these results demonstrated that cholinergic neuron activity plays a major role on controlling extracellular nitric oxide concentration, probably via somatodendritic nitric oxide production.

Finally, the group of R. M. Barbosa recently developed in 2005 carbon fiber microelectrodes with Nafion and *o*-phenylenediamine to measure $NO^{\bullet}$ in brain slices from CA1 region of the hippocampus.[307] Nafion films were deposited onto the microelectrode surface by simply dipping it into a 5% solution followed by a drying stage for 10 min at 170 °C. *o*-Phenylenediamine was then electropolymerized over the electrode surface by holding it at +0.9 V vs Ag/AgCl. $NO^{\bullet}$ concentrations were monitored in brain slices as a function of L-glutamate and *N*-methyl-D-aspartate perfusion (Figure 14C). The principal result of this study was to establish that such sensors were sensitive enough to follow $NO^{\bullet}$ concentration changes in the brain with a sensitivity of 954 ± 271 pA/μM and a detection limit of 6 ± 2 nM. This detection was shown to be independent of the presence of interferents like ascorbate, nitrite anions, or H_2O_2. Furthermore, these sensors appear ideally suited for the discovery of $NO^{\bullet}$-regulated pathways for memory and learning processes in the rat hippocampus.

These seminal investigations established that the electrochemical measurements of in vivo $NO^{\bullet}$ concentrations bring crucial information about $NO^{\bullet}$ pathways, which are difficult or impossible to achieve by other methods since $NO^{\bullet}$ is a fast diffusible messenger molecule, which plays an essential role on numerous physiological processes in the brain.

3.6.2. Electrochemical Detection of Nitric Oxide Directly in the Brain

From 1993 and over the ensuing years, A. Meulemans reported the possibility of direct oxidative detection of nitric oxide upon using commercial carbon fiber microelectrodes (Tacussel, France). These cylindrical sensors had a 8 μm diameter and ca. 500 μm length. For measurements, they were pretreated by performing 200 scans from 0 to +2 V vs SCE in PBS, at pH 7.4, and then coated with a cellulose membrane (to prevent the effects of protein adsorption). $NO^{\bullet}$ measurements were performed by differential pulse voltammetry based on the electrochemical wave detected at +0.95 V vs Ag/AgCl. Calibrations involved $NO^{\bullet}$ solutions in PBS. The sensor sensitivity was reported to vary from 250 to 500 pA/μM, although this depended on the success of the microelectrode treatment. The detection limit was around the micromolar range. The electrodes did not respond to nitrite anions, ascorbic acid, or serotonine up to millimolar concentrations. However, these sensors did not detect $NO^{\bullet}$ either in biological samples such as solutions of purified NO synthases or directly into brain tissues. This prompted A. Meulemans to raise an interesting and uncommon hypothesis according to which NO synthases transform L-arginine to *N*-nitroso-L-arginine but do not lead to liberation of free $NO^{\bullet}$.[308–313] This was backed on direct measurements of *N*-nitroso-L-arginine (NA) in rat brain frontal cortex with these carbon fiber microelectrodes and differential pulse voltammetry. On that purpose, a carbon microelectrode was inserted at a fixed depth (125 μm) into the frontal cortex of a living animal.[312] A constant level of neuronal NA of 0.66 mM was found in this region of the rat brain over a few hours. Applications of competitive inhibitors of brain NO synthase and $NO^{\bullet}$ donors resulted in the disappearance of NA levels. On the contrary, perfusions of classical ROS scavengers had no effects on NA frontal cortex concentrations, which remained at a constant level. These interesting

results seemed to indicate that NA is produced continuously at a high level by rat cortex neurons. Moreover, they represent an elegant measurement of an uncommon species associated with nitrosative stress directly in the intact brain of a living animal. The use of 8 μm diameter sensors allowed NA detection from a very few neurons, that is, closer to the single cell level than what was achieved in other studies cited in this subsection.

In vitro and in vivo performances of *o*-phenylenediamine- and Nafion-covered carbon fiber microelectrodes were tested in terms of their ability to detect $NO^{\bullet}$ and then used to measure $NO^{\bullet}$ diffusion in the extracellular space of the rat brain.[305] These electrodes were of 30 μm diameter and were compared with nickel porphyrin type $NO^{\bullet}$ sensors to determine which system had the most sensitivity and selectivity for $NO^{\bullet}$. It appears that electrodes treated with Nafion first, followed by *o*-phenylenediamine, offered better analytical detection charactericties than the others. They were very sensitive to $NO^{\bullet}$ with a detection limit of 35 ± 7 nM. Besides, they were highly selective against nitrite anions (>900:1), dopamine (>300:1), and ascorbate (>600:1). They displayed good linearity in 0−6 μM $NO^{\bullet}$ range ($R^2 \geq 0.997$). The authors also reported preliminary direct measurements of diffusion of $NO^{\bullet}$ from a point source in the rat striatum. Male rats were anesthetized and prepared for in vivo electrochemical recordings. An Ag/AgCl reference electrode (200 μm diameter) was implanted into the brain at a site remote from the recordings areas. $NO^{\bullet}$ (2 mM in PBS, pH 7.4) was loaded into a single-barrel micropipette with a 10−15 μm o.d. tip diameter. The micropipette was attached to the $NO^{\bullet}$ sensor with a tip separation of 325−375 μm, a distance that was accurately measured after introduction for calculation of $NO^{\bullet}$ diffusion coefficient. Typical profiles of diffusion curves following injection of $NO^{\bullet}$ were obtained, and interestingly, the decay of the curve shows that $NO^{\bullet}$ is not degraded or removed as rapidly as one might expect for such a reactive molecule in an overall aerobic environment. The apparent diffusion coefficient of $NO^{\bullet}$ was calculated on the basis of the rise times of all of the signals recorded in the brain striatum. The mean value was $1.2 \pm 0.2 \times 10^{-5}$ cm^2/s, that is, higher than those of other present molecules such as ascorbate, as predicted. These electrodes seemed to offer good recording features necessary for the reliable detection of $NO^{\bullet}$ in intact brains.

B. Fabre et al. showed an interesting voltammetric detection of $NO^{\bullet}$ in rat cortex based upon a carbon fiber microelectrode modified by a poly(*N*-methylpyrrole), incorporating a $[(H_2O)Fe^{III}PW_{11}O_{39}]^{4-}$ sublayer and covered by Nafion, and upon using differential normal pulse voltammetry (DNPV).[314] In solution, a linear response was reported between $NO^{\bullet}$ oxidation currents measured by DNPV and $NO^{\bullet}$ concentrations ranging from 10^{-7} to 10^{-3} M, with a sensitivity of 2.65 ± 0.15 nA/μM. This probe was then inserted in the rat brain and displayed good efficiency to detect in real time $NO^{\bullet}$ release. The validation of this last statement was supported by the electrode response decay after injections in the brain of a NO synthase inhibitor. Anesthetized male rats were used, and the rat head was immobilized in a stereotaxic frame. Then, the craniectomy was achieved by incising the cranial cutaneous plane. The skull was accessible, and the orifices allowing reference (occipital cortex), auxiliary (occipital cortex), and working (right frontal cortex) electrodes to be placed were made with a dentist's drill. As soon as the electrodes were implanted at 1 mm depth, DNPV measurements started (one cycle every 2 min). Over the +0.4 and 1.35 V range, an anodic peak was observed at 0.65 ± 0.02 V. This value was identical to the one determined by other authors.[238] The electrochemical response of this system was stabilized after 15 cycles. These results were encouraging because they demonstrated the ability of these sensors to detect $NO^{\bullet}$ under chronic conditions when inserted in the brain of a freely moving animal.

Commercial $NO^{\bullet}$ probes from WPI, based on Clark oxygen electrodes equipped with a gas permeable membrane (of unknown composition), were directly used by L. Cherian et al. in 2000.[315] Their tip diameter was 200 μm (ISO-NOP200, World Precision Instruments, Sarasota, FL), and their detection was based on the oxidation of $NO^{\bullet}$ at a working electrode potential of +0.85 V vs Ag/AgCl. Each electrode was calibrated before and after measurements with a $NO^{\bullet}$ donor: *S*-nitroso-*N*-acetly-D,L-pencillamine (SNAP). They were inserted into a rat brain at a depth of 1.5 mm after controlled cortical impact injury performed with an impactor tip (8 mm diameter) at a velocity of ~5 m/s, during ~130 ms and producing a brain deformation of 3 mm. Immediately after the injury, the $NO^{\bullet}$ sensor could be placed and an increase in $NO^{\bullet}$ concentrations was noted rising from baseline values up to a level of 83 ± 16 nM as compared with 0.5 ± 4 nM in the control animals. Then within minutes, $NO^{\bullet}$ concentrations fell and remained at an average of 25 nM lower than initial levels for at least 3 h after injury. The initial $NO^{\bullet}$ concentration increase was correlated with the rise in blood pressure and intracranial pressure in response to the initial injury. Pre-injury treatment with the NO synthase inhibitor L-NAME decreased the $NO^{\bullet}$ signal just after injury but resulted in higher intracranial hypertension. Henceforth, mortality was of 67% with L-NAME pre-treatment, as compared with 1% for untreated animals. These data suggested that reduced $NO^{\bullet}$ production plays a major role in the reduction of the cerebral blood flow after a severe traumatic brain injury.

Voltammetric measurements of extracellular $NO^{\bullet}$ in vivo directly in rat brain (nucleus tractus solitarius) were performed with carbon fiber microelectrode coated with Nafion and electropolymerized with *o*-phenylenediamine by W. C. Wu et al.[316] The sensors used were based on those proposed by M. N. Friedemann et al. in 1996.[305] This study was aimed to support increasing evidence that $NO^{\bullet}$ was involved in the central cardiovascular regulation. Therefore, the authors directly measured extracellular $NO^{\bullet}$ levels in anesthetized cats. They established that local application of L-arginine induced $NO^{\bullet}$ overflow, hypotension, and bradycardia in the nucleus tractus solitarius (NTS). Microinjections of L-NAME into the NTS elicited dose-dependent hypertension and decrease of $NO^{\bullet}$ levels, giving evidence that $NO^{\bullet}$ is tonically active on vessels in NTS and alternation of $NO^{\bullet}$ levels in NTS altering blood pressure in this region of brain. This last study brought another piece of evidence about the role of nitric oxide in controlling the brain vascular system, suggesting that $NO^{\bullet}$ is central for the control of vasodilation of blood vessels. This particular role of nitric oxide will be the subject of the following subsection.

3.7. Neurovascular Coupling: Toward the Electrochemical Detection of Nitric Oxide on a Single Cell Neuron

Neurons are the cells that perform the fundamental tasks of information integration and control. They gather, depending on the circuit to which they belong, process and relay specific types of information in the brain. There are increasing evidences that the neuronal activity itself can act as a key regulation factor for local cerebral perfusion and control of cerebral blood flow (CBF). It is well-established that when a local or global neuronal activity occurs in the brain, CBF does increase proportionally to the level of this activity.[317] This experimental fact named "neurovascular coupling" is localized to the active brain regions, and this close relationship "neuronal activity/CBF" has provided strategies for functional brain imaging and mapping using the changes in CBF as a clue of "brain working".[318,319] However, the vascular mechanisms by which a local neural activity commands CBF were still poorly understood at the beginning of the nineties despite the fact that this main hypothesis was developed by C. S. Roy and C. S. Sherrington since 1890.[320] These authors lucidly proposed that active neurons release vasoactive substances that diffuse to local vessels and induce their vasodilation leading to increasing local CBF.[321] In this section, we will report the works through which different authors have correlated measurements of vasoactive substances production, namely, nitric oxide, with CBF in brain tissues or intact brains. In this presentation, we will consider first studies involving groups of neurons to proceed up to recent studies investigating this correlation at the single cell level.

The group of T. Malinski proposed first the use of porphyrin microsensors (4−6 μm carbon fiber diameters) to measure cortical $NO^{\bullet}$ concentration within ischemic tissue (ischemia features inadequate blood supply to a local area due to blockade of the blood vessels to the area), in parallel with local cerebral blood flows measured by laser Doppler flowmetry.[322] Rat animals were anesthetized, and arterial catheters were placed in the right femoral artery and vein for continuous monitoring of mean blood pressure. A three-electrodes system was used for measurement of $NO^{\bullet}$ release. The working $NO^{\bullet}$ electrode was stereotaxically implanted perpendicularly in the ipsilateral parietal cortex; the counter (platinum wire of 0.25 mm) and reference electrodes were placed slightly further outside of the zone investigated. The regional CBF was measured with a flowmeter, and its changes were expressed as percentage change in flow. The preischemic or basal $NO^{\bullet}$ concentration in brain was found to be below the sensor's detection limit, that is, 10 nM. The maximum concentrations of $NO^{\bullet}$ during middle cerebral artery occlusion and reperfusion raised, respectively, up to 1.47 ± 0.45 and 0.54 ± 0.24 μM. Use of a NO synthase inhibitor, L-NAME, before inducing ischemia reduced $NO^{\bullet}$ release to 0.04 ± 0.02 μM during artery occlusion and totally inhibited it after reperfusion. Administration of L-arginine restored $NO^{\bullet}$ release but did not overcome the effect of L-NAME on mean arterial blood pressure. The appearance of the $NO^{\bullet}$ signal at +0.65 V (differential pulse voltammetry) as well as the sensitivity of the $NO^{\bullet}$ response to L-NAME injections were invoked as proof as the specificity of the sensors. Thanks to the reduced size of these $NO^{\bullet}$ sensors, $NO^{\bullet}$ production was detected in the cortex region of living rats from a few stimulated neurons. However, the stimulation was not selective but affected necessarily all of the neurons of the cortex, and the released $NO^{\bullet}$ could not be taken as originating from a single cell production.

The group of D. G. Buerk reported four interesting studies on the same subject from 1996 to 2004.[323−326] First, they performed direct electrochemical measurements of $NO^{\bullet}$ and simultaneous measurements of cat optic nerve head (ONH) blood flow by laser Doppler flowmetry (LDF) during neuronal activity increased by diffuse luminance flickering light stimuli. Cats were anesthetized. Nafion polymer-coated recessed gold microsensors with tip dimensions around 5 μm or less were used.[324] The microsensors were checked by detecting dissolved $NO^{\bullet}$ gas based on the electrochemical oxidation reaction:

$$NO^{\bullet} + 4OH^{-} \rightarrow NO_3^{-} + 2H_2O + 3e^{-} \qquad (19)$$

at a potential of +800 mV vs Ag/AgCl (amperometric techniques). Electrodes were placed near the ONH (<10 μm away) under microscope viewing, avoiding visible blood vessels. Experimental LDF and $NO^{\bullet}$ values were obtained during 10−15 Hz flicker at the maximum luminance from a photic stimulator. For normal physiological conditions, there was a consistent increase in ONH blood flow with each flicker stimulus. During the stimulus, $NO^{\bullet}$ increased by 88 $\pm$ 23 nM above basal $NO^{\bullet}$ levels. After inhibition by NO synthase inhibitors, $NO^{\bullet}$ concentrations were significantly lower. The authors concluded that $NO^{\bullet}$ plays a key vasodilatory role in the ONH by modulating blood flow during the enhancement of neuronal activity by light flicker stimuli.

Second, they determined the impact of elevated partial pressures of oxygen, or hyperoxia, on the steady state concentration of $NO^{\bullet}$ in the cerebral cortex. After animals were anesthetized, the scalp was removed, and a 4 mm hole was drilled through the skull with a bone drill. Rodents with implanted O_2- and NO-specific microelectrodes (these last are based on the ones of their first study) were analyzed.[325] In summary, cerebral cortex blood flow, measured by LDF probes, increased during hyperoxia (excess oxygen in body tissues or higher than normal partial pressure of oxygen) and caused elevations of steady-state NO concentrations. Hyperoxia was thus considered to initiate increase in $NO^{\bullet}$ synthesis.

Third, dynamic measurements of $NO^{\bullet}$ in tissue during functional activation of rat somatosensory cortex by forepaw stimulation associated with simultaneous blood flow measurements with LDF were performed.[323] In these two types of measurements, the electrodes were basically the same as before, a small opening being made in the thinned skull for positioning the $NO^{\bullet}$ sensing electrode at a precise angle so as to penetrate in the brain under the LDF probe. The $NO^{\bullet}$ microelectrode sampled over a much smaller and more spatially localized tissue volume than the LDF measurements. An initial peak of 125.5 ± 32.8 nM of $NO^{\bullet}$ was reported to occur within 400 ms after forepaw stimulation, followed by a rapid peak increase in blood flow. The delay noted between the $NO^{\bullet}$ peak and the change in blood flow might reflect the time required for the vascular muscle to relax. Indeed, this is thought to involve $NO^{\bullet}$ reaction with guanylate cyclase (supposedly active on dilation once activated by $NO^{\bullet}$ release from neuronal tissue) followed by an additional time featuring the effective vascular smooth muscle relaxation. Although the interpretation of local $NO^{\bullet}$ changes may be further complicated by its transport, the $NO^{\bullet}$ microelectrodes used herein in combination with LDF were crucial in linking the spatial and temporal changes in $NO^{\bullet}$ and blood flow.

In a fourth study, the same authors investigated the changes in $NO^{\bullet}$ concentrations in the cerebral cortex during experimental CO poisoning. In particular, *N*-methyl-D-aspartate (NMDA) sensitive neurons were investigated.[326] Rats were anesthetized, the $NO^{\bullet}$ electrode was placed into the cerebral cortex together with the LDF probe as described above, and the rats immobilized in a chamber were led to breath CO. Elevations in cortical $NO^{\bullet}$ concentration and in blood flow recorded as LDF were observed within minutes of exposure to CO. This was ascribed to neuronal NOS (nNOS) activation thanks to control experiments involving a selective nNOS inhibitor and experiments with nNOS knockout mice. Neuronal NOS activation appeared to be a consequence of NMDA neuronal receptors activation. In conclusion, these results demonstrated that the perivascular oxidative stress involving $NO^{\bullet}$ contributes to NMDA receptors activation. Large elevations in brain of $NO^{\bullet}$ concentration during CO exposure were attributable to nNOS activity linked to calcium influx through NMDA channels. Albeit they brought extremely important informations, the authors concluded that a precise understanding of the process by which each regional event communicates from the perivascular zone to neurons requires additional investigations.

This important dense work of the group of D. G. Buerk about the existence of links between species production ($NO^{\bullet}$) and cerebral perfusion offered a comprehensive view of the phenomenon to a local, yet macroscopic, level. However, as for T. Malinski's work, the stimulations were not selective and thus certainly triggered activity of all neurons of the scanned brain region. So, the $NO^{\bullet}$ signals were certainly due to a massive population of cells and maybe to collective/synergetic effects.

R. H. Fabian et al. developed an original study where they used a modification of a previously described electrochemical method to monitor superoxide anion and CBF in a model for understanding focal ischemia and reperfusion in cortical brain regions of living anesthetized rats.[257,327] A platinized carbon fiber electrode was coated with cytochrome *c* to respond to superoxide anion thanks to the fact that superoxide reduces cytochrome *c*, which is restored by giving back an electron to the electrode. This type of platinized carbon fiber electrode was initially designed for hydrogen−oxygen fuel cells; it used the same hydrogen−oxygen reaction as that sewing for hydrogen clearance measurements of CBF. This led the authors to propose that this sensor was ideal for coupling superoxide detection and CBF measurements. Superoxide anion concentration levels and CBF could then be measured simultaneously at almost the same tissue localization so that both local parameters could be correlated. Their results indicated that exposure of pial and cerebral vasculatures to a proinflammatory cytokine, IL-1β, increased cerebrovascular injury by accelerating recruitment of neutrophils, which produced superoxide anion during the reperfusion phase. However, the sensor was not specific for superoxide and could also react with H_2, for example. Moreover, the location of the probe in brain, because of its relatively big size (4 mm^2 surface area), was delicate and could even be critical because the probe could not detect local variability of CBF but averaged out the CBF variability over the pial surface.

The experimental limits encountered in the studies described above led recently the groups of C. Amatore and J. Rossier to define and apply a protocol for examining the nature of the neurovascular coupling at the level of a neuron and a few vessels in the cerebellum. As reported before in section 3.3.3, our group developed previously platinized carbon fiber microelectrodes for single-cell measurements of oxidative stress species. This type of simple modified electrode has been shown recently to match very well the conditions for measurements of species such as nitric oxide in brain tissues.[328] Platinized carbon microelectrodes were characterized in vitro in a configuration of μ-FIA (flow injection analysis at micrometric scale) vs solutions of nitric oxide, obtained from pure $NO^{\bullet}$ gas solubilized in PBS or from a $NO^{\bullet}$ donor (DEA-NO) in PBS.[328] The main advantages of these microelectrodes are their fast time response, their linear response in current over almost four decades of $NO^{\bullet}$ concentration, and their adjustable sensitivity through precise control of the quantity of black platinum deposited on their carbon-bevelled surface. Moreover, these microelectrodes of about 10 μm final diameter were designed to be sensitive only at the surface of their tip. In comparison with carbon fiber electrodes where the whole surface (shaft) of the fiber is uncovered and sensitive (see the review by R. M. Wightman in this issue), this property is essential for localized analyses aimed to investigate single cell behavior in a tissue such as the brain.

Studies of the neurovascular coupling could thus be achieved on acute slices of rat cerebellum with the aim of investigating the underlying hypothesis that certain neurons, the interneurons (stellate, basket, and granule cells), are the major actors involved in the control of cerebellar flow.[329,330] Practically, the tip of a 10 μm diameter platinized carbon fiber microelectrode was inserted via micromanipulation in the cerebellar slice (300 μm thick) at a few tens of micrometers depth to reach the undamaged molecular layer, which contains interneurons and microvessels (Figure 15). Simultaneously, microvessels dilatation or constriction was followed by infrared video microscopy. To warrant the validity and selectivity of the measurements, these studies were conducted in three steps. First, the slice was perfused with a solution of $NO^{\bullet}$ donor (DEA-NONoate 100 μM in PBS). The flux of nitric oxide diffusing into the slice was monitored by amperometry (650 mV vs SSCE) at the microelectrode surface, and a simultaneous dilatatation of microvessels was observed, asserting the direct relation between the two phenomena. Second, a selective pharmacological stimulation of nNOS containing neurons (see above) was achieved by NMDA. Although the whole slice was perfused, the release of $NO^{\bullet}$ was detected by the microelectrode in the close environment of a few neurons around that stimulated in the molecular layer. Local fluxes of about 150 amol of $NO^{\bullet}$ per second were recorded, which was sufficient to induce the dilatation of surrounding vessels. Control experiments with nNOS or neuronal activity inhibitors, or by applying a different detection potential at the microelectrode, demonstrated the strong specificity for nitric oxide in the monitored responses. These checks confirmed the validity of the electroanalytical approach so that the more challenging experiment consisting of measuring the release of $NO^{\bullet}$ by a single interneuron (stellate cells) of the cerebellum during the neuro-vascular coupling (Figure 15) was undertaken. This was achieved by placing the sensitive surface of a platinized microelectrode at less than 5 μm from a cell body while stimulating it electrically by patch clamp (whole cell technique) with a glass microelectrode (Figure 15A). Thus, the evoked neuronal activity was followed by a local minute release of $NO^{\bullet}$ at a rate of a few tens of amol/s,

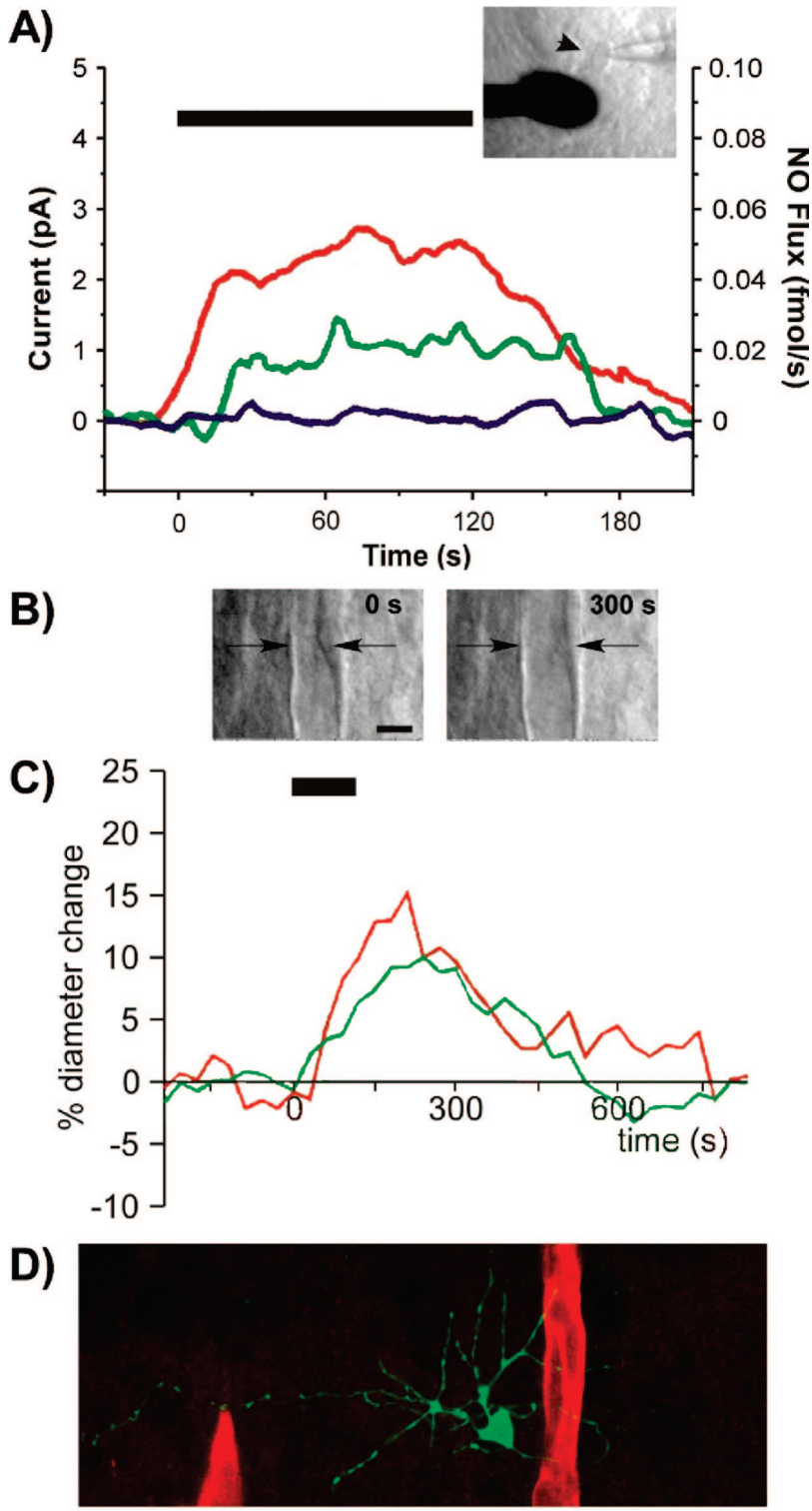

Figure 15. (A) Left axis, mean $NO^{\bullet}$ current induced by 2 min evoked firing (black line) of stellate neuron cells (containing NO synthases) recorded at 20−25 (green) or 30−35 °C (red) and of Purkinje neuron cells ("control" cells without NO synthases) recorded at 20−25 °C. Right axis, equivalent $NO^{\bullet}$ flux measured by the platinized carbon fiber microelectrode. Inset, location of the $NO^{\bullet}$ probe in the vicinity of a patched cell. (B) Infrared images of a responsive microvessel to depolarization of a stellate neuron cell illustrating diameter changes (indicated by the arrows) during the dilatation (left, preconstricted; right, evoked firing); scale bar, 10 μm. (C) Mean vascular dilation induced by 2 min of evoked firing (black line) of stellate neuron cells recorded at 20−25 (green) or 30−35 °C (red), showing no statistical differences between the two conditions. (D) Confocal image of a stimulated stellate neuron cell (biocytin labeled, green) and the responsive blood vessel (immunodetected for the protein laminin, red). The stimulated cell exhibits several neuronal processes coursing towards the reactive blood vessel, which is also shown in part B. Adapted from ref 329.

while a concomitant increase of nearby microvessels diameter was measured (Figure 15B,C). Besides, the stimulation in the same conditions of non-nitrergic cells such as Purkinje cells did not produce any release of electroactive compound nor vasodilatation. These experimentally challenging results thus demonstrated and quantified the major role of specific interneurons, namely, the stellate cells, in the fine-tuning of blood flow at the surface of cerebellum (illustrated by

fluorescence staining in Figure 15D) through local $NO^{\bullet}$ release during their activation. In addition, as apparent in Figure 15B microscopic views, the capillary dilatations occurred at specific areas where the capillary is initially constricted so as to impede the transit of red cells. The moderate but effective dilatation of such constrictions by the $NO^{\bullet}$ flux released by active neurons located within ca. 50 μm of such features allows the blood red cells transit. In other words, this work identified that blood supply regulation in the brain is finely controlled by a series of valves commanded by active neurons in their vicinity.

Finally, theorical models were reported to provide quantitative information on the local concentration of the flux of nitric oxide in the brain. Theoretical treatments were essentially designed to model the diffusion and action of $NO^{\bullet}$ in the brain (cerebellum) to quantify nitric oxide release in normal and pathological mechanisms of brain function.[331–334]

It was thus shown that the stimulated neuron produced an exceptional concentration of a few 100 nM at its surface. This concentration wave diffused spherically around the source so that a few nanomolar basal $NO^{\bullet}$ level was restored beyond a spherical volume of ca. 50 μm radius. In other words, the stimulated neuron "spoke" efficiently to any blood vessel located within this volume (50−70 μm mean separation between blood capillaries) and had no influence on the capillaries located further apart. In retrospect, this established that activation of large continuous domains of the brain, as evidenced by functional IRM or PET scan investigations, necessarily implies a continuous chain of active neurons stimulating an adjacent network of blood flow through a hopscotch pathway of local capillary controlled dilatation.[331]

4. Conclusions

The different aspects reviewed above clearly evidence that molecular electrochemistry at microelectrodes has brought many beneficial and original views to enhance the fine understanding of central processes of cellular biology. Initially, this field was considered as a topical curiosity, bringing notes of exotism among the community of electrochemistry. Yet, because of its growing success in addressing several central issues that could not be examined by any other techniques and to its spreading interest among neurobiologists, the area has rapidly widened; this is now a mature tool able to tackle the most difficult problems of cellular metabolism either at the single cell stage or in living tissues (see R. M. Wightman et al. in this issue).

This does not mean that the methods will stay in their present state of development because their successes claim for specific improvements so as to increase their time and topological resolution and adapt them to specific issues.

Also, it should be mentioned that since cells have highly variable metabolism even among single genetic lines, studies performed at the single cell level allow delineating precisely the extent and limits of these variabilities. However, the price for such performance is that substantiation of statistical issues generally requires fastidious repetition of series of experiments. A way to overcome this difficulty is offered by microfluidic manipulations of living cells. Because microelectrodes may be easily implemented onto microfluidic driven chips, it is expected that the next generation of methods will involve chips in which any selected and precise number of cells may be stimulated and examined electrochemically. This will also enable their coupling to different spectroscopic methods. Such devices are already appearing in the literature as outlined in the present review. Another predictable development is the coupling of the nanoelectrochemical biological probes to AFM, STM stages, or SECM to enable examination of cellular properties at the nanoscale level. Finally, decreasing the size of the electrodes to nanometric scales, including a few nanometer length of their shaft, should enable the harmless penetration of cellular compartments so as to more precisely investigate the central contribution of intracellular organelles, which presently cannot be resolved.

5. Acknowledgments

This work has been supported in parts by CNRS (UMR 8640-ENS-UPMC), Ecole Normale Supérieure (ENS), Universite Pierre and Marie Curie-Paris 6 (UPMC) and by the French Ministry of Research. We wish also to thank hearthly some of our collaborators whose names appear in the references regarding our group. This extends with a particular pleasure to Dr. Monique Vuillaume, with whom the studies on oxidative stress were initiated, and our more recent collaborators, viz., the group of Dr. Jean-Claude Drapier (ICSN-CNRS, France) and the group of Pr. Jean Rossier (ESPCI-CNRS, France).

6. References

(1) Burgoyne, R. D.; Morgan, A. *Physiol. Rev.* **2003**, *83*, 581.
(2) Sulzer, D.; Pothos, E. N. *Rev. Neurosci.* **2000**, *11*, 159.
(3) Sorensen, J. B. *Trends Neurosci.* **2005**, *28*, 453.
(4) Meldolesi, J.; Chieregatti, E.; Malosio, M. L. *Trends Cell Biol.* **2004**, *14*, 13.
(5) Chen, G. Y.; Ewing, A. G. *Crit. Rev. Neurobiol.* **1997**, *11*, 59.
(6) Cooper, B. R.; Jankowski, J. A.; Leszczyszyn, D. J.; Wightman, R. M.; Jorgenson, J. W. *Anal. Chem.* **1992**, *64*, 691.
(7) Ciolkowski, E. L.; Cooper, B. R.; Jankowski, J. A.; Jorgenson, J. W.; Wightman, R. M. *J. Am. Chem. Soc.* **1992**, *114*, 2815.
(8) Cooper, B. R.; Wightman, R. M.; Jorgenson, J. W. *J. Chromatogr. B: Biomed. Sci. Appl.* **1994**, *653*, 25.
(9) Kennedy, R. T.; Jorgenson, J. W. *Anal. Chem.* **1989**, *61*, 436.
(10) Kennedy, R. T.; Oates, M. D.; Cooper, B. R.; Nickerson, B.; Jorgenson, J. W. *Science* **1989**, *246*, 57.
(11) Hawley, M. D.; Tatawawa, S. V.; Piekarsk, S.; Adams, R. N. *J. Am. Chem. Soc.* **1967**, *89*, 447.
(12) Leszczyszyn, D. J.; Jankowski, J. A.; Viveros, O. H.; Diliberto, E. J.; Near, J. A.; Wightman, R. M. *J. Biol. Chem.* **1990**, *265*, 14736.
(13) Leszczyszyn, D. J.; Jankowski, J. A.; Viveros, O. H.; Diliberto, E. J.; Near, J. A.; Wightman, R. M. *J. Neurochem.* **1991**, *56*, 1855.
(14) Wightman, R. M.; Jankowski, J. A.; Kennedy, R. T.; Kawagoe, K. T.; Schroeder, T. J.; Leszczyszyn, D. J.; Near, J. A.; Diliberto, E. J.; Viveros, O. H. *Proc. Natl. Acad. Sci. U.S.A.* **1991**, *88*, 10754.
(15) Pihel, K.; Schroeder, T. J.; Wightman, R. M. *Anal. Chem.* **1994**, *66*, 4532.
(16) Paras, C. D.; Kennedy, R. T. *Anal. Chem.* **1995**, *67*, 3633.
(17) Paras, C. D.; Kennedy, R. T. *Electroanalysis* **1997**, *9*, 203.
(18) Travis, E. R.; Wightman, R. M. *Annu. Rev. Biophys. Biomol. Struct.* **1998**, *27*, 77.
(19) Westerink, R. H. S. *Neurotoxicology* **2004**, *25*, 461.
(20) Amatore, C. *C. R. Acad. Sci. Ser. IIb* **1996**, *323*, 757.
(21) Grabner, C. P.; Price, S. D.; Lysakowski, A.; Fox, A. P. *J. Neurophysiol.* **2005**, *94*, 2093.
(22) Jankowski, J. A.; Finnegan, J. M.; Wightman, R. M. *J. Neurochem.* **1994**, *63*, 1739.
(23) Haller, M.; Heinemann, C.; Chow, R. H.; Heidelberger, R.; Neher, E. *Biophys. J.* **1998**, *74*, 2100.
(24) Elhamdani, A.; Brown, M. E.; Artalejo, C. R.; Palfrey, H. C. *J. Neurosci.* **2000**, *20*, 2495.
(25) Elhamdani, A.; Palfrey, H. C.; Artalejo, C. R. *Neuron* **2001**, *31*, 819.
(26) Oberhauser, A. F.; Robinson, I. M.; Fernandez, J. M. *J. Physiol. (Paris)* **1995**, *89*, 71.
(27) Mosharov, E. V.; Sulzer, D. *Nat. Methods* **2005**, *2*, 651.
(28) Schroeder, T. J.; Borges, R.; Finnegan, J. M.; Pihel, K.; Amatore, C.; Wightman, R. M. *Biophys. J.* **1996**, *70*, 1061.
(29) Schroeder, T. J.; Jankowski, J. A.; Kawagoe, K. T.; Wightman, R. M.; Lefrou, C.; Amatore, C. *Anal. Chem.* **1992**, *64*, 3077.

(30) Koh, D. S.; Moody, M. W.; Nguyen, T. D.; Hille, B. *J. Gen. Physiol.* **2000**, *116*, 507.
(31) Jung, S. R.; Kim, M. H.; Hille, B.; Nguyen, T. D.; Koh, D. S. *Am. J. Physiol., Cell. Physiol.* **2004**, *286*, C573.
(32) Jung, S. R.; Kim, K.; Hille, B.; Nguyen, T. D.; Koh, D. S. *J. Physiol. (London)* **2006**, *576*, 163.
(33) Clark, R. A.; Ewing, A. G. *Mol. Neurobiol.* **1997**, *15*, 1.
(34) Tang, K. S.; Tse, A.; Tse, F. W. *J. Neurochem.* **2005**, *92*, 1126.
(35) Amatore, C.; Arbault, S.; Bonifas, I.; Bouret, Y.; Erard, M.; Guille, M. *ChemPhysChem* **2003**, *4*, 147.
(36) Elhamdani, A.; Palfrey, C. H.; Artalejo, C. R. *Neurobiol. Aging* **2002**, *23*, 287.
(37) Chen, T. K.; Luo, G. O.; Ewing, A. G. *Anal. Chem.* **1994**, *66*, 3031.
(38) Anderson, B. B.; Zerby, S. E.; Ewing, A. G. *J. Neurosci. Methods* **1999**, *88*, 163.
(39) Pothos, E.; Desmond, M.; Sulzer, D. *J. Neurochem.* **1996**, *66*, 629.
(40) Pihel, K.; Travis, E. R.; Borges, R.; Wightman, R. M. *Biophys. J.* **1996**, *71*, 1633.
(41) Oberhauser, A. F.; Robinson, I. M.; Fernandez, J. M. *Biophys. J.* **1996**, *71*, 1131.
(42) Borges, R.; Jaen, R.; Freire, F.; Gomez, J. F.; Villafruela, C.; Yanes, E. *Cell Tissue Res.* **2001**, *304*, 159.
(43) Kim, T. D.; Eddlestone, G. T.; Mahmoud, S. F.; Kuchtey, J.; Fewtrell, C. *J. Biol. Chem.* **1997**, *272*, 31225.
(44) Mahmoud, S. F.; Fewtrell, C. *J. Cell Biol.* **2001**, *153*, 339.
(45) Kennedy, R. T.; Huang, L.; Atkinson, M. A.; Dush, P. *Anal. Chem.* **1993**, *65*, 1882.
(46) Smith, P. A.; Duchen, M. R.; Ashcroft, F. M. *Pflügers Arch.* **1995**, *430*, 808.
(47) Aspinwall, C. A.; Brooks, S. A.; Kennedy, R. T.; Lakey, J. R. T. *J. Biol. Chem.* **1997**, *272*, 31308.
(48) Ardiles, A. O.; Maripillan, J.; Lagos, V. L.; Toro, R.; Mora, I. G.; Villarroel, L.; Ales, E.; Borges, R.; Cardenas, A. M. *J. Neurochem.* **2006**, *99*, 29.
(49) Bian, X. C.; Patel, B.; Dai, X. L.; Galligan, J. J.; Swain, G. *Gastroenterology* **2007**, *132*, 2438.
(50) Patel, B. A.; Bian, X. H.; Quaiserova-Mocko, V.; Galligan, J. J.; Swain, G. M. *Analyst* **2007**, *132*, 41.
(51) Bruns, D.; Jahn, R. *Nature* **1995**, *377*, 62.
(52) Bruns, D.; Riedel, D.; Klingauf, J.; Jahn, R. *Neuron* **2000**, *28*, 205.
(53) Bruns, D. *Methods* **2004**, *33*, 312.
(54) Chen, G. Y.; Gavin, P. F.; Luo, G. O.; Ewing, A. G. *J. Neurosci.* **1995**, *15*, 7747.
(55) Chen, G. Y.; Ewing, A. G. *Brain Res.* **1995**, *701*, 167.
(56) Chen, G. Y.; Gutman, D. A.; Zerby, S. E.; Ewing, A. G. *Brain Res.* **1996**, *733*, 119.
(57) Anderson, B. B.; Ewing, A. G. *J. Pharm. Biomed. Anal.* **1999**, *19*, 15.
(58) Anderson, B. B.; Chen, G. Y.; Gutman, D. A.; Ewing, A. G. *J. Neurosci. Methods* **1999**, *88*, 153.
(59) Patel, B. A.; Arundell, M.; Parker, K. H.; Yeoman, M. S.; O'Hare, D. *J. Chromatogr., B: Anal. Technol. Biomed. Life Sci.* **2005**, *818*, 269.
(60) Marinesco, P.; Carew, T. J. *J. Neurosci.* **2002**, *22*, 2299.
(61) Zhou, Z.; Misler, S. *Proc. Natl. Acad. Sci. U.S.A.* **1995**, *92*, 6938.
(62) Staal, R. G. W.; Mosharov, E. V.; Sulzer, D. *Nat. Neurosci.* **2004**, *7*, 341.
(63) Gillis, M. A.; Anctil, M. *J. Neurochem.* **2001**, *76*, 1774.
(64) Jaffe, E. H.; Marty, A.; Schulte, A.; Chow, R. H. *J. Neurosci.* **1998**, *18*, 3548.
(65) Pothos, E. N.; Davila, V.; Sulzer, D. *J. Neurosci.* **1998**, *18*, 4106.
(66) Hochstetler, S. E.; Puopolo, M.; Gustincich, S.; Raviola, E.; Wightman, R. M. *Anal. Chem.* **2000**, *72*, 489.
(67) Cahill, P. S.; Walker, Q. D.; Finnegan, J. M.; Mickelson, G. E.; Travis, E. R.; Wightman, R. M. *Anal. Chem.* **1996**, *68*, 3180.
(68) Chow, R. H.; Vonruden, L.; Neher, E. *Nature* **1992**, *356*, 60.
(69) Zhou, Z.; Misler, S. *J. Biol. Chem.* **1996**, *271*, 270.
(70) Kawagoe, K. T.; Jankowski, J. A.; Wightman, R. M. *Anal. Chem.* **1991**, *63*, 1589.
(71) Zhang, X. J.; Ogorevc, B.; Rupnik, M.; Kreft, M.; Zorec, R. *Anal. Chim. Acta* **1999**, *378*, 135.
(72) Huang, L.; Shen, H.; Atkinson, M. A.; Kennedy, R. T. *Proc. Natl. Acad. Sci. U.S.A.* **1995**, *92*, 9608.
(73) Fernandez-Peruchena, C.; Navas, S.; Montes, M. A.; De Toledo, G. A. *Brain Res. Rev.* **2005**, *49*, 406.
(74) De Toledo, G. A.; Fernandez-Chacon, R.; Fernandez, J. M. *Nature* **1993**, *363*, 554.
(75) Wightman, R. M.; Schroeder, T. J.; Finnegan, J. M.; Ciolkowski, E. L.; Pihel, K. *Biophys. J.* **1995**, *68*, 383.
(76) Amatore, C.; Arbault, S.; Bonifas, I.; Bouret, Y.; Erard, M.; Ewing, A. G.; Sombers, L. A. *Biophys. J.* **2005**, *88*, 4411.
(77) Jankowski, J. A.; Schroeder, T. J.; Ciolkowski, E. L.; Wightman, R. M. *J. Biol. Chem.* **1993**, *268*, 14694.
(78) Amatore, C.; Bouret, Y.; Midrier, L. *Chem. Eur. J.* **1999**, *5*, 2151.
(79) Sombers, L. A.; Hanchar, H. J.; Colliver, T. L.; Wittenberg, N.; Cans, A.; Arbault, S.; Amatore, C.; Ewing, A. G. *J. Neurosci.* **2004**, *24*, 303.
(80) Pothos, E. N.; Mosharov, E.; Liu, K. P.; Setlik, W.; Haburcak, M.; Baldini, G.; Gershon, M. D.; Tamir, H.; Sulzer, D. *J. Physiol. (London)* **2002**, *542*, 453.
(81) Amatore, C.; Arbault, S.; Bonifas, I.; Guille, M.; Lemaître, F.; Verchier, Y. *Biophys. Chem.* **2007**, *129*, 181.
(82) Sombers, L. A.; Maxson, M. M.; Ewing, A. G. *J. Neurochem.* **2005**, *93*, 1122.
(83) Braun, M.; Wendt, A.; Karanauskaite, J.; Galvanovskis, J.; Clark, A.; MacDonald, P. E.; Rorsman, P. *J. Gen. Physiol.* **2007**, *129*, 221.
(84) Duncan, R. R.; Greaves, J.; Wiegand, U. K.; Matskovich, I.; Bodammer, G.; Apps, D. K.; Shipston, M. J.; Chow, R. H. *Nature* **2003**, *422*, 176.
(85) Grabner, C. P.; Fox, A. P. *J. Neurophysiol.* **2006**, *96*, 3082.
(86) Bonifas, I. Ph.D. Thesis, Université Pierre et Marie Curie, Paris 6, Paris, France, 2004.
(87) Zhou, Z.; Misler, S.; Chow, R. H. *Biophys. J.* **1996**, *70*, 1543.
(88) Neher, E. *Nature* **1993**, *363*, 497.
(89) Wang, C. T.; Grishanin, R.; Earles, C. A.; Chang, P. Y.; Martin, T. F. J.; Chapman, E. R.; Jackson, M. B. *Science* **2001**, *294*, 1111.
(90) Constable, J. R. L.; Graham, M. E.; Morgan, A.; Burgoyne, R. D. *J. Biol. Chem.* **2005**, *280*, 31615.
(91) Barclay, J. W.; Aldea, M.; Craig, T. J.; Morgan, A.; Burgoyne, R. D. *J. Biol. Chem.* **2004**, *279*, 41495.
(92) Graham, M. E.; Barclay, J. W.; Burgoyne, R. D. *J. Biol. Chem.* **2004**, *279*, 32751.
(93) Borisovska, M.; Zhao, Y.; Tsytsyura, Y.; Glyvuk, N.; Takamori, S.; Matti, U.; Rettig, J.; Sudhof, T.; Bruns, D. *EMBO J.* **2005**, *24*, 2114.
(94) Schutz, D.; Zilly, F.; Lang, T.; Jahn, R.; Bruns, D. *Eur. J. Neurosci.* **2005**, *21*, 2419.
(95) Han, X.; Jackson, M. B. *J. Cell Biol.* **2006**, *172*, 281.
(96) Albillos, A.; Dernick, G.; Horstmann, H.; Almers, W.; De Toledo, G. A.; Lindau, M. *Nature* **1997**, *389*, 509.
(97) Dernick, G.; De Toledo, G. A.; Lindau, M. *Nat. Cell Biol.* **2003**, *5*, 358.
(98) Tabares, L.; Lindau, M.; De Toledo, G. A. *Biochem. Soc. Trans.* **2003**, *31*, 837.
(99) Schroeder, T. J.; Jankowski, J. A.; Senyshyn, J.; Holz, R. W.; Wightman, R. M. *J. Biol. Chem.* **1994**, *269*, 17215.
(100) Robinson, I. M.; Finnegan, J. M.; Monck, J. R.; Wightman, R. M.; Fernandez, J. M. *Proc. Natl. Acad. Sci. U.S.A.* **1995**, *92*, 2474.
(101) Gutierrez, L. M.; Gil, A.; Viniegra, S. *Eur. J. Cell Biol.* **1998**, *76*, 274.
(102) Paras, C. D.; Qian, W. J.; Lakey, J. R.; Tan, W. H.; Kennedy, R. T. *Cell Biochem. Biophys.* **2000**, *33*, 227.
(103) Qian, W. J.; Aspinwall, C. A.; Battiste, M. A.; Kennedy, R. T. *Anal. Chem.* **2000**, *72*, 711.
(104) Wu, W. Z.; Huang, W. H.; Wang, W.; Wang, Z. L.; Cheng, J. K.; Xu, T.; Zhang, R. Y.; Chen, Y.; Liut, J. *J. Am. Chem. Soc.* **2005**, *127*, 8914.
(105) Zhang, B.; Adams, K. L.; Luber, S. J.; Eves, D. J.; Heien, M. L.; Ewing, A. G. *Anal. Chem.* **2008**, *80*, 1394.
(106) Burgoyne, R. D.; Barclay, J. W. *Trends Neurosci.* **2002**, *25*, 176.
(107) Amatore, C.; Arbault, S.; Bonifas, I.; Lemaître, F.; Verchier, Y. *ChemPhysChem* **2007**, *8*, 578.
(108) Anderson, B. B.; Chen, G. Y.; Gutman, D. A.; Ewing, A. G. *Brain Res.* **1998**, *788*, 294.
(109) Westerink, R. H. S.; de Groot, A.; Vijverberg, H. P. M. *Biochem. Biophys. Res. Commun.* **2000**, *270*, 625.
(110) Amatore, C.; Bouret, Y.; Travis, E. R.; Wightman, R. M. *Biochimie* **2000**, *82*, 481.
(111) Amatore, C.; Bouret, Y.; Travis, E. R.; Wightman, R. M. *Angew. Chem., Int. Ed.* **2000**, *39*, 1952.
(112) Chizmadzhev, Y. A.; Cohen, F. S.; Shcherbakov, A.; Zimmerberg, J. *Biophys. J.* **1995**, *69*, 2489.
(113) Chizmadzhev, Y. A.; Kuzmin, P. I.; Kumenko, D. A.; Zimmerberg, J.; Cohen, F. S. *Biophys. J.* **2000**, *78*, 2241.
(114) Farrell, B.; Cox, S. J. *Bull. Math. Biol.* **2002**, *64*, 979.
(115) Fan, T. H.; Fedorov, A. G. *Anal. Chem.* **2004**, *76*, 4395.
(116) Amatore, C.; Arbault, S.; Guille, M.; Lemaître, F. *ChemPhysChem* **2007**, *8*, 1597.
(117) Teschemacher, A. G. *Auton. Neurosci. Basic Clin.* **2005**, *117*, 1.
(118) Kennedy, R. T.; Lan, H. A.; Aspinwall, C. A. *J. Am. Chem. Soc.* **1996**, *118*, 1795.
(119) Taylor, S. C.; Roberts, M. L.; Peers, C. *J. Physiol. (London)* **1999**, *519*, 765.
(120) Camacho, M.; Machado, J. D.; Montesinos, M. S.; Criado, M.; Borges, R. *J. Neurochem.* **2006**, *96*, 324.
(121) Haynes, C. L.; Buhler, L. A.; Wightman, R. M. *Biophys. Chem.* **2006**, *123*, 20.

(122) Almers, W. *Nature* **2001**, *409*, 567.
(123) An, S. J.; Almers, W. *Science* **2004**, *306*, 1042.
(124) Gil, A.; Viniegra, S.; Gutierrez, L. M. *Eur. J. Neurosci.* **1998**, *10*, 3369.
(125) Fisher, R. J.; Burgoyne, R. D. *Pflügers Arch.* **1999**, *437*, 754.
(126) Graham, M. E.; Fisher, R. J.; Burgoyne, R. D. *Biochimie* **2000**, *82*, 469.
(127) Quetglas, S.; Iborra, C.; Sasakawa, N.; De Haro, L.; Kumakura, K.; Sato, K.; Leveque, C.; Seagar, M. *EMBO J.* **2002**, *21*, 3970.
(128) Criado, M.; Gil, A.; Viniegra, S.; Gutierrez, L. M. *Proc. Natl. Acad. Sci. U.S.A.* **1999**, *96*, 7256.
(129) Graham, M. E.; Burgoyne, R. D. *J. Neurosci.* **2000**, *20*, 1281.
(130) Fisher, R. J.; Pevsner, J.; Burgoyne, R. D. *Science* **2001**, *291*, 875.
(131) Burgoyne, R. D.; Fisher, R. J.; Graham, M. E.; Haynes, L. P.; Morgan, A. *Biochem. Soc. Trans.* **2001**, *29*, 467.
(132) Archer, D. A.; Graham, M. E.; Burgoyne, R. D. *J. Biol. Chem.* **2002**, *277*, 18249.
(133) Amatore, C.; Arbault, S.; Guille, M.; Lemaître, F.; Verchier, Y. *ChemBioChem* **2006**, *7*, 1998.
(134) Uchiyama, Y.; Maxson, M. M.; Sawada, T.; Nakano, A.; Ewing, A. G. *Brain Res.* **2007**, *1151*, 46.
(135) Borges, R.; Travis, E. R.; Hochstetler, S. E.; Wightman, R. M. *J. Biol. Chem.* **1997**, *272*, 8325.
(136) Troyer, K. P.; Wightman, R. M. *J. Biol. Chem.* **2002**, *277*, 29101.
(137) Marszalek, P. E.; Farrell, B.; Verdugo, P.; Fernandez, J. M. *Biophys. J.* **1997**, *73*, 1169.
(138) Taylor, S. C.; Peers, C. *J. Neurochem.* **2000**, *75*, 1583.
(139) Tang, Y. M.; Travis, E. R.; Wightman, R. M.; Schneider, A. S. *J. Neurochem.* **2000**, *74*, 702.
(140) Lerner, I.; Trus, M.; Cohen, R.; Yizhar, O.; Nussinovitch, I.; Atlas, D. *J. Neurochem.* **2006**, *97*, 116.
(141) Haynes, C. L.; Siff, L. N.; Wightman, R. M. *Biochim. Biophys. Acta, Mol. Cell Res.* **2007**, *1173*, 728.
(142) Walker, A.; Glavinovic, M. I.; Trifaro, J. M. *Pflugers Arch.* **1996**, *432*, 885.
(143) Mundorf, M. L.; Hochstetler, S. E.; Wightman, R. M. *J. Neurochem.* **1999**, *73*, 2397.
(144) Machado, J. D.; Gomez, J. F.; Betancor, G.; Camacho, M.; Brioso, M. A.; Borges, R. *Circ. Res.* **2002**, *91*, 830.
(145) Taylor, S. C.; Peers, C. *Biochem. Biophys. Res. Commun.* **1998**, *248*, 13.
(146) Fu, X. W.; Nurse, C. A.; Wong, V.; Cutz, E. *J. Physiol. (London)* **2002**, *539*, 503.
(147) Machado, J. D.; Segura, F.; Brioso, M. A.; Borges, R. *J. Biol. Chem.* **2000**, *275*, 20274.
(148) Westerink, R. H. S.; Vijverberg, H. P. M. *Neurosci. Lett.* **2002**, *326*, 81.
(149) Angleson, J. K.; Betz, W. J. *Trends Neurosci.* **1997**, *20*, 281.
(150) Henry, J. P.; Darchen, F.; Cribier, S. *Biochimie* **1998**, *80*, 371.
(151) Fernandez-Chacon, R.; De Toledo, G. A. *FEBS Lett.* **1995**, *363*, 221.
(152) Engisch, K. L.; Chernevskaya, N. I.; Nowycky, M. C. *J. Neurosci.* **1997**, *17*, 9010.
(153) Xu, T.; Binz, T.; Niemann, H.; Neher, E. *Nat. Neurosci.* **1998**, *1*, 192.
(154) Bokvist, K.; Holmqvist, M.; Gromada, J.; Rorsman, P. *Pflügers Arch.* **2000**, *439*, 634.
(155) Di, A.; Krupa, B.; Bindokas, V. P.; Chen, Y. M.; Brown, M. E.; Palfrey, H. C.; Naren, A. P.; Kirk, K. L.; Nelson, D. J. *Nat. Cell Biol.* **2002**, *4*, 279.
(156) Chan, S. A.; Smith, C. *J. Physiol. (London)* **2001**, *537*, 871.
(157) Chan, S. A.; Chow, R.; Smith, C. *Pflügers Arch.* **2003**, *445*, 540.
(158) Takahashi, N.; Kadowaki, T.; Yazaki, Y.; Miyashita, Y.; Kasai, H. *J. Cell Biol.* **1997**, *138*, 55.
(159) Dernick, G.; Gong, L. W.; Tabares, L.; De Toledo, G. A.; Lindau, M. *Nat. Methods* **2005**, *2*, 699.
(160) Ales, E.; Tabares, L.; Poyato, J. M.; Valero, V.; Lindau, M.; De Toledo, G. A. *Nat. Cell Biol.* **1999**, *1*, 40.
(161) Gong, L. W.; Hafez, I.; De Toledo, G. A.; Lindau, M. *J. Neurosci.* **2003**, *23*, 7917.
(162) Finnegan, J. M.; Borges, R.; Wightman, R. M. *Neuroscience* **1996**, *71*, 833.
(163) Anderova, M.; Duchene, A. D.; Barbara, J. G.; Takeda, K. *Brain Res.* **1998**, *809*, 97.
(164) Kang, G. X.; Holz, G. G. *J. Physiol. (London)* **2003**, *546*, 175.
(165) Xin, Q.; Wightman, R. M. *Anal. Chem.* **1998**, *70*, 1677.
(166) Hafez, I.; Kisler, K.; Berberian, K.; Dernick, G.; Valero, V.; Yong, M. G.; Craighead, H. G.; Lindau, M. *Proc. Natl. Acad. Sci. U.S.A.* **2005**, *102*, 13879.
(167) Amatore, C.; Arbault, S.; Chen, Y.; Crozatier, C.; Lemaître, F.; Verchier, Y. *Angew. Chem., Int. Ed.* **2006**, *45*, 4000.
(168) Koh, D. S.; Hille, B. *J. Neurosci. Methods* **1999**, *88*, 83.
(169) Borges, R.; Diaz, J.; Camacho, M.; Machado, J. D. *Pflügers Arch.* **2005**, *450*, 280.
(170) Chen, P.; Xu, B.; Tokranova, N.; Feng, X. J.; Castracane, J.; Gillis, K. D. *Anal. Chem.* **2003**, *75*, 518.
(171) Sun, X. H.; Gillis, K. D. *Anal. Chem.* **2006**, *78*, 2521.
(172) Chen, X. H.; Gao, Y. F.; Hossain, M.; Gangopadhyay, S.; Gillis, K. D. *Lab Chip* **2008**, *8*, 161.
(173) Amatore, C.; Arbault, S.; Lemaître, F.; Verchier, Y. *Biophys. Chem.* **2007**, *127*, 165.
(174) Spégel, C.; Heiskanen, A.; Acklid, J.; Wolff, A.; Taboryski, R.; Emneus, J.; Ruzgas, T. *Electroanalysis* **2007**, *19*, 263.
(175) Spegel, C.; Heiskanen, A.; Pedersen, S.; Emneus, J.; Ruzgas, T.; Taboryski, R. *Lab Chip* **2008**, *8*, 323.
(176) Cui, H. F.; Ye, J. S.; Chen, Y.; Chong, S. C.; Liu, X.; Lim, T. M.; Sheu, F. S. *Sens. Actuators, B* **2006**, *115*, 634.
(177) Hengstenberg, A.; Blochl, A.; Dietzel, I. D.; Schuhmann, W. *Angew. Chem., Int. Ed.* **2001**, *40*, 905.
(178) Liebetrau, J. M.; Miller, H. M.; Baur, J. E. *Anal. Chem.* **2003**, *75*, 563.
(179) Bauermann, L. P.; Schuhmann, W.; Schulte, A. *Phys. Chem. Chem. Phys.* **2004**, *6*, 4003.
(180) Amemiya, S.; Guo, J. D.; Xiong, H.; Gross, D. A. *Anal. Bioanal. Chem.* **2006**, *386*, 458.
(181) Finkel, T. *Curr. Opin. Cell Biol.* **2003**, *15*, 247.
(182) *The Oxygen Paradox*; Davies, K. J. A., Ursini, F., Eds.; CLEUP University Press: Padova, 1995.
(183) Halliwell, B.; Gutteridge, J. M. C. *Free Radicals in Biology and Medecine*, 3rd ed.; Oxford University Press: Oxford, 1999.
(184) Balaban, R. S.; Nemoto, S.; Finkel, T. *Cell* **2005**, *120*, 483.
(185) Inoue, M.; Sato, E. F.; Nishikawa, M.; Park, A. M.; Kira, Y.; Imada, I.; Utsumi, K. *Curr. Med. Chem.* **2003**, *10*, 2495.
(186) Kinnula, V. L.; Crapo, J. D. *Free Radical Biol. Med.* **2004**, *36*, 718.
(187) Landis, G. N.; Tower, J. *Mech. Ageing Dev.* **2005**, *126*, 365.
(188) Maier, C. M.; Chan, P. H. *Neuroscientist* **2002**, *8*, 323.
(189) Miller, A. F. *Curr. Opin. Chem. Biol.* **2004**, *8*, 162.
(190) Niviere, V.; Fontecave, M. *J. Biol. Inorg. Chem.* **2004**, *9*, 119.
(191) Zelko, I. N.; Mariani, T. J.; Folz, R. J. *Free Radical Biol. Med.* **2002**, *33*, 337.
(192) Burkitt, M. J. *Prog. React. Kinet. Mech.* **2003**, *28*, 75.
(193) Arnes, B. N.; Shigenagra, M. K., In *Molecular Biology of Free Radical Scavenging Systems*; Scandalios, J. S., Ed.; Cold Spring Harbor Laboratory Press: New York, 1992; pp 1–122.
(194) Chance, B. *Arch. Biochem. Biophys.* **1952**, *41*, 404.
(195) Chance, B.; Maehly, A. C. *Methods Enzymol.* **1955**, *2*, 764.
(196) *Metabolic Compartmentation*; Sies, H., Ed.; Academic Press: New York, 1982.
(197) Dequaire, M.; Limoges, B.; Moiroux, J.; Saveant, J. M. *J. Am. Chem. Soc.* **2002**, *124*, 240.
(198) Lardinois, O. M.; Mestdagh, M. M.; Rouxhet, P. G. *Biochim. Biophys. Acta, Protein Struct. Mol. Enzymol.* **1996**, *1295*, 222.
(199) Bedard, K.; Krause, K. H. *Physiol. Rev.* **2007**, *87*, 245.
(200) Groemping, Y.; Rittinger, K. *Biochem. J.* **2005**, *386*, 401.
(201) Robinson, J. M.; Ohira, T.; Badwey, J. A. *Histochem. Cell Biol.* **2004**, *122*, 293.
(202) Segal, A. W. *Mol. Med. Today* **1996**, 129.
(203) Segal, A. W.; Abo, A. *Trends Biochem. Sci.* **1993**, *18*, 43.
(204) Alderton, W. K.; Cooper, C. E.; Knowles, R. G. *Biochem. J.* **2001**, *357*, 593.
(205) Li, H. Y.; Poulos, T. L. *J. Inorg. Biochem.* **2005**, *99*, 293.
(206) Southan, G. J.; Szabo, C. *Biochem. Pharmacol.* **1996**, *51*, 383.
(207) Stuehr, D. J. *Biochim. Biophys. Acta, Bioenerg.* **1999**, *1411*, 217.
(208) Koppenol, W. H. *Free Radical Biol. Med.* **1998**, *25*, 385.
(209) Koppenol, W. H.; Moreno, J. J.; Pryor, W. A.; Ischiropoulos, H.; Beckman, J. S. *Chem. Res. Toxicol.* **1992**, *5*, 834.
(210) Nauser, T.; Koppenol, W. H. *J. Phys. Chem. A* **2002**, *106*, 4084.
(211) Kissner, R.; Beckman, J. S.; Koppenol, W. H. *Methods Enzymol.* **1999**, *301*, 342.
(212) Kissner, R.; Koppenol, W. H. *J. Am. Chem. Soc.* **2002**, *124*, 234.
(213) Pacher, P.; Beckman, J. S.; Liaudet, L. *Physiol. Rev.* **2007**, *87*, 315.
(214) Meli, R.; Nauser, T.; Latal, P.; Koppenol, W. H. *J. Biol. Inorg. Chem.* **2002**, *7*, 31.
(215) Nauser, T.; Merkofer, M.; Kissner, R.; Koppenol, W. H. *Chem. Res. Toxicol.* **2001**, *14*, 348.
(216) Herold, S.; Exner, M.; Boccini, F. *Chem. Res. Toxicol.* **2003**, *16*, 390.
(217) Kirsch, M.; Korth, H. G.; Wensing, A.; Sustmann, R.; de Groot, H. *Arch. Biochem. Biophys.* **2003**, *418*, 133.
(218) Pfeiffer, S.; Gorren, A. C. F.; Schimdt, K.; Werner, E. R.; Hansert, B.; Bohle, D. S.; Mayer, B. *J. Biol. Chem.* **1997**, *272*, 3465.
(219) Ford, P. C.; Wink, D. A.; Stanbury, D. M. *FEBS Lett.* **1993**, *326*, 1.
(220) Pogrebnaya, V. L.; Usov, A. P.; Baranov, A. V.; Nesterenko, A. I.; Bezyazychnyi, P. I. *J. Appl. Chem. USSR* **1975**, *48*, 1004.
(221) Koppenol, W. H. *Methods Enzymol.* **1996**, *268*, 7.
(222) Lee, K. Y.; Amatore, C.; Kochi, J. K. *J. Phys. Chem.* **1991**, *95*, 1285.

(223) Gaudry-Talarmain, Y. M.; Moulian, N.; Meunier, F. A.; Blanchard, B.; Angaut-Petit, D.; Faille, L.; Ducrocq, C. *Nitric Oxide-Biol. Chem.* **1997**, *1*, 330.
(224) Possel, H.; Noack, H.; Augustin, W.; Keilhoff, G.; Wolf, G. *FEBS Lett.* **1997**, *416*, 175.
(225) Possel, H.; Noack, H.; Keilhoff, G.; Wolf, G. *Glia* **2002**, *38*, 339.
(226) Wang, P. H.; Zweier, J. L. *J. Biol. Chem.* **1996**, *271*, 29223.
(227) Kurz, C.; Zeng, X. Q.; Hannemann, S.; Kissner, R.; Koppenol, W. H. *J. Phys. Chem. A* **2005**, *109*, 965.
(228) Amatore, C.; Arbault, S.; Bruce, D.; De Oliveira, P.; Erard, M.; Vuillaume, M. *Chem. Eur. J.* **2001**, *7*, 4171.
(229) Green, M. J.; Hill, H. A. O.; Tew, D. G.; Walton, N. J. *FEBS Lett.* **1984**, *170*, 69.
(230) Hill, H. A. O.; Tew, D. G.; Walton, N. J. *FEBS Lett.* **1985**, *191*, 257.
(231) Yuasa, M.; Oyaizu, K. *Curr. Org. Chem.* **2005**, *9*, 1685.
(232) Shibuki, K. *Neurosci. Res.* **1990**, *9*, 69.
(233) Lee, Y.; Kim, J. *Anal. Chem.* **2007**, *79*, 7669.
(234) Lee, Y.; Oh, B. K.; Meyerhoff, M. E. *Anal. Chem.* **2004**, *76*, 536.
(235) Pinsky, D. J.; Patton, S.; Mesaros, S.; Brovkovych, V.; Kubaszewski, E.; Grunfeld, S.; Malinski, T. *Circ. Res.* **1997**, *81*, 372.
(236) Bedioui, F.; Villeneuve, N. *Electroanalysis* **2003**, *15*, 5.
(237) Ciszewski, A.; Milczarek, G. *Talanta* **2003**, *61*, 11.
(238) Malinski, T.; Taha, Z. *Nature* **1992**, *358*, 676.
(239) Lantoine, F.; Trevin, S.; Bedioui, F.; Devynck, J. *J. Electroanal. Chem.* **1995**, *392*, 85.
(240) Mitchell, K. M.; Michaelis, E. K. *Electroanalysis* **1998**, *10*, 81.
(241) Xue, J.; Ying, X. Y.; Chen, J. S.; Xian, Y. H.; Jin, L. T.; Jin, J. *Anal. Chem.* **2000**, *72*, 5313.
(242) Cortes, J. S.; Granados, S. G.; Ordaz, A. A.; Jimenez, J. A. L.; Griveau, S.; Bedioui, F. *Electroanalysis* **2007**, *19*, 61.
(243) Green, M. J.; Hill, H. A. O.; Tew, D. G. *FEBS Lett.* **1987**, *216*, 31.
(244) Isogai, Y.; Tsuyama, T.; Osada, H.; Iizuka, T.; Tanaka, K. *FEBS Lett.* **1996**, *380*, 263.
(245) Tanaka, T. T.; Yusho, K.; Tetsutaro, I. *Bioelectrochem. Bioenerg.* **1996**, *41*, 201.
(246) Mesaros, S.; Vankova, Z.; Grunfeld, S.; Mesarosova, A.; Malinski, T. *Anal. Chim. Acta* **1998**, *358*, 27.
(247) Pontie, M.; Bedioui, F. *Analusis* **1999**, *27*, 564.
(248) Villeneuve, N.; Bedioui, F.; Voituriez, K.; Avaro, S.; Vilaine, J. P. *J. Pharmacol. Toxicol. Methods* **1998**, *40*, 95.
(249) Xue, J. A.; Xian, Y. Z.; Ying, X. Y.; Chen, J. S.; Wang, L.; Jin, L. T. *Anal. Chim. Acta* **2000**, *405*, 77.
(250) Privat, C.; Stepien, O.; David-Dufilho, M.; Brunet, A.; Bedioui, F.; Marche, P.; Devynck, J. *Free Radical Biol. Med.* **1999**, *27*, 554.
(251) McNeil, C. J.; Smith, K. A.; Bellavite, P.; Bannister, J. V. *Free Radical Res. Commun.* **1989**, *7*, 89.
(252) Cooper, J. M.; Greenough, K. R.; McNeil, C. J. *J. Electroanal. Chem.* **1993**, *347*, 267.
(253) Manning, P.; McNeil, C. J.; Cooper, J.; Hillhouse, E. *Free Radical Biol. Med.* **1998**, *24*, 1304.
(254) Tammeveski, K.; Tenno, T. T.; Mashirin, A. A.; Hillhouse, E. W.; Manning, P.; McNeil, C. J. *Free Radical Biol. Med.* **1998**, *25*, 973.
(255) Tolias, C. M.; McNeil, C. J.; Kazlauskaite, J.; Hillhouse, E. W. *Free Radical Biol. Med.* **1999**, *26*, 99.
(256) Kelm, M.; Dahmann, R.; Wink, D.; Feelisch, M. *J. Biol. Chem.* **1997**, *272*, 9922.
(257) Fabian, R. H.; Dewitt, D. S.; Kent, T. A. *J. Cereb. Blood Flow Metab.* **1995**, *15*, 242.
(258) Manning, P.; Cookson, M. R.; Eggett, C. J.; Tolias, C. M.; Read, S. J.; Hunter, A. J.; Tsatmali, M.; Thody, A. J.; Hillhouse, E. W.; Shaw, P. J.; McNeil, C. J. *Analusis* **2000**, *28*, 493.
(259) Thomson, L.; Trujillo, M.; Telleri, R.; Radi, R. *Arch. Biochem. Biophys.* **1995**, *319*, 491.
(260) Arbault, S.; Pantano, P.; Jankowski, J. A.; Vuillaume, M.; Amatore, C. *Anal. Chem.* **1995**, *67*, 3382.
(261) Ikariyama, Y.; Yamauchi, S.; Yukiashi, T.; Ushioda, H. *Anal. Lett.* **1987**, *20*, 1407.
(262) Ikariyama, Y.; Yamauchi, S.; Yukiashi, T.; Ushioda, H. *J. Electroanal. Chem.* **1988**, *251*, 267.
(263) de Boer, J.; Hoeijmakers, J. H. J. *Carcinogenesis* **2000**, *21*, 453.
(264) Ford, J. M.; Hanawalt, P. C. *Curr. Top. Microbiol. Immunol.* **1997**, *221*, 47.
(265) Arbault, S.; Pantano, P.; Sojic, N.; Amatore, C.; Best-Belpomme, M.; Sarasin, A.; Vuillaume, M. *Carcinogenesis* **1997**, *18*, 569.
(266) Arbault, S.; Sojic, N.; Bruce, D.; Amatore, C.; Sarasin, A.; Vuillaume, M. *Carcinogenesis* **2004**, *25*, 509.
(267) Lachgar, A.; Sojic, N.; Arbault, S.; Bruce, D.; Sarasin, A.; Amatore, C.; Bizzini, B.; Zagury, D.; Vuillaume, M. *J. Virol.* **1999**, *73*, 1447.
(268) Brovkovych, V.; Stolarczyk, E.; Oman, J.; Tomboulian, P.; Malinski, T. *J. Pharm. Biomed. Anal.* **1999**, *19*, 135.
(269) Malinski, T.; Mesaros, S.; Tomboulian, P. *Methods Enzymol.* **1996**, *268*, 58.
(270) Mesaros, S.; Grunfeld, S.; Mesarosova, A.; Bustin, D.; Malinski, T. *Anal. Chim. Acta* **1997**, *339*, 265.
(271) Mao, L. Q.; Tian, Y.; Shi, G. Y.; Liu, H. Y.; Jin, L. T.; Yamamoto, K.; Tao, S.; Jin, J. Y *Anal. Lett.* **1998**, *31*, 1991.
(272) Mao, L. Q.; Yamamoto, K.; Zhou, W. L.; Jin, L. T. *Electroanalysis* **2000**, *12*, 72.
(273) Xian, Y. Z.; Zhang, W.; Xue, J.; Ying, X. Y.; Jin, L. T.; Jin, J. Y. *Analyst* **2000**, *125*, 1435.
(274) Kubant, R.; Malinski, C.; Burewicz, A.; Malinski, T. *Electroanalysis* **2006**, *18*, 410.
(275) Amatore, C.; Arbault, S.; Bruce, D.; De Oliveira, P.; Erard, M.; Sojic, N.; Vuillaume, M. *Analusis* **2000**, *28*, 506.
(276) Amatore, C.; Arbault, S.; Bruce, D.; De Oliveira, P.; Erard, M.; Vuillaume, M. *Faraday Discuss.* **2000**, 356.
(277) Amatore, C.; Arbault, S.; Bouton, C.; Coffi, K.; Drapier, J. C.; Ghandour, H.; Tong, Y. H. *ChemBioChem* **2006**, *7*, 653.
(278) Arbault, S.; Edeas, M.; Legrand-Poels, S.; Sojic, N.; Amatore, C.; Piette, J.; Best-Belpomme, M.; Lindenbaum, A.; Vuillaume, M. *Biomed. Pharmacother.* **1997**, *51*, 430.
(279) Isik, S.; Schuhmann, W. *Angew. Chem., Int. Ed.* **2006**, *45*, 7451.
(280) Pailleret, A.; Oni, J.; Reiter, S.; Isik, S.; Etienne, M.; Bedioui, F.; Schuhmann, W. *Electrochem. Commun.* **2003**, *5*, 847.
(281) Wang, W.; Xiong, Y.; Du, F. Y.; Huang, W. H.; Wu, W. Z.; Wang, Z. L.; Cheng, J. K.; Yang, Y. F.; Yang, Y. F. *Analyst* **2007**, *132*, 515.
(282) Yasukawa, T.; Kaya, T.; Matsue, T. *Electroanalysis* **2000**, *12*, 653.
(283) Zhao, X. C.; Petersen, N. O.; Ding, Z. F. *Can. J. Chem.* **2007**, *85*, 175.
(284) Andersson, H.; van den Berg, A. *Curr. Opin. Biotechnol.* **2004**, *15*, 44.
(285) Amatore, C.; Arbault, S.; Chen, Y.; Crozatier, C.; Tapsoba, I. *Lab Chip* **2007**, *7*, 233.
(286) Borgmann, S.; Radtke, I.; Erichsen, T.; Blochl, A.; Heumann, R.; Schuhmann, W. *ChemBioChem* **2006**, *7*, 662.
(287) Cai, X. X.; Klauke, N.; Glidle, A.; Cobbold, P.; Smith, G. L.; Cooper, J. M. *Anal. Chem.* **2002**, *74*, 908.
(288) Chang, S. C.; Pereira-Rodrigues, N.; Henderson, J. R.; Cole, A.; Bedioui, F.; McNeil, C. J. *Biosens. Bioelectron.* **2005**, *21*, 917.
(289) Chang, S. C.; Rodrigues, N. P.; Zurgil, N.; Henderson, J. R.; Bedioui, F.; McNeil, C. J.; Deutsch, M. *Biochem. Biophys. Res. Commun.* **2005**, *327*, 979.
(290) Kintzios, S.; Marinopoulou, I.; Moschopoulou, G.; Manganab, O.; Nomikou, K.; Endo, K.; Papanastasiou, I.; Simonian, A. *Biosens. Bioelectron.* **2006**, *21*, 1365.
(291) Klauke, N.; Smith, G. L.; Cooper, J. M. *Anal. Chem.* **2007**, *79*, 1205.
(292) Rodrigues, N. P.; Bedioui, F.; Deutsch, A.; Zurgil, N.; Afrimzon, E.; Shafran, Y.; Deutsch, M. *Electrochem. Commun.* **2006**, *8*, 341.
(293) Yasukawa, T.; Glidle, A.; Cooper, J. M.; Matsue, T. *Anal. Chem.* **2002**, *74*, 5001.
(294) Isik, S.; Berdondini, L.; Oni, J.; Blochl, A.; Koudelka-Hep, M.; Schuhmann, W. *Biosens. Bioelectron.* **2005**, *20*, 1566.
(295) Pereira-Rodrigues, N.; Zurgil, N.; Chang, S. C.; Henderson, J. R.; Bedioui, F.; McNeil, C. J.; Deutsch, M. *Anal. Chem.* **2005**, *77*, 2733.
(296) Bedioui, F.; Trevin, S.; Devynck, J. *Electroanalysis* **1996**, *8*, 1085.
(297) Bedioui, F.; Trevin, S.; Devynck, J.; Lantoine, F.; Brunet, A.; Devynck, M. A. *Biosens. Bioelectron.* **1997**, *12*, 205.
(298) Wightman, R. M. *Science* **2006**, *311*, 1570.
(299) Baur, J. E.; Kristensen, E. W.; May, L. J.; Wiedemann, D. J.; Wightman, R. M. *Anal. Chem.* **1988**, *60*, 1268.
(300) Venton, B. J.; Wightman, R. M. *Anal. Chem.* **2003**, *75*, 414A
(301) Shibuki, K.; Okada, D. *Nature* **1991**, *349*, 326.
(302) Shibuki, K. *Brain Res.* **1989**, *487*, 96.
(303) Tuzel, I. H. *J. Clin. Pharmacol.* **1974**, *14*, 494.
(304) Smith, D. A.; Hoffman, A. F.; David, D. J.; Adams, C. E.; Gerhardt, G. A. *Neurosci. Lett.* **1998**, *255*, 127.
(305) Friedemann, M. N.; Robinson, S. W.; Gerhardt, G. A. *Anal. Chem.* **1996**, *68*, 2621.
(306) Leonard, C. S.; Michaelis, E. K.; Mitchell, K. M. *J. Neurophysiol.* **2001**, *86*, 2159.
(307) Ferreira, N. R.; Ledo, A.; Frade, J. G.; Gerhardt, G. A.; Laranjinha, J.; Barbosa, R. M. *Anal. Chim. Acta* **2005**, *535*, 1.
(308) Meulemans, A. *Neurosci. Lett.* **1993**, *157*, 7.
(309) Meulemans, A. *Neurosci. Lett.* **1994**, *171*, 89.
(310) Meulemans, A. *Neurosci. Lett.* **2000**, *294*, 125.
(311) Meulemans, A. *Neurosci. Lett.* **2002**, *321*, 115.
(312) Meulemans, A. *Neurosci. Lett.* **2003**, *347*, 116.
(313) Meulemans, A. *C. R. Biol.* **2005**, *328*, 271.
(314) Fabre, B.; Burlet, S.; Cespuglio, R.; Bidan, G. *J. Electroanal. Chem.* **1997**, *426*, 75.
(315) Cherian, L.; Goodman, J. C.; Robertson, C. S. *J. Neurophysiol.* **2000**, *83*, 2171.
(316) Wu, W. C.; Wang, Y.; Kao, L. S.; Tang, F. I.; Chai, C. Y. *Brain Res. Bull.* **2002**, *57*, 171.

(317) Iadecola, C.; Nakai, M.; Mraovitch, S.; Ruggiero, D. A.; Tucker, L. W.; Reis, D. J. *Brain Res.* **1983**, *272*, 101.
(318) Belliveau, J. W.; Kennedy, D. N.; McKinstry, R. C.; Buchbinder, B. R.; Weisskoff, R. M.; Cohen, M. S.; Vevea, J. M.; Brady, T. J.; Rosen, B. R. *Science* **1991**, *254*, 716.
(319) Raichle, M. E. *Annu. Rev. Psychol.* **1994**, *45*, 333.
(320) Roy, C. S.; Sherrington, C. S. *J. Physiol. (London)* **1890**, *11*, 85.
(321) Iadecola, C. *Trends Neurosci.* **1993**, *16*, 206.
(322) Zhang, Z. G.; Chopp, M.; Bailey, F.; Malinski, T. *J. Neurol. Sci.* **1995**, *128*, 22.
(323) Buerk, D. G.; Ances, B. M.; Greenberg, J. H.; Detre, J. A. *NeuroImage* **2003**, *18*, 1.
(324) Buerk, D. G.; Riva, C. E.; Cranstoun, S. D. *Microvasc. Res.* **1996**, *52*, 13.
(325) Thom, S. R.; Bhopale, V.; Fisher, D.; Manevich, Y.; Huang, P. L.; Buerk, D. G. *J. Neurobiol.* **2002**, *51*, 85.
(326) Thom, S. R.; Fisher, D.; Zhang, J.; Bhopale, V. M.; Cameron, B.; Buerk, D. G. *Toxicol. Appl. Pharmacol.* **2004**, *194*, 280.
(327) Fabian, R. H.; Perez-Polo, J. R.; Kent, T. A. *J. Neurosci. Res.* **2000**, *60*, 795.
(328) Amatore, C.; Arbault, S.; Bouret, Y.; Cauli, B.; Guille, M.; Rancillac, A.; Rossier, J. *ChemPhysChem* **2006**, *7*, 181.
(329) Rancillac, A.; Rossier, J.; Guille, M.; Tong, X. K.; Geoffroy, H.; Amatore, C.; Arbault, S.; Hamel, E.; Cauli, B. *J. Neurosci.* **2006**, *26*, 6997.
(330) Cauli, B.; Tong, X. K.; Rancillac, A.; Serluca, N.; Lambolez, B.; Rossier, J.; Hamel, E. *J. Neurosci.* **2004**, *24*, 8940.
(331) Oleinick, A. I.; Amatore, C.; Guille, M.; Arbault, S.; Klymenko, O. V.; Svir, I. *Math. Med. Biol.-A J. Ima* **2006**, *23*, 27.
(332) Rice, M. E.; Okada, Y. C.; Nicholson, C. *J. Neurophysiol.* **1993**, *70*, 2035.
(333) Schweighofer, N.; Ferriol, G. *Proc. Natl. Acad. Sci. U.S.A.* **2000**, *97*, 10661.
(334) Wood, J.; Garthwaite, J. *Neuropharmacology* **1994**, *33*, 1235.

CR068062G